THESIS ON NATURAL AND EXACT SCIENCES B98

Optical Properties of Multinary Semiconductor Compounds for Photovoltaic Applications

MAARJA GROSSBERG

TUT PRESS

TALLINN UNIVERSITY OF TECHNOLOGY
Faculty of Chemical and Materials Technology
Department of Materials Science
Chair of Semiconductor Materials Technology

Dissertation was accepted for the defence of the degree of Doctor of Philosophy in Natural and Exact Sciences on October 5, 2010.

Supervisor: Professor Jüri Krustok, Department of Materials Science, Tallinn University of Technology

Opponents: Professor Rajmund Bacewicz, Faculty of Physics, Warsaw University of Technology

Dr. Raivo Jaaniso, Institute of Physics, University of Tartu

Defence: November 26, 2010, at 11.00
Lecture hall: VII-226
Tallinn University of Technology, Ehitajate tee 5, Tallinn

Declaration: Hereby I declare that this doctoral thesis, my original investigation and achievement, submitted for the doctoral degree at Tallinn University of Technology has not been submitted for any academic degree.

Maarja Grossberg

ISSN 1406-4723
ISBN 978-9949-23-039-6

LOODUS- JA TÄPPISTEADUSED B98

Päikesepatareides kasutatavate mitmikpooljuhtühendite optilised omadused

MAARJA GROSSBERG

TTÜ KIRJASTUS

Table of Contents

LIST OF PUBLICATIONS

The present doctoral thesis is based on the following papers, which are referred to in the text by their Roman numerals.

I **M. Grossberg**, J. Krustok, A. Jagomägi, M. Leon, E. Arushanov, A. Nateprov, I. Bodnar. Investigation of potential and compositional fluctuations in $CuGa_3Se_5$ crystals using photoluminescence spectroscopy. *Thin Solid Films*, 515 (2007) 6204-6207.

II **M. Grossberg**, J. Krustok, I. Bodnar, S. Siebentritt, J. Albert. Photoluminescence and Raman spectra of the ordered vacancy compound $CuGa_5Se_8$. *Physica B : Condenced Matter* 403 (2008) 184-189.

III **M. Grossberg**, J. Krustok, S. Siebentritt, J. Albert. Compositional dependence of Raman scattering and photoluminescence emission in Cu-Ga-Se films grown by MOCVD, *Physica B: Condenced Matter* 404 (14-15) (2009) 1984-1988.

IV **M. Grossberg**, J. Krustok, K. Timmo, M. Altosaar. Radiative recombination in $Cu_2ZnSnSe_4$ monograins studied by photoluminescence spectroscopy, *Thin Solid Films* 517 (2009) 2489-2492.

V **M. Grossberg**, J. Krustok, J. Raudoja, K. Timmo, M. Altosaar, T. Raadik. Photoluminescence and Raman study of $Cu_2ZnSn(Se_xS_{1-x})_4$ monograins for photovoltaic applications, *Thin Solid Films* (in press)

In Appendix A, copies of the following papers are included.

Author`s own contribution

The contribution by the author to the papers included in the thesis is as follows:

I Characterization of $CuGa_3Se_5$ crystals by photoluminescence, analysis of the results and major part of writing

II Characterization of $CuGa_5Se_8$ crystals and films by photoluminescence and Raman spectroscopy, analysis of the results and major part of writing

III Characterization of Cu-Ga-Se films by photoluminescence and Raman spectroscopy, analysis of the results and major part of writing

IV Characterization of $Cu_2ZnSnSe_4$ monograins by photoluminescence and Raman spectroscopy, analysis of the results and major part of writing

V Characterization of $Cu_2ZnSn(Se_xS_{1-x})_4$ monograins by photoluminescence and Raman spectroscopy, analysis of the results and major part of writing

List of abbreviations and symbols

a_B	Bohr radius
BB	band-to-band
BI	band-to-impurity
BT	band-to-tail
CBM	conduction band minimum
CZTS	Cu_2ZnSnS_4
CZTSe	$Cu_2ZnSnSe_4$
DADC	donor-acceptor defect complex
DAP	donor-acceptor pair
EDS	energy dispersive x-ray spectroscopy
E_C	percolation level of electrons
E_{C0}	bottom of the conduction band
E_e	energy of an electron
E_g	bandgap energy
E_h	energy of a hole
E_T	thermal activation energy
E_V	percolation level of holes
E_{V0}	top of the valence band
EQE	external quantum efficiency
f	focal length
f_e	Fermi function
F_n	Fermi level
FWHM	full width at half maximum

hv_{max}	band`s peak position
I_a	ionization energy of a defect
MGL	monograin layer
MOCVD	metal organic chemical vapor deposition
n	concentration of free electrons
N	defect concentration
N_V	effective density of states in the valence band
ODC	ordered defect compound
p	concentration of free holes
PL	photoluminescence
q_h	distribution function for holes
r_0	screening radius
$\rho\ (E)$	density of states function
ρ_c	electron density of states
ρ_v	hole density of states
SEM	scanning electron microscopy
SPC	solid phase crystallization
T_m	melting point temperature
VBM	valence band maximum
XRD	X-ray diffraction
θ	ratio of electron and hole capture probabilities
γ	average amplitude of potential fluctuations
γ^*	average amplitude of band edge fluctuations

INTRODUCTION

Chalcopyrite type semiconductors such as $CuInSe_2$ and $CuGaSe_2$ are used as absorbers in high-efficiency heterojunction solar cells. They are promising materials for photovoltaic applications due to their optimal direct bandgap and high absorption coefficient. Solar cells based on $CuIn_{1-x}Ga_xSe_2$ have demonstrated efficiencies up to 20.3 % [1]. Another attractive property is their tolerance to the large range of anion-to-cation off stoichiometry, manifested by the existence of ordered defect compounds (ODCs) [2]. In some high-efficiency $CuIn_{1-x}Ga_xSe_2$ based solar cells, the existence of an In-rich n-type material surface layer of $Cu(In_{1-x}Ga_x)_3Se_5$ on the absorber has been shown [3,4]. This ODC layer is expected to play an important role in the perfomance of the high-efficiency solar cells. Also, in the studies of surface properties of wide-gap $CuGaSe_2$ (E_g = 1.68 eV) thin films, the evidence of bandgap widening [5] together with deviations from stoichiometry, pointing to the formation of ODC-related phases were shown [6]. In addition, it was found by deep-level-transient and admittance spectroscopy that compositional variations decrease the density of the dominant type defect states and increase the device performance of $CuGaSe_2$ based solar cells [7]. It is wellknown that ternary chalcopyrites allow us to control their electronic properties just by changing the native defect composition instead of introducing additional impurities. However, the native defects in the absorber material may create unwanted recombination channels and limit the efficiency of a solar cell. Therefore, a detailed study of the electronic properties of the ODCs is essential. Different defect related recombination mechanisms can be identified by the temperature and excitation power dependent photoluminescence (PL) studies. The typical PL spectra of the ODCs of the Cu-Ga-Se system are dominated by broad asymmetric emission bands that can be characterized with the model of highly doped and compensated semiconductors. The aim of the first part of my work was to study the defect structure of the ODCs of the Cu-Ga-Se system by using PL and Raman spectroscopy.

The second part is dedicated to the first steps in the investigation of the PL properties and vibrational spectra of kesterite compounds $Cu_2ZnSnSe_4$, Cu_2ZnSnS_4 and their solid solutions $Cu_2ZnSn(Se_xS_{1-x})_4$. These compounds have gained recent interest as absorber materials of solar cells due to the limited amount of In and Ga in the Earth`s crust. The kesterites are obtained by replacing half of the In atoms in chalcopyrite $CuInSe_2$ or $CuInS_2$ by Zn and the other half by Sn. These compounds are believed to have electronic and optical properties similar to the widely studied ternary chalcopyrites such as $CuInSe_2$ and $CuGaSe_2$. However, there is still not enough knowledge about the properties of kesterites to draw a parallel to the chalcopyrites. Moreover, the crystallization process of the kesterite is still not very well understood. Unlike ternary chalcopyrites, the kesterite structure is very sensitive to deviations from stoichiometry, leading to the formation of additional phases. Therefore, it is essential to determine growth conditions and chemical

composition for the single phase formation. To broaden the knowledge about the opto-electronic properties of kesterites we performed the PL and Raman measurements of $Cu_2ZnSn(Se_xS_{1-x})_4$ small single crystal particles (monograins). Similarly to the ODCs, we found the PL spectra of $Cu_2ZnSn(Se_xS_{1-x})_4$ monograin powders to result from the recombination related to the spatial potential fluctuations that are present in highly doped and compensated semiconductors. We also present the first results of the Raman characterization of $Cu_2ZnSn(Se_xS_{1-x})_4$ compounds.

The present thesis is based on five published papers. The thesis is divided into three Chapters. Chapter 1 reviews the known optical, vibrational, and electronic properties of the ODCs and the kesterites based on the literature. Chapter 2 describes the sample preparation and the experimental setup of PL and Raman measurements. Chapter 3 introduces the theory of the PL of heavily doped semiconductors and describes the Raman modes of the chalcopyrites. With the help of the theory, the results of the PL and Raman experiments of the ODCs and the kesterites are discussed. Finally, the main results are summarized.

The work was financially supported by Estonian Science Foundation grants G-5149, G-6554, G6160, G-8282, by INTAS grant no. 03-51-6314 and by the target financing by HTM (Estonia) No. SF0140099s08. Financial support was also received from the World Federation of Scientists National Scholarship Programme and Estonian Doctoral School of Materials Science and Materials Technology.

1. LITERATURE REVIEW AND THE AIM OF THE WORK

1.1. Ordered defect compounds

It has been shown by first-principles calculations [2] that the formation of interacting donor-acceptor defect complexes (DADCs) like $\left(2V_{Cu}^{-1} + In_{Cu}^{+2}\right)$ can take place in $CuInSe_2$ due to their very small energy of formation. The array of DADCs is formed spontaneously due to the negative formation energy. The existence of In-rich phases such as $CuIn_5Se_8$, $CuIn_3Se_5$, $Cu_2In_4Se_7$, $Cu_5In_9Se_{16}$, and $Cu_3In_5Se_9$ is explained as the repetition of the defect complex of $\left(2V_{Cu}^{-1} + In_{Cu}^{+2}\right)$ after each n = 4, 5, 7, 8, 9 unit cells of $CuInSe_2$, respectively. For this reason, these compounds are called *ordered defect compounds*. Since one of the defects related to the ordering is copper vacancy, these compunds are also called *ordered vacancy compounds* (OVCs). Similarly, the existence of ODCs in Cu-Ga-Se, Cu-In-Te and Cu-Ga-Te systems has been explained [8]. In the Cu-Ga-Se system, the Ga-rich phases are formed by the ordering of DADCs that consist of 2 V_{Cu} and Ga_{Cu} [2] (see an example in Figure 1).

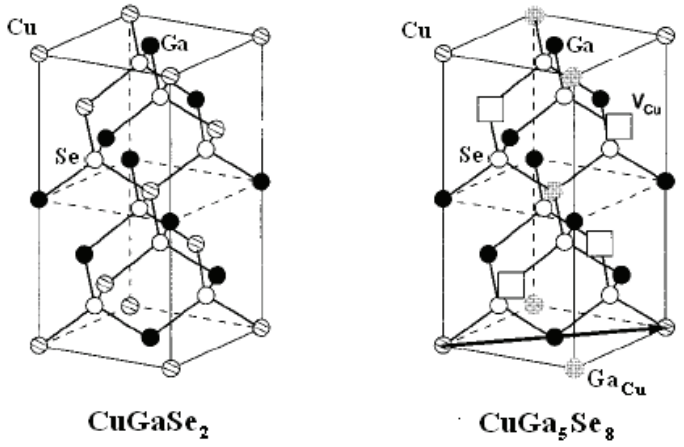

Figure 1. Chalcopyrite crystal structure of $CuGaSe_2$ and related ODC $CuGa_5Se_8$ that includes defect ordering ....Cu – V_{Cu} – Ga_{Cu} – V_{Cu} – Cu....

It has been confirmed [9-11] that the relatively low concentration of majority carriers in the ODCs compared to the corresponding 1:1:2 phase is due to the attractive interaction between V_{Cu}^{-1} and In_{Cu}^{+2}. This interaction leads to the partial annihilation of the corresponding shallow acceptor and deep donor levels and forms an electrically passive defect pair. Therefore, deep defect states that act as

traps for carriers are almost absent in the ODCs of the Cu-In-Se system. However, it was calculated by Wei *et al.* [12] that the donor formation energy is larger in $CuGaSe_2$ and the Ga_{Cu} donor level in $CuGaSe_2$ is deeper than the In_{Cu} donor level in $CuInSe_2$. Also, the attraction between V_{Cu} and Ga_{Cu} is not sufficient to push the Ga_{Cu} level close to the conduction band minimum (CBM). As a result, even when it is passivated by V_{Cu}, Ga_{Cu} always behaves as an electron trap in Ga-rich $CuGaSe_2$. Their calculations also show that the valence band maximum (VBM) of $CuGaSe_2$ is about 0.04 eV lower than the VBM of $CuInSe_2$, whereas the CBM of $CuGaSe_2$ is about 0.6 eV higher than the CBM of $CuInSe_2$, suggesting that p-type doping in $CuInSe_2$ and $CuGaSe_2$ should be similar, whereas n-type doping is more difficult in $CuGaSe_2$. Therefore, one should not expect the type inversion in $CuGaSe_2$ with an increasing Ga concentration, as it is found in In-rich $CuInSe_2$.

The ODCs also show a blueshift of the bandgap energy as compared to the corresponding 1:1:2 phase. According to Zhang *et al.* [2] the creation of periodic V_{Cu} reduces the Se p – Cu d interband repulsion in the ODCs, as compared to the corresponding 1:1:2 phase. Although, the defect complex $\left(2V_{Cu}^{-1} + III_{Cu}^{+2}\right)$ also lowers the CBM, the first effect predominates, because the *p-d* repulsion is very strong in the selenides of the ODCs [13]. Therefore the bandgap of the ODCs is wider than the corresponding 1:1:2 phase and the PL emission is observed at higher energies. The published values of the room-temperature bandgap energies of $CuGaSe_2$, $CuGa_3Se_5$ and $CuGa_5Se_8$ thin films and polycrystalline bulk samples are 1.64 - 1.70 eV [8,14], 1.74 – 1.87 eV [15-19] and 1.78 – 1.97 eV [8, 18-20], respectively. The wide range of bandgap energies is probably related to the presence of Urbach`s tail in the optical absorption spectra, making the precise bandgap determination somewhat complicated. The formation of ternary Cu-Ga-Se compounds with varying bandgaps enables the formation of heterojunctions that are used in the design of high-performance electronic and optoelectronic devices. For these applications, it is important to know the recombination processes in the ODCs. In order to determine the recombination channels in $CuGa_3Se_5$ and $CuGa_5Se_8$ crystals and films, we performed the PL analysis [I-III].

The presence of DADC arrays in the ODCs also reduces the frequencies of some of the optical phonon modes [21], as compared to the corresponding 1:1:2 phase. It is obvious that the dimensions of the unit cell of the defect structures are always larger than those of the ideal chalcopyrite structure. Therefore the Brillouin zone of the ODC structure is smaller than the Brillouin zone of the chalcopyrite structure. All reciprocal-lattice points of the defect structure which are inside or at the zone boundaries of the larger Brillouin zone are equivalent to $k = 0$. Therefore, the vibrations corresponding to these k vectors in the large Brillouin zone can be optically active. Our Raman spectra of the Cu-Ga-Se films and the results reported in the literature are compared in [II, III].

1.1.1. $CuGa_3Se_5$

$CuGa_3Se_5$ is the most investigated ODC compound in the Cu-Ga-Se system. The bandgap energy of $CuGa_3Se_5$ obtained from optical absorption measurements for bulk samples at room temperature is 1.754 eV and for thin films 1.855 eV [15]. Rincon *et al*. report in [23] that the PL spectrum of $CuGa_3Se_5$ that consists of one broad band hv_{max} = 1.63 eV (T = 15 K). The band was suggested to result from donor-acceptor pair (DAP) recombination. Guastavino *et al*. [24] measured the PL spectrum of $CuGa_3Se_5$ that consisted of one broad asymmetric edge emission band at hv_{max} = 1.6 eV (T = 4.2 K) and one deeper band at $hv_{max} \sim$ 1.2 eV (T = 4.2 K). The broadness of the PL bands (150–200 meV) was also interpreted by DAP transitions.

The typical asymmetric shape of the PL band in ternary chalcopyrites is often caused by the band tails of the density of states function induced by spatial potential fluctuations due to the high concentration of intrinsic defects [25-27]. Furthermore, compositional fluctuations also affect the shape of the PL bands by creating the fluctuations of the bandgap energy. Also, Wasim *et al*. [28] found from the absorption measurements that the optical absorption coefficient of $CuGa_3Se_5$ just below the absorption edge varies exponentially with photon energy, showing the so-called Urbach`s tail. We studied the PL properties of $CuGa_3Se_5$ in connection with compositional and spatial potential fluctuations [I]. These results are presented in Section 3.4 in the present thesis.

Structural measurements showed that the $CuGa_3Se_5$ structure fits to the $P\bar{4}2c$ spatial group, point group $\bar{4}2m$ [22]. The unit cell parameters are: a = 0.54995 nm, c = 1.0946 nm. Rincon *et al*. [23] have studied the Raman spectra of $CuGa_3Se_5$ and determined 14 Raman lines at 48, 64, 72, 90, 105, 142, 166, 187, 200, 220, 252, 274, and 287 cm^{-1}, where the most intense peak at 166 cm^{-1} was assigned to the A_1 mode. The Raman peaks at 72 and 90 cm^{-1} were assigned to B_1 modes, the peaks at 64, 187 and 274 cm^{-1} to B_2 modes and the rest of the peaks to E modes.

1.1.2. $CuGa_5Se_8$

In comparison with $CuGa_3Se_5$, very little information on the physical properties of $CuGa_5Se_8$ have appeared in the literature and no papers can be found on the PL properties of $CuGa_5Se_8$. The temperature dependence of the energy gap of the bulk samples of $CuGa_5Se_8$ has been reported by Marin *et al.* [21]. It was found that the bandgap energy varies from 1.917 to 1.811 eV in the temperature range from 10 to 300 K. Xu *et al*. [29] have investigated the Raman spectra of $Cu(In_{1-x}Ga_x)_5Se_8$ thin films with varying x. To our knowledge, this is the only Raman spectrum of $CuGa_5Se_8$ reported in the literature. From the room-temperature Raman measurements they found six peaks at 78, 93, 107, 160, 259

and 289 cm^{-1}, the peak at 160 cm^{-1} being the dominant A_1 mode of $CuGa_5Se_8$. However, neither fitting of the spectra nor detailed identification or assignment of the observed peaks have been conducted. Orlova *et al*. [30,31] have investigated the structural parameters, the axial thermal expansion coefficients and the characteristic Debye temperature of the $CuGa_5Se_8$ single crystals by using X-ray diffraction (XRD). The unit cell parameters a = 0.54682 nm and c = 1.09116 nm that are very close to the crystal lattice parameters of $CuGa_3Se_5$ were determined. It was also found that the thermal expansion coefficient of $CuGa_5Se_8$ is very close to $CuGa_3Se_5$. These properties of ODC compounds are essential to obtain high-quality epitaxial layers, to form heterojunctions and to produce solar cells based on these ternary compounds. Leon *et al.* [32] have studied $CuGa_5Se_8$ by spectroscopic ellipsometry and determined the dielectric function related optical constants, such as the complex refractive index, extinction coefficient, absorption coefficient, and normal-incidence reflectivity.

In order to understand the role of the ordered defects in the recombination processes, my analysis focused on the PL and Raman spectra of $CuGa_5Se_8$ polycrystalline thin films and single crystals [II]. The results of this study are presented in Sections 3.3.1 and 3.5.

1.2. Kesterites

Kesterite is the name of the mineral Cu_2ZnSnS_4 (CZTS) that belongs to the space group $I\bar{4}$ [33]. Its ordering of the metals is slightly different from the mineral stannite (Cu_2FeSnS_4), which belongs to the space group $I\bar{4}2m$. The $Cu_2ZnSnSe_4$ (CZTSe) compound is also reported to crystallize in the kesterite structure [34], although some authors suggest that stannite structure is characteristic of CZTSe [35,36]. Both structures are topologically identical (see Figure 2), but differ in the distribution of the metal atoms. The difference between the structures is barely discernible with XRD that shows that kesterite has a sligthly larger peak intensity ratio I(211):I(202) than stannite. Moreover, the calculations of the crystal structure and electronic band structure made by Chen and co-workers [37] show only 3 meV/atom energy difference between the kesterite and stannite structure, indicating that kesterite and stannite ordering may coexist in the synthesized samples.

CZTSe and CZTS are believed to have electronic and optical properties similar to the widely studied ternary chalcopyrites such as $CuInSe_2$, $CuGaSe_2$ and $CuInS_2$. The reason is that they are obtained by replacing half of the In atoms in chalcopyrite $CuInSe_2$ or $CuInS_2$ by Zn and by replacing the other half by Sn. The kesterites have p-type conductivity, high absorption coefficient 10^4 cm^{-1} and direct band gap in CZTSe around 1 eV [37] or 1.5 eV [35], and in CZTS around 1.6 eV [38]. These properties make the kesterites attractive for solar cell applications. Todorov *et al.* [39] have reported a $Cu_2ZnSn(S,Se)_4$ solar cell efficiency of 9.66 %. However, very little is still known about the electrical and optical properties of the kesterites.

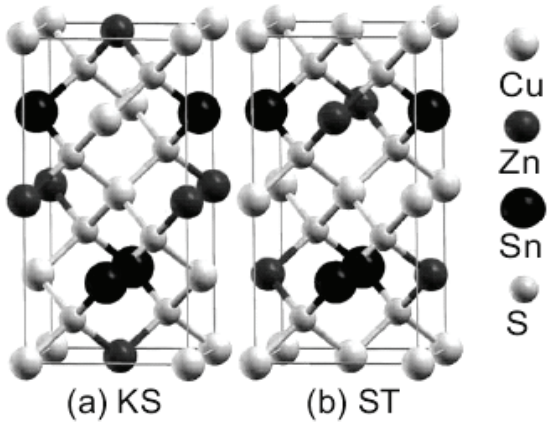

Figure 2. The (a) kesterite and (b) stannite crystal structures of CZTS [37].

Currently the main problem seems to be the formation of different binary and ternary phases during the growth of the kesterites. The ZnSe, $Cu_{2-x}Se$, SnSe, $SnSe_2$, and Cu_2SnSe_3 phases are most commonly observed in CZTSe [34, 40]. Nagoya *et al.* [41] performed first-principles studies that show the thermodynamic stability of the CZTS phase for the very small confined domain of chemical potentials, i.e. even slight deviations from the optimal growth conditions will result in the formation of other sulfidic precipitates, including ZnS, Cu_2SnS_3, SnS, SnS_2 and CuS. Our studies have focused on CZTSe monograins that are synthesized at temperatures over 700 ^{o}C and should obviously include less additional phases than thin films prepared at low temperatures, and should accordingly be more suitable for electronic devices such as solar cells. In order to detect the presence of additional phases in the monograins, we used Raman spectroscopy that is very sensitive to small amounts of material and enables us to distinguish between different phases better than XRD, where the peaks of the phases often closely match. In [IV] and [V] the Raman spectra of CZTSe and $Cu_2ZnSn(Se_xS_{1-x})_4$ monograin powders are presented.

The uncontrolled composition variations are probably one reason for the wide range of bandgap energies obtained by different groups. For CZTS, values between 1.4 eV [42] and 1.6 eV [38] have been reported. Nevertheless, the situation with CZTSe is even more peculiar; the obtained bandgap energies vary from 0.8 eV [43] to 1.65 eV [40], the latter being basically the same as that for CZTS. Selenides with larger lattice constants and higher *p* orbital energies usually have much smaller bandgaps than sulfides. The variation in bandgap values could also be related to the coexcistence of stannite and kesterite crystal structures. However, Chen *et al*. [37] have determined the bandgap energy difference of 0.12 eV for the kesterite and stannite phase in CZTS, which is too small to explain the differences in bandgap values obtained from the absorption measurements.

They also calculated the bandgap energy of kesterite CZTSe that is about 0.4 eV smaller than CZTS in the same crystal structure, which is consistent with the expectation that the selenides have smaller bandgaps than the corresponding sulfides.

Very little information about the PL properties of the kesterites can be found from the literature. Tanaka *et al.* [44] have determined DAP recombination with a thermal quenching activation energy E_T = 48 meV that was considered to be the ionization energy of an acceptor defect. They determined the room-temperature bandgap energy of 1.3 eV in S-poor CZTS single crystals grown by the iodine transport method. In addition, they have also studied the PL spectra of CZTS thin films and found similar results to the single crystals [45]. The origin of the PL for the stoichiometric and Cu-poor, Zn-rich films was attributed to DAP recombination with E_T = 39 meV and E_T = 59 meV, respectively. Recently, Hönes *et al*. [46] have observed edge emission at 1.5 eV from vapor phase grown CZTS crystals and proposed a defect recombination model with a shallow donor 5 ± 3 meV below the conduction band and two shallow acceptors 10 ± 5 meV and 30 ± 5 meV above the valence band. Broad PL band at 1.45 eV was observed by Oishi *et al*. [47], however, no detailed analysis were presented. We were first to publish the detailed analysis of the PL spectra of CZTSe [IV]. Recently, Salome *et al.* [48] have observed very weak PL emission from polycrystalline CZTSe thin films in the same spectral range.

1.2.1. $Cu_2ZnSnSe_4$

Due to contradictory information about its properties in the literature, the focus of the study of kesterites is on the properties of CZTSe. As mentioned above, there are some difficulties in determining the bandgap energy of $Cu_2ZnSnSe_4$ due to the formation of secondary phases during the low temperature growth. Several groups have determined the bandgap value of CZTSe around 1.44 eV from optical absorption measurements [35, 40, 49]. On the other hand, the *ab initio* calculations of the electronic structure of CZTSe by Raulot *et al*. [43] and Chen *et al*. [37] show a bandgap around 0.8 eV and 0.96 eV, respectively. Based on the external quantum efficiency (EQE) curves of the CZTSe monograin layer solar cells, in [50] we suggested that CZTSe has lower bandgap energy than proposed by the authors of the absorption measurements. According to the EQE and PL measurements [IV], the bandgap energy of CZTSe is expected to be in the vicinity of 1 eV. Recently, Krustok *et al.* [51] have studied the temperature dependence of EQE curves of the CZTSe solar cells and determined the room temperature bandgap energy of CZTSe Eg = 1.017 eV.

Only few papers about the defect structure of CZTSe can be found from the literature. Raulot *et al*. [43] have studied the defect formation energies of CZTSe. The lowest formation energy was found for V_{Cu} that can be considered as a dominating defect in CZTSe. They also calculated the formation energies of

neutral complex defects and found that defect complexes involving Zn have lower formation energies than the defects with Sn. The formation energy of $Cu_{Zn} + Zn_{Cu}$ complex defect was calculated to be 0.09 eV that may easily lead to some disorder in the CZTSe crystal structure in Cu and Zn sub-lattices like has been observed in ternary chalcopyrites. Krustok has proposed a novel method [51] for studying defect related spatial potential fluctuations in compensated absorber materials based on the analysis of the temperature dependence of EQE curves of solar cells. The results on CZTSe-based monograin layer (MGL) solar cells show the presence of spatial potential fluctuations with an average energetic depth of 25 meV. As mentioned above, we used PL studies to investigate the defect related radiative recombination in CZTSe [IV]. The results are presented in Section 3.7.1.

1.3. Aim of the work

Ordered defect compounds:

Understanding the behaviour of intrinsic defects in materials is essential to improve their electrical and optical properties. As can be seen from the literature review, only few papers report the PL and Raman results of ODCs of the Cu-Ga-Se system. The asymmetric shape of the PL bands was suggested to result from the DAP recombination in the $CuGa_3Se_5$. However, in ternary chalcopyrites the asymmetry of the PL bands is often caused by the band tails induced by spatial potential fluctuations due to the high concentration of native defects [25-27]. Furthermore, compositional fluctuations also affect the shape of PL bands by creating the fluctuations of the bandgap energy. Accordingly, the first task of this doctoral thesis was to study the PL properties of $CuGa_3Se_5$ in connection with compositional and potential fluctuations.

There are no PL studies published and only one Raman spectrum of $CuGa_5Se_8$ appears in the literature [29]. Therefore, in order to understand more about the role of the ordered defects in recombination processes, the second task of this thesis was to perform a detailed study of the PL and Raman properties of $CuGa_5Se_8$ polycrystalline thin films and single crystals.

In addition, to see the general trend of Raman properties with an increasing Ga concentration, the third task was to study the compositional dependence of the Raman spectra of the Ga-rich Cu-Ga-Se films with different composition grown by Metal Organic Chemical Vapor Deposition (MOCVD).

Kesterites:

Kesterites are very promising materials for photovoltaic applications, however, their fundamental physical properties have still been poorly studied. Very different values of the bandgap energy of CZTSe appear in the literature and no PL studies have been conducted to investigate the recombination in these compounds.

As a result, the fourth task in this thesis was to study the PL properties of the $Cu_2ZnSn(Se_xS_{1-x})_4$ monograins and to perform more detailed analysis of the PL spectra of the CZTSe monograins to clarify the contradiction in the bandgap energy values presented in the literature.

Secondly, since the kesterite structure is very sensitive to deviations from stoichiometry, additional phases are very easily formed. The fifth task in this thesis was to use PL and Raman measurements to investigate the phase composition of the studied $Cu_2ZnSn(Se_xS_{1-x})_4$ monograins.

2 EXPERIMENTAL DETAILS

2.1. Photoluminescence measurements

The photoluminescence is a non-destructive, contactless and sensitive method for studying defects in semiconductor materials. PL is very sensitive to small changes in the crystal structure, enabling us to establish its defect composition both qualitatively and quantitatively. The schematic view of the PL setup is shown in Figure 3.

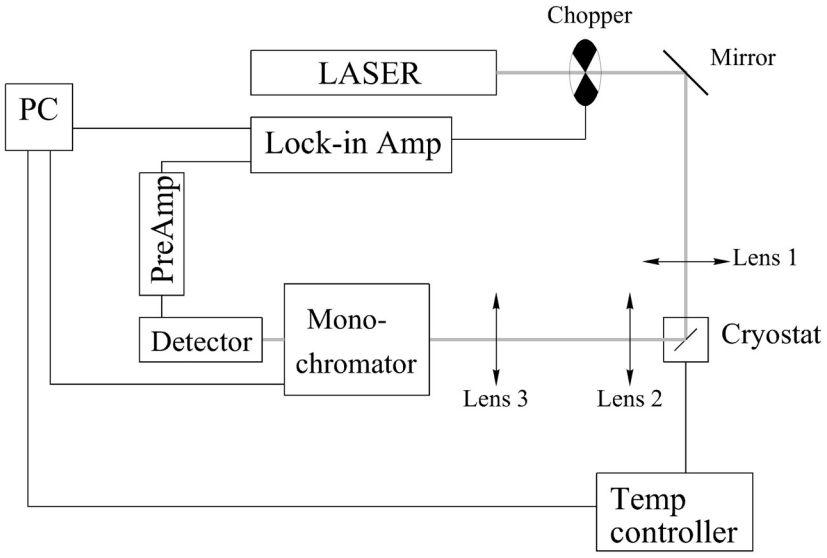

Figure 3. Experimental setup for photoluminescence measurements.

For PL measurements the samples were mounted inside the closed-cycle He cryostat that enables us to measure in the temperature range from 10 K to 325 K. The samples were mounted inside the cryostat on a vertical surface of the cold finger using silicon grease as an adhesive material. For comparison, the PL signal from the silicon grease was measured separately. For the PL measurements of the monograin powders, the powder was glued onto a thin copper plate that was mounted on the cold head of the cryostat using silicon grease.

For excitation the He-Cd laser with the maximum output power of 45 meV and the wavelength of 441 nm was used. The laser beam passes through the chopper that is connected to the lock-in amplifier. With the help of a mirror and a lens 1 (f = 20 cm) the laser beam is then focused on the sample with the spot

diameter of about 100 μm. A parallel beam is formed from the PL signal by lens 2 (f = 10 cm). The beam is then focused into the monochromator entrance slit by lens 3 (f = 40 cm). Computer controlled *Carl Zeiss SPM-2* monochromator (f = of 40 cm) is used to analyze the PL signal. Depending on the spectral region and required spectral resolution, either grating (600 lines per mm) or prism was used as the dispersive element.

The PL signal was detected either by the photomultiplier tube *R632* in the visible spectral region or by the InGaAs detector in the infrared spectral region. The electrical signal was amplified using the low-noise phase sensitive lock-in technique (*Stanford Research Systems SR810DSP*). The resulting spectra were corrected for grating efficiency variations and for the spectral response of the detectors.

For laser power dependencies of the PL spectra, natural density filters were used to reduce the intensity of the laser signal. The output power of the laser beam was measured with laser power meter *Melles Griot 13PEM001*.

All the PL and Raman spectra were fitted by using *MS Excel*, *Microcal Origin* or *PeakFit* software.

2.2. Raman measurements

Raman spectroscopy allows the compositional and crystal structural investigation of the surface region of the samples. This method is based on the inelastic scattering of light by the medium, leading to a change in the frequency of the incident light. The information depth of Raman spectroscopy depends on the absorption coefficient of the material and on the chosen laser wavelength.

The room temperature Raman spectra were recorded by using the *Horiba`s Labram HR* high resolution confocal spectrometer equipped with a multichannel CCD detection system in the backscattering configuration.

In micro-Raman measurements, the incident laser light with the wavelength of 532 nm can be focused on the sample with the spot diamater of 10 μm. The spot size can be altered by changing the objective (Olympus) from 10 x to 100 x. For changing the light intensity on the sample there are 6 neutral filters installed with the optical densities 0.3, 0.6, 1, 2, 3 or 4. The incident laser intensity can be decreased from 2 times (D0.3) to 10000 times (D4). The grating with 1800 lines/mm was chosen and the width of the confocal hole was 100 μm. The spectral resolution of the spectrometer was 0.1 cm^{-1}. The information depth was up to 1 μm. The spectrometer was equipped with a motorized xyz table. All measurements took place at room temperature and in the ambient air.

2.3. Chemical composition and structural analysis

The phase composition and the crystal structure of the $CuGa_3Se_5$ crystals were determined by XRD (in Universidad Autonoma de Madrid, Spain). The XRD patterns were recorded by the Siemens D 500 diffractometer. The Rietveld method was used for the derivation of crystal structure information from powder XRD data.

The chemical composition of the ODC crystals and $Cu_2ZnSn(Se_xS_{1-x})_4$ monograin powders was determined by EDS performed on Leo Supra 35 SEM. EDS analyses were done by Dr. Olga Volobujeva.

2.4. Sample preparation

2.4.1. Ordered defect compounds

The **$CuGa_3Se_5$** crystals were grown by the solid phase crystallization (SPC) method and by the Bridgman method by Dr. Ernest Arushanov at the Institute of Applied Physics in Moldova, and by Dr. Ivan Bodnar at the Belarussian State University of Informatics and Radioelectronics in Belarus, respectively.

For the SPC growth, the stoichiometric amounts of Cu (99.999% of purity), Ga (99.9999%) and Se (99.999%) (~20g total) were placed together in a quartz ampoule with the inner surface coated by carbon. The ampoule was evacuated up to 10^{-2} Pa and sealed. For synthesis, an one-zone vertical resistance furnace was used. The ampoule with precursors was heated up to 873 K and kept at this temperature for 24 hours. Then, the temperature was raised with the rate of 50 K/h up to 1223 K. This temperature is about 136 K lower than the melting point temperature of $CuGa_3Se_5$ (T_m=1359 K [31]). The ampoule was held at this temperature for 10 days before cooling. An ingot consisting of a few single crystal blocks of $CuGa_3Se_5$ was obtained.

The other **$CuGa_3Se_5$** crystals were grown by directed crystallization of the melt in the a vertical one-zone resistance furnace in the double quartz ampoules. The ampoules containing the stoichiometric amounts of the precursors were sealed under a vacuum of 10^{-3} Pa. Then they were placed in the furnace wherein the single crystals were grown. The furnace temperature was first raised to 900 K at a rate of 50 K/h. Then, vibrational stirring was switched on, and the charge was held at this temperature for 2 h. Next, the temperature was elevated up to 1450 K at the same rate, and the melt was vibrated at this temperature for 1 h. Thereafter the vibration was stopped and the directed crystallization was carried out by cooling the furnace to 1070 K at a rate of 2-3 K/h until the melt completely solidified. For homogenization, the obtained crystals were annealed for 120 h.

The **$CuGa_5Se_8$** single crystals were grown by the horizontal Bridgman method by Dr. Ivan Bodnar at the Belarussian State University of Informatics and Radioelectronics in Belarus. The stoichiometric amounts of the metals with purities of 6N purity were placed in a boat, which was put in the one end of the quartz ampoule. In the opposite end of the quartz ampoule an excess amount of selenium was placed. The ampoule was vacumized to 10^{-3} Pa of the residual pressure, sealed, and placed into the two-zone horizontal resistance furnace. Then the boat with metallic components was located in the hot furnace zone, where the temperature was rapidly (within ~ 2h) raised up to 1400 K. At first the temperature in the cold zone was first elevated at a rate of 50 K/h up to 900 K and held at this constant temperature during ~ 2 h for proceeding chemical reactions between the metallic components and selenium vapours. Then the temperature was raised at the same rate up to 1100 K with the exposure during 1 h. The directed crystallization of the melt was performed by cooling of the furnace at a rate of ~ 2 K/h. For homogenisation, annealing of the obtained ingots was made for ~ 240 h.

The studied **$CuGa_xSe_y$ films** were grown in the Aixtron AIX200 MOCVD reactor by Dr. Jürgen Albert in Helmholtz Zentrum Berlin. GaAs wafer in (100) orientation from Wafer Technologies were used as substrates. Cyclopentadienyl-copper, triethyl-gallium and ditertiary-butyl-selenide supplied from Epichem were used as Cu-, Ga- and Se-precursor, respectively. The growth process was derived from the process for $CuGaSe_2$ [52]. The growth temperature of 570^{o}C was used and

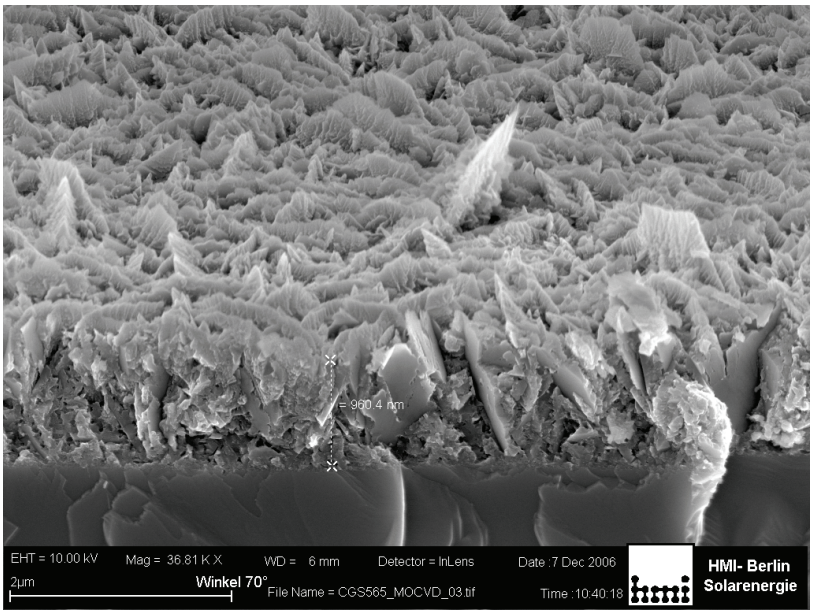

Figure 4. Cross-sectional SEM image of the polycrystalline $CuGa_5Se_8$ film with thickness around 1 μm.

pressure in the reactor was kept at 50 mbar during the processing time of 4 h. The compositions with concentration ratio of elements Cu to Ga [Cu]/[Ga] varied from 1 to 0.19, as was determined by EDS. SEM images of the samples showed the surface roughness and polycrystallinity of the Ga-rich films (see Figure 4). Despite the polycrystallinity it is wellknown that the chalcopyrites do not lose their good electrical properties since many defects are neutral.

2.4.2. $Cu_2ZnSn(Se_xS_{1-x})_4$ monograin powders

The $Cu_2ZnSn(Se_xS_{1-x})_4$ monograins were synthesized from CuSe(S), ZnSe(S) and SnSe(S) precursors in molten KI by doctoral student Kristi Timmo and Dr. Jaan Raudoja at Tallinn University of Technology. The binary compounds in the stoichiometric relation of $Cu_2ZnSnSe(S)_4$ and KI were mixed and ground in the planetary ball mill. The mixture was degassed and sealed into quartz ampoules. The recrystallization temperature was 1000 K. Crystal size was controlled by the temperature and duration of the recrystallization process. Crystals of the synthesized powders were released from flux by washing with deionizated water.

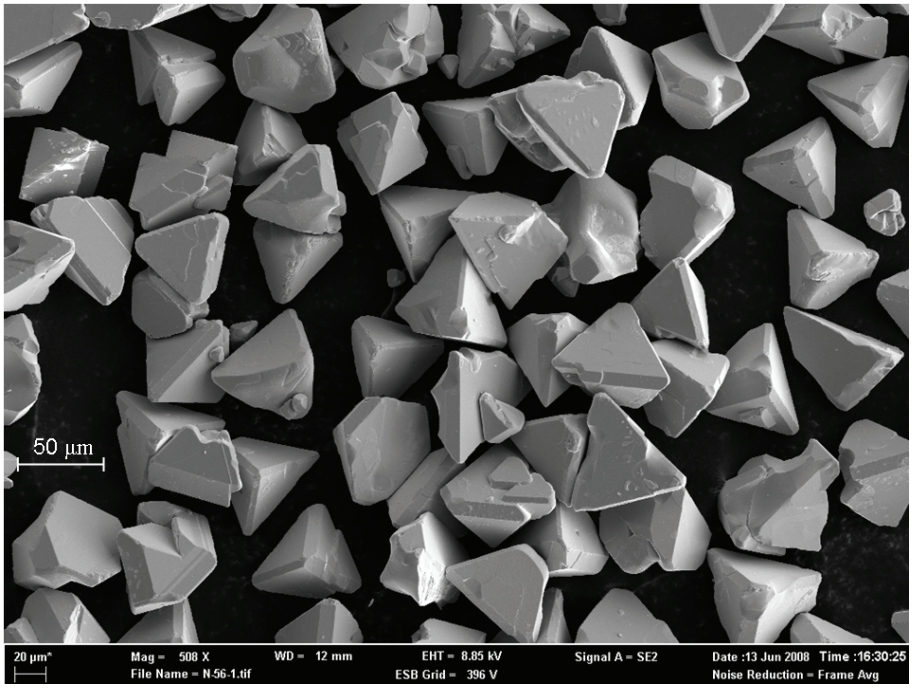

Figure 5. SEM image of the $Cu_2ZnSnSe_4$ monograin powder.

The obtained material consisted of single crystalline particles with diameters of around 100 µm in tertagonal shape and rounded grain edges (see Figure 5). The chemical composition of the monograin powders was determined by

EDS (see Table 1). The XRD measurements confirmed the formation of solid solutions. According to the hot probe measurements, the monograins had p-type conductivity.

In order to modify the surface of the monograins, vacuum annealing was performed to the crystals.

For the comparison of the results, polycrystalline Cu_2SnSe_3 was synthesized by melting of CuSe and SnSe in a vacuum ampoule at 1170 K.

Table 1. Compositions of the studied $Cu_2ZnSn(Se_xS_{1-x})_4$ solid solutions as determined by EDS

x	[Cu]/([Zn]+[Sn])	[Zn]/[Sn]
1	0.88	1.03
0.75	0.93	0.99
0.55	0.97	0.98
0.26	0.95	0.98
0	0.95	0.98

3. RESULTS AND DISCUSSION

3.1. Photoluminescence of heavily doped semiconductors

Photoluminescence is the optical radiation emitted by a physical system (in excess of the thermal equilibrium blackbody radiation) resulting from excitation to a nonequilibrium state by irradiation with light [53]. The carrier distribution resulting from the excitation of the sample is inhomogeneous and nonequilibrium. In attempting to regain homogeneity and equilibrium, the excess carriers will diffuse away from the surface of the sample while being depleted by both radiative and nonradiative recombination processes. The excess energy released in the nonradiative recombination process is given to the crystal lattice while as a result of radiative recombination a photon is emitted. The radiative recombination resulting in the PL spectrum of the material can occur through several recombination channels: (1) band-to-band recombination that involves a free electron in the conduction band and a free hole in the valence band, (2) excitonic emission, (3) band-to-acceptor recombination involving free electron in the conduction band and a hole in the acceptor state, (4) donor-to-band recombination involving an electron in the donor state and a free hole in the valence band, and (5) donor-acceptor pair recombination involving an electron in the donor state and a hole in the acceptor state.

The edge emission close to the bandgap energy of the material has rather complicated shape of the spectrum. The excitonic emission results in the bands of Lorentzian shape at energies close to the bandgap energy, while recombination involving defect states usually gives rise to PL bands with the Gaussian shape more distant from the bandgap energy. In the case of high quality crystals with low concentration of defects, the phonon structure of the PL bands can be observed, while very high concentration of defects in the material leads to asymmetric shape of the PL bands [54]. The latter case involves so-called heavily doped semiconductors, where the concentration of impurities or native defects is very high. The theory describing the electrical and optical properties of highly doped and compensated semiconductors was developed by Levanjuk and Osipov [54] and by Shklovskii and Efros [55].

Heavily doped semiconductors are those in which the average distance between impurities is less than the Bohr radius of an impurity state [54]:

$$N \cdot a_B^3 > 1, \qquad (3.1.1.)$$

where N is defect concentration and a_B is the Bohr radius of the defect state. In this case, the kinetic energy of an electron localized in a region of size $r \approx N^{-1/3}$ is higher than the energy of the Coulomb attraction by a donor. Also, the screening radius r_0 of the Coulomb potential is less than the Bohr radius a_B.

In heavily doped semiconductors spatial potential fluctuations are induced due to the random distribution of unscreened charged defects. These Coulomb

potential fluctuations will lead to a local perturbation of the band structure, thus broadening the defect level distribution and forming band tails (see Figure 6). Therefore, in a p-type semiconductor at low temperature, holes are captured at deep states in the valence band tail. Very deep states in the tail resemble acceptor rather than band states, i.e. they are strongly localized in that sense that the conductivity involving these states is close to zero. In the case of shallower states, the mobility increases abruptly at energies E_C and E_V, which are called the percolation levels of electrons and holes, respectively (see Figure 6). The percolation level E_V above which holes can be considered as free, differs from the energy E_{V0} corresponding to the top of the valence band of an undoped semiconductor and the difference is $\gamma_h \approx (2/3)\gamma$, where γ is the average amplitude of potential fluctuations. Due to the potential fluctuations the density of states function $\rho(E)$ does not vanish at the edges of the forbidden band. Also, a distribution of deep defect levels is broadened by the fluctuating potential field in the material and we have a distribution of defect levels instead of only one defect energy level with the ionization energy I_a.

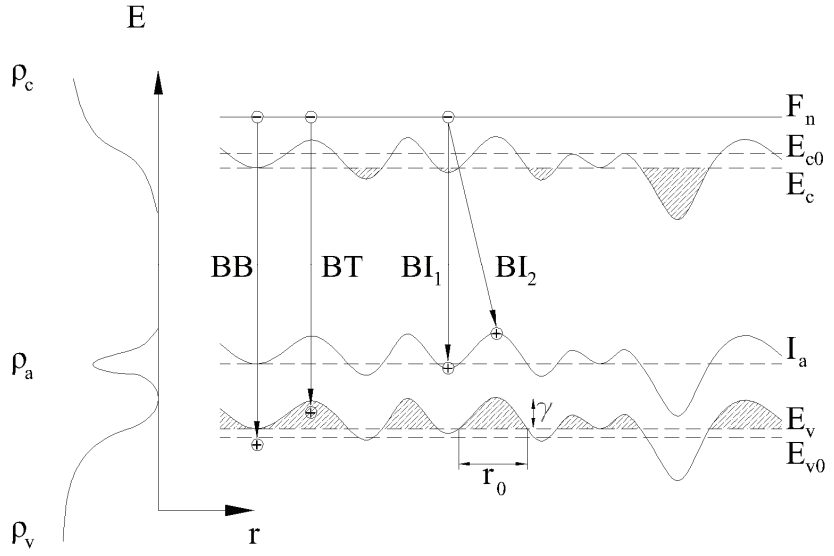

Figure 6. Energy band diagram and radiative recombination channels in a heavily doped semiconductor. On the left, the density of states function $\rho(E)$ is shown for the conduction band ρ_c, the valence band ρ_v and the defect state ρ_a. On the right, the fluctuating band edges are shown together with the main recombination channels: BB, BT and BI transitions. Here, the E_{v0} and E_{c0} represent the band edges of the undisturbed crystal, E_c and E_v are the percolation levels of electrons and holes, F_n is the Fermi level and I_a is the ionization energy of an acceptor. γ and r_0 represent the average potential well depth and width.

The average amplitude of the potential fluctuations γ is the average energetic difference between the hole energy in the potential fluctuation minimum and maximum [54]:

$$\gamma = \sqrt{2\pi}\,\frac{e^2}{\varepsilon r_0}\sqrt{N r_0^3}\,, \qquad (3.1.2.)$$

where e is the elementary charge, ε the static dielectric constant, N the total concentration of charged defects and r_0 is the screening radius which is equal to the extension of the fluctuation. γ is strongly dependent on the level of doping and compensation.

According to the theory of heavily doped semiconductors with spatially varying potential fluctuations, the radiative recombination can mainly arise from three different channels (see Figure 6). Firstly, band-to-band (BB) recombination involves a free electron and a free hole. Secondly, in band-to-tail (BT) recombination, a free electron recombines with a hole that is localized in the valence band tail. Thirdly, in band-to-impurity (BI) recombination free electron recombines with a hole that is localized on a deep acceptor state that does not overlap with the valence band tail. In a p-type semiconductor, if the electrons are localized in a potential well of the conduction band, the radiative recombination can also arise from the tail-to-tail (TT) or tail-to-impurity (TI) channel. In ternary chalcopyrites the effective mass of electrons is many times greater than the effective mass of holes, which allows us to assume that electrons are not confined in a potential well of a conduction band but can be considered as free. Due to the similarity of the crystal structures of chalcopyrites and kesterites, we can assume that the latter assumption is valid for kesterites as well.

In this thesis we have found that the PL spectra of ODC-s and kesterites arise either from the BT or BI recombination. Therefore, the next Sections 3.1.1. and 3.1.2. describe these recombination channels in more detail.

3.1.1. BT-band

BT recombination involves a free electron and a hole that is localized in the valence band tail. The theoretical PL spectrum of the BT-band is defined by the following expression [54]:

$$I_{BT}(h\nu) \propto \iint W_{BT}(E_e, E_h)\rho_c(E_e) f_e(E_e)\rho_v(E_h) q_h(E_h) \times \delta(E_e - E_h - h\nu) dE_e dE_h\,, \qquad (3.1.1.1.)$$

where $W_{BT}(E_e, E_h)$ is the recombination probability of a free electron and a localized hole with energies E_e and E_h, respectively, ρ_c is the electron density of states in the conduction band, f_e is the Fermi function, ρ_v is the density of states function for the localized holes and q_h is the distribution function for the localized holes. Since the effective mass of an electron in the compounds studied in this

thesis is presumed to be small compared to the effective mass of holes, the electron part of the intergral can be considered the same for all types of ρ_v.

The low-energy side of the BT-band is determined by the ρ_v function while the high-energy side is of much more complex nature. In most semiconductors with a very high defect concentration, the density of states function for the localized holes ρ_v and the emission intensity on the low-energy side I_{LE} at low temperatures have the following shapes [54]:

$$\rho_v(\varepsilon) = \rho_0 \exp\left(-\frac{E}{\gamma}\right) \quad , \; E = E_h - E_V > 0 \,, \tag{3.1.1.2}$$

$$I_{LE}(h\nu) \propto \exp\left[-\frac{E_g - h\nu}{\gamma}\right]. \tag{3.1.1.3}$$

The resulting BT-band at low temperatures has an asymmetrical shape with an exponential slope on the low-energy side and a steeper Gaussian incline on the high-energy side [56]. It is obvious that the shape of the low-energy side of the BT-band does not depend on the temperature and excitation intensity. At the same time, the slope of the low-energy side of the BT-band depends on the amplitude of the spatial potential fluctuations enabling the determination of γ from the PL spectra.

The intensity on the high-energy side I_{HE} of the BT-band has several common properties for all types of the density of states function for localized holes. At low temperatures ($kT < \gamma$) the curvature of I_{HE} $(h\nu)$ does not depend on the temperature but at higher temperatures ($kT > \gamma$) its slope decreases linearly with the temperature and the BT-band becomes more symmetrical.

The easiest way to identify the BT-band is to find its maximum energy $h\nu_{max}$ and study its temperature and excitation intensity dependencies. The $h\nu_{max}$ for the BT-band at low temperatures may be expressed as [54]:

$$h\nu_{\max} = E_g - kT \ln(N_V/(p+\theta n)) \,, \tag{3.1.1.4}$$

where N_V is the effective density of states in the valence band, n and p are the concentrations of free electrons and holes, respectively, θ is the ratio of electron and hole capture probabilities by the localized state. Therefore, the BT-band can be taken as a result of a recombination of a free electron from a Fermi level F_n with a hole, captured by the localized state in the valence band tail with the depth $kT \ln(N_V/(p+\theta n))$. As can be seen from Eq. (3.1.1.4), the $h\nu_{max}$ shifts towards lower energies linearly with an increasing temperature and more rapidly than the bandgap. At higher temperatures $kT > kT_1 = \gamma \ln(N_V/(p+\theta n))^{-1/2}$, starting from a characteristic temperature T_1 where the BT transition has a maximum probability and after which the thermal activation process starts to dominate, the $h\nu_{max}$ shifts towards higher energies until above some characteristic temperature T_2 it will follow the temperature dependence of the energy gap. At temperatures where all localized holes are thermally released, the BB recombination dominates.

It can also be seen from Eq. (3.1.1.4) that the $h\nu_{max}$ shifts towards higher energies with higher energies with increasing n and p, i. e. with increasing

excitation intensity. Because of a blueshift with excitation intensity, the BT-band is often misinterpreted to be the DAP band to which this is also a characteristic feature. However, the magnitude of the blueshift is in the order of few meV per decade for the DAP recombination. In the case of compensated semiconductors it usually exceeds 10 meV per decade [25,26].

3.1.2. BI-band

BI recombination involves a free electron and a hole that is localized on a deep acceptor state that does not overlap with the valence band tail, i.e. ionization energy of the acceptor I_a has to be larger than the average fluctuation depth of the potential energy of the holes γ_h. The theoretical PL spectrum of the BI-band is defined by the following expression [54]:

$$I_{BI}(h\nu) = h\nu \iint W(E_e, E_h)\rho_c(E_e) f_e(E_e)\rho_a(E_h) q_a(E_h)\delta(E_e - E_h - h\nu) dE_e dE_h , \quad (3.1.2.1)$$

where ρ_a is the hole density of states, and q_a is the filling probability of the hole states. In heavily doped semiconductors, the acceptor level is broadened by the fluctuating potential field in the material creating a distribution of the acceptor states instead of a single acceptor level. According to [54], the hole density of states has its maximum at the acceptor´s activation energy and has a Gaussian shape:

$$\rho_v(E_h) = \rho_a(E_h) = (N_a / \sqrt{2\pi}\gamma) \exp\left[-(E_h - E_{V0} - I_a)^2 / 2\gamma^2\right]. \quad (3.1.2.2)$$

BI recombination involves two types of transitions: BI_1 and BI_2 (see Figure 6). BI_1 transition involves a free electron and a hole localized in the acceptor state with an energy above the percolation level E_V. There the impurity potential represents a hump for holes. BI_2 transition involves acceptor levels located in those regions where the valence band edge lies above the percolation level. BI_2 transition is a two-step process: a free hole is captured nonradiatively by a localized tail state and then captured by a neutral acceptor from which it will recombine with a free electron. The BI-band is the sum of the BI_1- and BI_2-band.

The temperature dependence of a BI-band is very similar to a BT-band, which is why it is sometimes difficult to separate these two recombination mechanisms. At low temperatures the BI_2 transition dominates, the peak position energy of a BI-band decreases with increasing temperature until it reaches a characteristic temperature T_1 where the transition probability is the highest. According to the theory in [54], at low temperatures the BI-band maximum is located at $h\nu_{\max} = E_g - I_a$. At higher temperatures $T > \gamma_h$, the $h\nu_{max}$ rises by an amount γ_h and the PL band broadens assuming the Gaussian shape. The shift of the BI-band is caused by the dominating thermal activation process. At higher temperatures when all localized holes are thermalized, the BI_2-band vanishes and recombination will go through the BI_1 channel. The changes in $h\nu_{max}$ are described approximately by the expression [57]:

$$h\nu_{\max}^{BI} = E_g - I_a + 0.5T + \frac{\gamma_h p}{p + p^*}, \qquad (3.1.2.3)$$

where $p^* = \left[\theta n + N_V \exp(-\frac{I_a}{T}) \right] \exp(\frac{\gamma_h}{T})$. It can be seen from Eq. (3.1.1.2.3) that $h\nu_{max}^{BI}$ depends weakly on the rate of excitation and changes only by an amount γ_h in a narrow range of temperatures and excitation rates.

For fitting the PL spectra of heavily doped semiconductors we use an empirical asymmetric double sigmoidal function:

$$I(h\nu) = A\left(1\Big/\left(1+\exp\left[-\frac{h\nu - E_1}{W_1}\right]\right)\right) \times \left(1 - 1\Big/\left(1+\exp\left[-\frac{h\nu - E_2}{W_2}\right]\right)\right). \qquad (3.1.2.4)$$

Here A, E_1, E_2, W_1 and W_2 are the fitting parameters. Parameters E_1 and W_1 represent the shape of the low-energy side of the PL bands while E_2 and W_2 belong to the high-energy side. This fitting function is purely empirical and was chosen from among several candidates because it always seemed to give the best result.

3.2. Raman modes of chalcopyrites

The chalcopyrite crystal $A^IB^{III}C_2^{VI}$, with the space group $I\bar{4}2d$, is the ternary analog of the cubic zincblende structure F43m. Its crystal structure has eight atoms per primitive cell that lead to 24 zone-center vibrational modes [58]: $1A_1 + 2A_2 + 3B_1 + 4B_2 + 7E$, where the E-modes are doubly degenerated. These modes are classified into 3 acoustic ($B_2 + E$) and 21 optical modes ($1A_1 + 2A_2 + 3B_1 + 3B_2 + 6E$). Except for two silent modes ($2A_2$), there are 22 Raman active modes:

$$1A_1 + 3B_1 + 3B_2(LO) + 3B_2(TO) + 6E(LO) + 6E(TO).$$

These modes can be classified, following the increasing frequency, into five groups related to the five high symmetry points in the $\Gamma \rightarrow X$ direction of the Brillouin zone of the zincblende structure [59]. They originate from TA, LA, LO, and TO branches, at the Γ_{15} point of the zincblende structure. The modes originating from the X_5, W_2 and W_4 points of the TA branch are: $E[X_{5l}] + B_1[W_{2l}]$, $B_2[W_{2l}] + E[W_{4l}]$; from the X_3 and W_3 points of the LA branch are: $B_1[X_3] + E[W_3]$; from the X_1 and W_1 points of the LO branch are: $A_2[X_1] + A_1[W_1] + A_2[W_1]$; from the X_5, W_2 and W_4 points of the TO branch are: $E[X_{5u}] + B_1[W_{2u}] + B_2[W_{2u}] + E[W_{4u}]$; and those from the Γ_{15} optical mode of the zincblende are: $B_2[\Gamma_{15}] + E[\Gamma_{15}]$. Here the space group notation (Γ_n, X_n, W_n) for the irreducible representations of the zincblende and the point group notation (A_n, B_n, E) at the Γ point of the chalcopyrite system are used.

The totally symmetric A_1 mode has purely ionic nature and originates from vibrations of anion atom while the rest of the atoms in the lattice are stationary.

This mode is the most intensive in the spectra of chalcopyrite compounds. The B_1 modes involve the motion of the cations and the B_2 and E modes correspond to the combined motion of all the atoms. Correct assignment of the lattice vibrations is of great importance for a fundamental understanding of the structural properties of chalcopyrites. However, this is not always an easy task because of the difficulties in growing high quality bulk crystals, the great variety of defects in the chalcopyrite materials and its dependence on a deviation from stoichiometry. The vibrational properties of the studied ODCs that have chalcopyrite-related crystal structure are discussed in Section 3.3.

Until now, no theoretical studies of the vibrational properties of the kesterites have been published. However, due to the similar crystal structure, one would expect the vibrational spectra of the kesterites and the corresponding chalcopyrites to be quite similar.

The vibrational spectra of solid solutions, such as $Cu_2ZnSn(Se_xS_{1-x})_4$ monograins studied in this thesis, add valuable information how the disorder in them influences the phonon frequencies at the center of the Brillouin zone in contrast to the constituent substances [60]. The solid solutions can be classified as unimodal or bimodal according to the type of behaviour of the optical modes [61]. Among the unimodal type are solid solutions, for which the optical mode frequencies vary with the composition in the range extending from frequencies typical of one of the constituent compounds to frequencies typical of another compound, while the mode intensity remains constant. In bimodal solid solutions, twice as many modes are observed for all intermediate compositions as for the constituent compounds, and the intensity of each mode is proportional to the mole fraction of the basic components. The results of the Raman analysis of $Cu_2ZnSn(Se_xS_{1-x})_4$ monograins are presented in Section 3.6.

3.3. Raman spectra of Ga-rich Cu-Ga-Se thin films

The compositional dependence of the room temperature Raman spectra of MOCVD grown Cu-Ga-Se films is shown in Figure 7. The appearance of $CuGa_3Se_5$ and $CuGa_5Se_8$ phases in the spectra of Cu-Ga-Se films is visible with decreasing [Cu]/[Ga] ratio. The dominating A_1 Raman peaks were detected at 185 cm^{-1}, 166 cm^{-1} and 159 cm^{-1} for $CuGaSe_2$, $CuGa_3Se_5$ and $CuGa_5Se_8$, respectively. The presence of binary phases in the films was not detected from the spectra.

According to the simplified version of Keating`s model [62], the frequency of the A_1 mode v is given by $v \approx \sqrt{k/M_{Se}}$, where M_{Se} is the mass of the Se atom and k being the force constant related to the cations-anion bond-stretching forces. Due to the presence of the vacancy in the ODC the stretching forces are relaxed, thus reducing slightly the corresponding vibrational frequencies compared to chalcopyrites with 1:1:2 stoichiometry. Since in the first approximation the vibrational frequencies in chalcopyrites depend mainly on the nearest neighbour

atoms interaction [62] and taking also into account that one vacancy exists for each four and five Se atoms in $CuGa_5Se_8$ and $CuGa_3Se_5$, respectively, it was proposed in [22] that for the A_1 mode k is reduced by 25% and 20% for $CuGa_5Se_8$ and $CuGa_3Se_5$, respectively, as compared to its value in the normal chalcopyrites. Under this assumption, frequencies $v' \approx \sqrt{0.75k/M_{Se}} \approx 0.87v$ and $v' \approx \sqrt{0.8k/M_{Se}} \approx 0.89v$ of this mode, where v is the frequency in the normal chalcopyrites, are to be expected for $CuGa_5Se_8$ and $CuGa_3Se_5$, respectively. The frequency of the A_1 mode for $CuGaSe_2$ at room temperature is 184 cm^{-1} [63], giving us the frequencies of 164 cm^{-1} and 161 cm^{-1} for the A_1 mode in $CuGa_3Se_5$ and $CuGa_5Se_8$, respectively. The recorded A_1 mode frequencies were 185 cm^{-1}, 166 cm^{-1} and 159 cm^{-1} for $CuGaSe_2$, $CuGa_3Se_5$ and $CuGa_5Se_8$, respectively. The obtained wavenumbers are in very good agreement with the theoretically expected values.

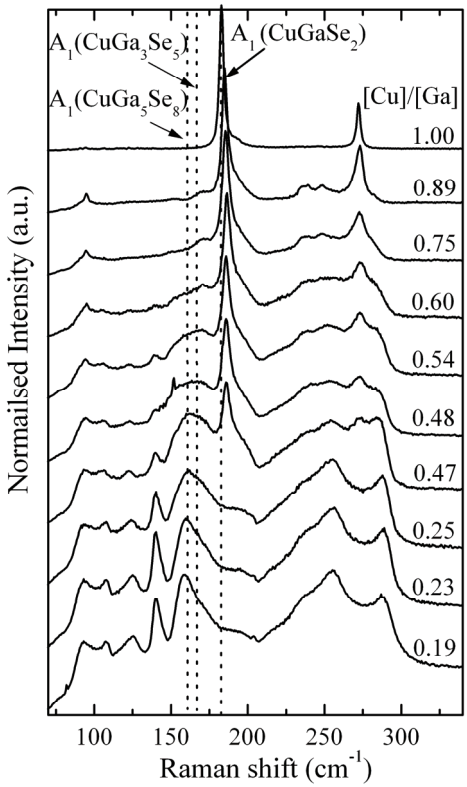

Figure 7. Room-temperature Raman spectra of Cu-Ga-Se films with different [Cu]/[Ga] ratios. The Raman peaks at 185 cm^{-1}, 166 cm^{-1} and 159 cm^{-1} correspond to the A_1 mode of $CuGaSe_2$, $CuGa_3Se_5$ and $CuGa_5Se_8$, respectively.

The A_1 mode frequency of $GuGaSe_2$ shows a nonlinear shift to higher wavenumbers with the decrease of Cu content up to [Cu]/[Ga] = 0.47 (see Figure 8 a). Apart from the frequency, also the full width at half maximum (FWHM) of the A_1 Raman band of $CuGaSe_2$ (see Figure 8 b) and all the other modes are broadening with the increase of the Ga content. Similar behaviour has been observed in $CuIn_{1-x}Ga_xSe_2$ [64], $Cu(In_{1-x}Ga_x)_5Se_8$ [29] and $Cu(In_{1-x}Ga_x)_3Se_5$ [65] films. Differences in the degree of disorder and increasing defect concentration are believed to be responsible for the observed changes in the Raman mode width as a function of the [Cu]/[Ga] ratio. Therefore, the broadening of the Raman bands is an indication of a large defect density in the ODC`s.

Since only one paper in the literature about the Raman results of $CuGa_5Se_8$ refers to no detailed identification of the Raman modes, we studied the Raman spectra of $CuGa_5Se_8$ in more detail. The results are presented in the next Section 3.3.1.

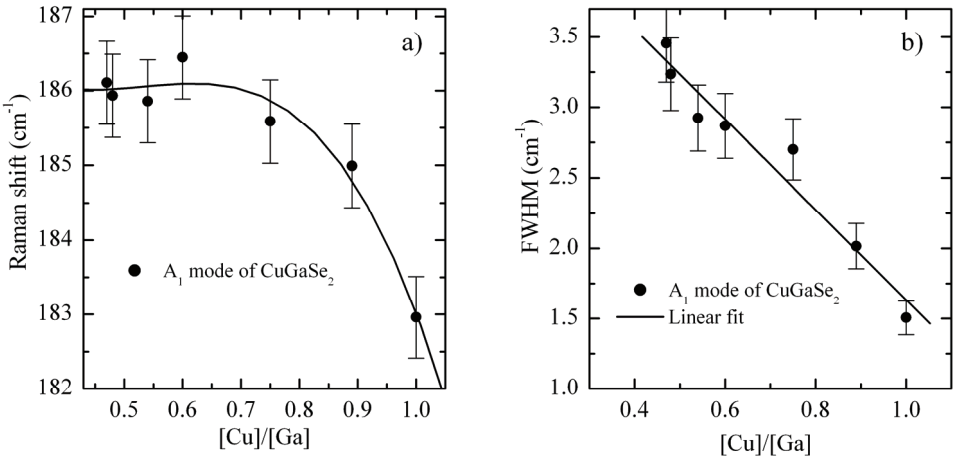

Figure 8. Compositional dependence of the peak position of the A_1 Raman mode of $CuGaSe_2$ (a) and its FWHM (b).

3.3.1. Raman spectra of $CuGa_5Se_8$

The Raman spectrum of the MOCVD grown $CuGa_5Se_8$ film with the fitting result is shown in Figure 9. The Bridgman grown $CuGa_5Se_8$ single crystal showed a very similar spectrum. Because of the slightly asymmetric shape of Raman peaks, each peak was fitted using the Pearson VII function [66]. 12 peaks were detected from these spectra. For comparison, Raman peak positions and possible mode assignments, as discussed in the following, are listed in Table 2. It is seen from the

table that the A_1 peak at 161 cm^{-1} of a $CuGa_5Se_8$ single crystal is shifted to higher wavenumbers by 3 cm^{-1} compared to the A_1 peak position at 158 cm^{-1} of a $CuGa_5Se_8$ polycrystalline thin film. Negative and positive shifts attributed to the stress in the polycrystalline films can also be observed for other Raman modes.

The B_1 modes involve the motion of the cations. Since the presence of ordered vacancies on Se sites is not expected to occur in these materials, the frequencies of these modes in the ODC are expected to be very similar to those observed in $CuGaSe_2$ [22]. Thus, the mode at 117 cm^{-1} and 124 cm^{-1} in the $CuGa_5Se_8$ single crystal and polycrystalline thin film, respectively, probably corresponds to the second-lowest frequency B_1 mode reported at 116 cm^{-1} in $CuGaSe_2$ at 300 K [63]. The lowest frequency B_1 mode whose corresponding values in $CuGaSe_2$ and $CuGa_3Se_5$ are 76 cm^{-1} and 72 cm^{-1} [23], respectively, is not observed in our spectrum due to the limitations of our experimental system. The highest frequency B_1 mode, which should be very weak because it corresponds to the motion of the cations in antiphase, is expected to be observed close to the A_1 peak. This mode has not yet been reported in $CuGa_3Se_5$ or $CuGa_5Se_8$ even at low temperatures.

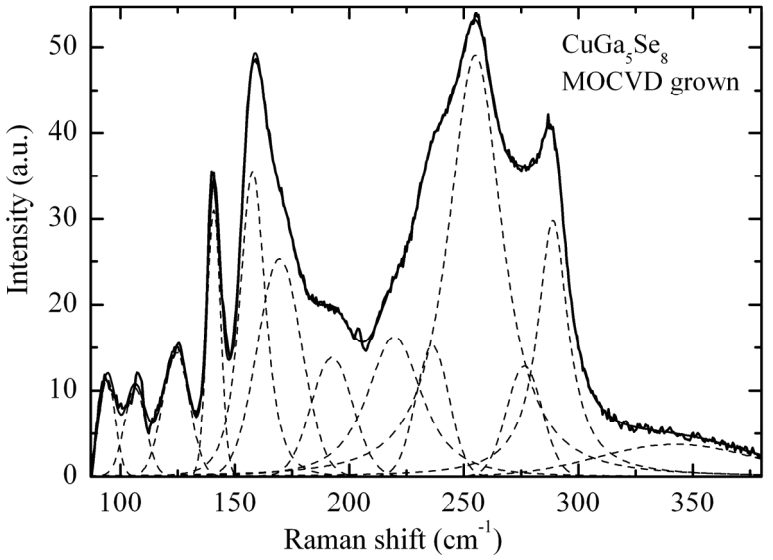

Figure 9. The room-temperature Raman spectra of the MOCVD grown $CuGa_5Se_8$ polycrystalline film and the result of fitting. The peak at 93 cm^{-1} is due to the cut-off of the filter and is not taken into account.

The remaining modes should be assigned as B_2 and E modes that mostly correspond to the combined motion of all the atoms. Hence, by similar considerations given for the A_1 mode, it is expected that its frequencies are slightly lower than those observed in $CuGaSe_2$ [22]. Thus the peaks at around 255, 236,

220 and 192 cm^{-1} in the polycrystalline $CuGa_5Se_8$ and at 253, 235, 216, 186 cm^{-1} in a $CuGa_5Se_8$ single crystal, can be related to 273, 261, 239 and 199 cm^{-1} in $CuGaSe_2$, respectively. The calculated ratio of each pair of the corresponding frequencies in $CuGa_5Se_8$ and $CuGaSe_2$ ν'/ν varies from 0.90 to 0.94, which was also found for $CuGa_3Se_5$ Raman peaks in [22]. The peak at 141 cm^{-1} probably corresponds to the E mode reported at 142 cm^{-1} in $CuGa_3Se_5$ [23]. The peak around 289 cm^{-1} in $CuGa_5Se_8$ probably corresponds to a combination of the lowest-energy B_2 mode, which is expected to occur at around 53 cm^{-1}, and the E mode at 236 cm^{-1}. Similarly, the peak around 170 cm^{-1} in $CuGa_5Se_8$ probably corresponds to a combination of B and the E modes. Such combinations have also been observed in $CuGaSe_2$ and $CuGa_3Se_5$ [22,23].

Table 2. Raman peak positions obtained from the fitting and possible mode assignments

Raman peak position (cm^{-1})					
MOCVD grown $CuGa_5Se_8$	**Bridgman grown $CuGa_5Se_8$**	**$CuGaSe_2$ Ref. [63]**	**$CuGa_3Se_5$ Ref. [23]**	**$CuGa_5Se_8$ Ref. [29]**	**Possible origin**
343	344	-	-	-	$B_2 + E$
289	293	-	286	289	$B_2 + E$
277	280	-	274	-	B_2
255	253	273	252	259	E
236	235	261	-	-	B_2 *or* E
220	216	239	220	-	E
-	-	-	200	-	E
192	186	199	187	-	B_2
170	168	-	-	-	$B_2 + E$
158	161	184	166	160	$\boldsymbol{A_1}$
141	142	-	142	-	E
124	117	116	-	-	B_1
106	99	96	105	107	E
-	-	-	90	93	B_1
-	-	-	72	78	B_1
-	-	60	64	-	B_2
-	-	-	48	-	E

3.4. Photoluminescence spectra of $CuGa_3Se_5$ crystals

The $CuGa_3Se_5$ crystals were grown by the SPC method and the vertical Bridgman method. The X-ray analysis demonstrated the single phase of the tetragonal chalcopyrite-related structure of $CuGa_3Se_5$. The Rietveld evaluation produced unit-cell parameters a = 0.54874 nm and c = 1.10049 nm for $CuGa_3Se_5$

crystal grown by the SPC method and a = 0.54803 nm, and c = 1.09734 nm for the crystal grown by the vertical Bridgman method. These values are close to data a = 0.544995(8) nm, and c = 1.0946(3) nm reported in [22]. However, the chemical composition determined by the EDS analysis in several points of crystals showed the presence of compositional fluctuations that were larger for the $CuGa_3Se_5$ samples grown by the SPC method, see Figure 10.

In the PL spectra of the $CuGa_3Se_5$ crystals, we found a broad (FWHM ~ 200 meV) asymmetric PL band at 1.76 eV. It has an exponential slope on the low-energy side and a steeper Gaussian incline on the high-energy side. This type of asymmetric PL bands is common for heavily doped compensated semiconductors where spatial potential fluctuations are present.

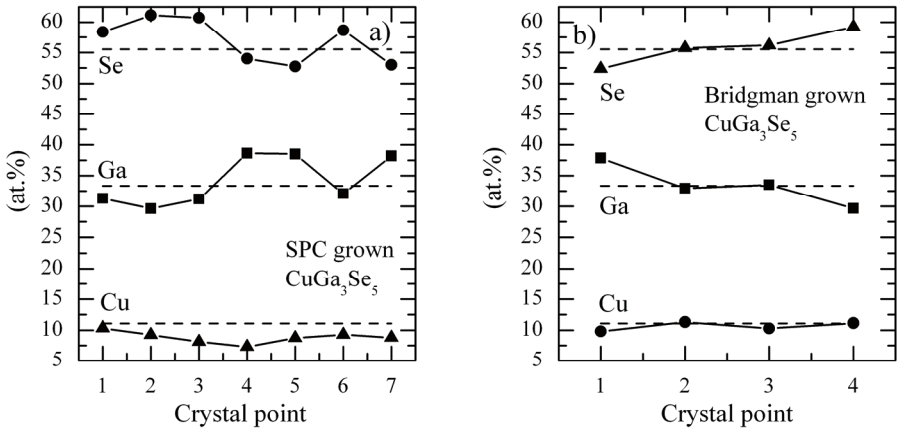

Figure 10. Chemical composition measured in several points of $CuGa_3Se_5$ crystals grown by the SPC method (a) and by the vertical Bridgman method (b). The dashed line represents the chemical composition of $CuGa_3Se_5$ (Cu:Ga:Se = 11.11:33.33:55.55 at.%).

Figure 11 shows normalized spectra of the asymmetric PL band for SPC grown $CuGa_3Se_5$, measured from different points of the crystal. The maximum energy difference of the corresponding peak positions is ~ 60 meV. This difference may be taken as the approximate value of the bandgap energy fluctuations. The average amplitude of band edge fluctuations γ^* in the presence of potential and compositional fluctuations is the mean difference of the energy of holes in the valence band fluctuation minimum and maximum, see Figure 12.

The slope of the low-energy side of the PL band is determined by the density of states in the valence band and therefore depends on the amplitude of both fluctuations. Thus, the value of the mean amplitude of the band edge fluctuations γ^* can be derived from the slope of the low-energy side of the PL band. The average value of γ^* was about 70 meV, and 90 meV for Bridgman, and SPC grown $CuGa_3Se_5$, respectively. The compositional fluctuations also affect the half-

width of the PL-band. The values of γ^* and the FWHM of the BT-band for several chalcopyrite compounds are shown in Table 3. These rather high values of γ^* and FWHM support the idea of the coexistence of potential and compositional fluctuations in these samples.

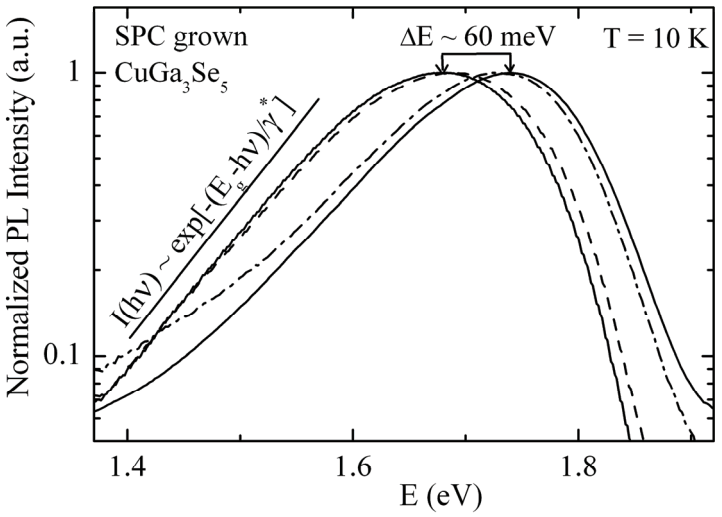

Figure 11. Normalized spectra of the 1.76 eV PL band for SPC grown $CuGa_3Se_5$, measured from different spots of the crystal. The energy difference of the peak positions is ~ 60 meV. The exponential slope of the low-energy side of the BT-band gives the average depth of the band edge fluctuations γ^*.

Excitation power and temperature dependent PL measurements indicate that our spectra are dominated by the BT-type recombination. Due to their small effective mass $m_e^* \approx 0.08 m_e$, almost all electrons are free. The activation energy of the thermal quenching of the BT-band allows us to evaluate the average depth of the acceptor states. From Arrhenius plot of thermal quenching of the PL bands, we obtained thermal activation energies 38 ± 12 meV, and 53 ± 17 meV for Bridgman, and SPC crystals, respectively. The *lnI(T)* versus *1000/T* dependence was fitted with the theoretical expression for discrete energy levels proposed in [68]:

$$\Phi(T) = \frac{\Phi_0}{1 + \alpha_1 T^{3/2} + \alpha_2 T^{3/2} \exp(-E_T / kT)}, \qquad (3.4.1)$$

where Φ is integrated intensity, α_1 and α_2 are the process rate parameters and E_T is the thermal activation energy. It is clear that in the case of BT type recombination, the fitting is not completely valid due to continuous tail states. However, the average activation energy of acceptor states can be estimated to be 45 meV, which is smaller than the average depth of the fluctuations.

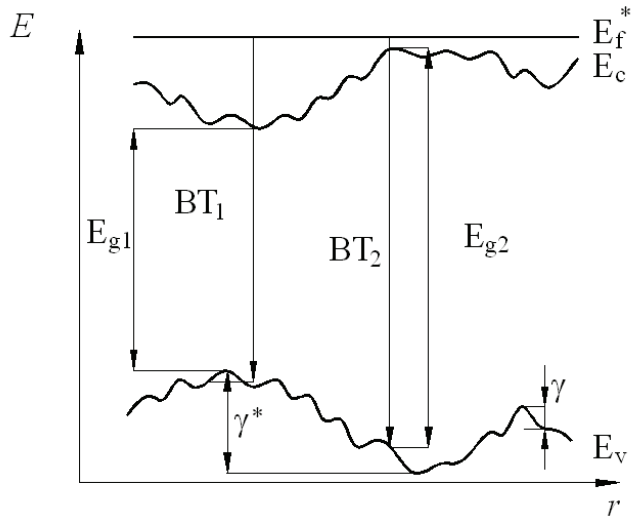

Figure 12. BT recombination model in $CuGa_3Se_5$ in the presence of potential- and compositional fluctuations. BT_1 and BT_2 emissions originate from different parts of the crystal with different bandgap energy (E_{g1} vs E_{g2}).

Table 3. Values of the average amplitude of the band edge fluctuations γ^* calculated from the low-energy slope of the PL band, and FWHM of the BT-band for several chalcopyrite compounds

Compound	γ^*(meV)	FWHM (meV)	References
$CuGaSe_2$	17.6	50	[26]
$CuIn_{0.5}Ga_{0.5}Se_2$	17.0	49	[25]
$AgGaTe_2$	4.5	16	[67]
$CuInSe_2$	24.1	51	Our data
$CuGa_3Se_5$ (Bridgman)	58.1 - 72.8	170 - 178	[I]
$CuGa_3Se_5$ (SPC)	71.4 - 94.5	188 - 220	[I]

In Figure 13, the temperature dependence of the peak position of the 1.76 eV PL band is shown along with the bandgap energy E_g of $CuGa_3Se_5$ [16]. The observed shift of the peak position energy exceeds the temperature dependence of the bandgap energy. This feature is predicted by the theory of heavily doped semiconductors. According to the theory, when the holes localized in the valence band tail are freed at higher temperatures, BB-transition that involves a free electron and a free hole dominates the spectra. However, the BB-band may not appear in the presence of large compositional fluctuations, because higher thermal energy is needed to liberate holes. In our case, the thermal energy is enough to

redistribute the holes between the potential wells and therefore the BB-band was not detected.

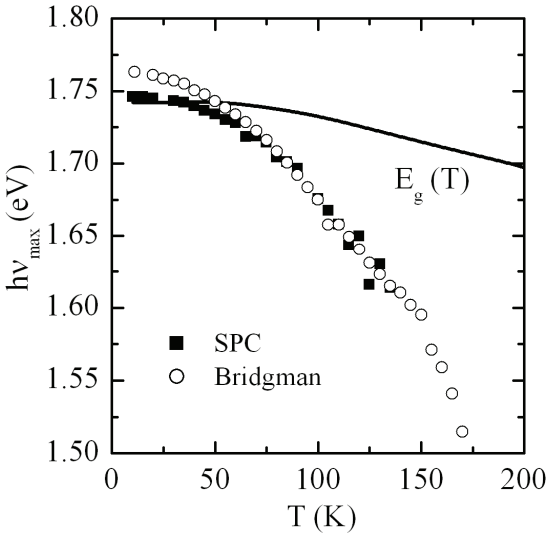

Figure 13. Temperature dependence of the peak position of the 1.76 eV PL band and the bandgap energy E_g [16] of $CuGa_3Se_5$.

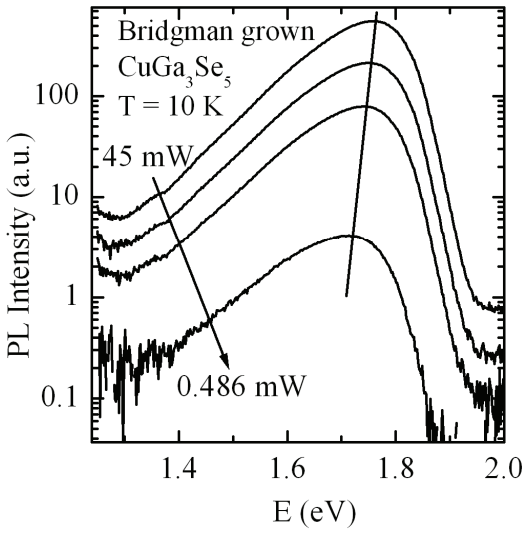

Figure 14. The laser power dependence of the PL spectrum of the $CuGa_3Se_5$ crystal grown by the Bridgman method.

The excitation power dependence of the PL peak at 1.76 eV is shown in Figure 14. The blueshift of the BT-band with the magnitude of about 19 meV per decade was detected. This confirms that the observed emission results from the BT recombination together with the bandgap fluctuations.

3.5. Photoluminescence spectra of $CuGa_5Se_8$ crystals and thin films

Only one broad asymmetric band at 1.788 eV and 1.765 eV was observed at 10 K in the PL spectra of Bridgman grown $CuGa_5Se_8$ single crystal and MOCVD grown polycrystalline film, respectively (see Figure 15). PL band positions are at much lower energies than the bandgap energy of $CuGa_5Se_8$ (E_g = 1.811 eV at 300 K and $E_g(0) \approx$ 1.917 eV [69]). Detailed analysis of the PL data suggests that the emission is due to BT- or BI- recombination because both emissions show a very similar behaviour.

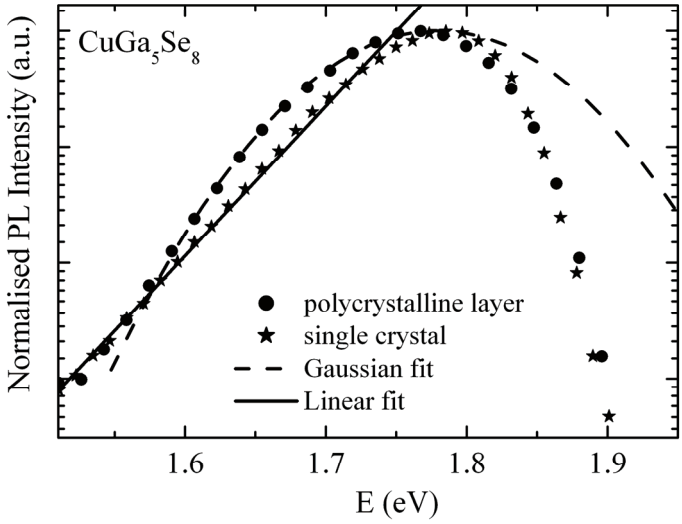

Figure 15. Normalized PL spectra of polycrystalline and single crystal $CuGa_5Se_8$ at 10 K. The lines represent the fittings of the low-energy side of the PL bands.

According to the theory of heavily doped semiconductors, the low-energy tail of PL emissions can be described by a Gaussian or an exponential spectral dependence. The low-energy side of the PL band of the $CuGa_5Se_8$ samples showed a Gaussian shape and an exponential decay for the polycrystalline film and single crystal, respectively. It is an indication of the presence of deeper fluctuations with the Gaussian shape density of states function in the polycrystalline film while the density of states function in the band tails of a single crystal has an exponential distribution. Deeper potential fluctuations in the $CuGa_5Se_8$ polycrystalline film also

explain the shift of the PL band position towards lower energies compared to the single crystal. The average amplitudes of the fluctuations $\gamma = 62 \pm 4$ meV and $\gamma = 113 \pm 7$ meV for the $CuGa_5Se_8$ single crystal and polycrystalline film, respectively, were determined from the exponential and Gaussian spectral dependencies, respectively [54]:

$$I(E) \sim \exp\left(-\frac{E}{\gamma}\right) \text{ or } I(E) \sim \exp\left(-\frac{(E-E_0)^2}{2\gamma^2}\right) \qquad (3.5.1)$$

where E_0 is assumed to represent an average emission energy in the case of fluctuating potentials. Similar results were obtained by Siebentritt *et al.* [70] for Cu-poor $CuGaSe_2$ thin films.

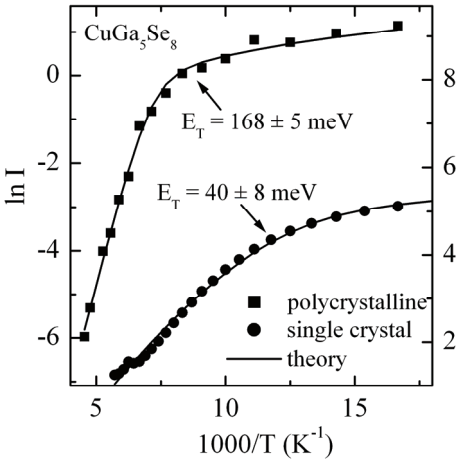

Figure 16. Arrhenius graph of the $CuGa_5Se_8$ single crystal and polycrystalline layer obtained from the temperature dependence of the PL spectra. Solid lines represent the fitting of the experimental data with the theoretical expression (3.4.1).

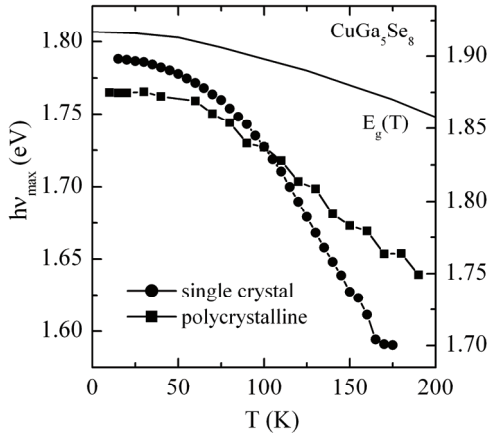

Figure 17. Temperature dependence of the PL band peak position. Solid line represents the temperature dependence of the bandgap energy E_g of $CuGa_5Se_8$ [69].

From the Arrhenius plot of thermal quenching of the PL band (Figure 16), we obtained an estimation of the thermal activation energy of the acceptor states 40 ± 8 meV and 168 ± 5 meV for a single crystal and polycrystalline $CuGa_5Se_8$, respectively. It can be seen from the Arrhenius plot (Figure 16) that the PL band of the polycrystalline film shows linear dependence of *lnI vs. 1000/T* at high temperatures, that is common for BI –recombination. Also, the activation energy of the acceptor states is larger than the average depth of the fluctuations, indicating that the recombination in the polycrystalline film is related to a deeper acceptor level. The Gaussian shape of the low-energy tail of PL emission supports this idea.

The PL band of the single crystal shows non-linear dependence of *lnI vs. 1000/T* at high temperatures, which is common for the BT-recombination. Also, the exponential decay of the low-energy side of the PL band and the thermal activation energy of the acceptor states being smaller than the average depth of the fluctuations support the idea of the BT-recombination in $CuGa_5Se_8$ single crystals.

Figure 17 shows the temperature dependence of the PL band peak position along with the bandgap energy E_g of $CuGa_5Se_8$ [69]. The peak position energy decreasing rate exceeds the bandgap energy decreasing rate with the temperature. This feature is predicted by the theory of heavily doped semiconductors [54] and was also observed in $CuGa_3Se_5$.

From the excitation power dependence, the blue shift of the PL band with the magnitude of about 15 meV and 23 meV per decade for $CuGa_5Se_8$ single crystal and polycrystalline layer, respectively, was detected. This again confirms that the observed emission results from the BT- or BI-recombination. The observed shift is larger for the sample with deeper potential fluctuations, as predicted by the theory.

3.6. Raman spectra of the $Cu_2ZnSn(Se_xS_{1-x})_4$ solid solutions

In this section, the Raman spectra of $Cu_2ZnSn(Se_xS_{1-x})_4$ monograins are presented. The dependence of the Raman spectra on the composition of the $Cu_2ZnSn(Se_xS_{1-x})_4$ solid solutions with x values of 1, 0.75, 0.55, 0.26 and 0 are presented in Figure 18. The A_1 Raman mode frequencies of CZTSe and CZTS (indicated by arrows in Figure 18) are 196 cm^{-1} and 338.5 cm^{-1}, respectively. A linear shift of the A_1 Raman modes of CZTS and CZTSe towards higher wavenumbers with increasing sulphur concentration in $Cu_2ZnSn(Se_xS_{1-x})_4$ is demonstrated in Figure 19. This linearity is expected to be useful in determining alloy composition. The other Raman peaks of CZTSe were detected at 167, 172, 230, 233, 243 cm^{-1} and the Raman peaks of CZTS at 167, 252, 288, 347, 366 cm^{-1} (labeled with numbers in Figure 18). The lattice vibrational properties of these solid solutions have not been discussed so far.

All Raman spectra of the studied $Cu_2ZnSn(Se_xS_{1-x})_4$ solid solutions show peaks of some secondary (mostly binary) phases (positions of the peaks are indicated by dotted lines in Figure 18). However, the Raman peaks corresponding to additional phases have very low intensities in comparison with the CZTSe or CZTS peak intensities. All Raman spectra were fitted using Lorentzian functions to resolve the peaks. In the Raman spectrum of CZTSe the presence of ZnSe (peak at 249 cm^{-1}) was detected and also a $SnSe_2$ phase might be present (peak at 191 cm^{-1}). The corresponding Raman frequencies of ZnSe and $SnSe_2$ reported in the literature are 252 cm^{-1} [71] and 186 cm^{-1} [72], respectively. In $Cu_2ZnSn(Se_{0.75}S_{0.25})_4$ the presence of ZnS (peak at 353 cm^{-1}) and SnS (peaks at 196 cm^{-1} and 217 cm^{-1}) was detected. According to the literature data, the corresponding Raman frequencies of ZnS and SnS are 353 cm^{-1} [73] and 192 cm^{-1}, 218 cm^{-1} [74], respectively. In the

spectrum of $Cu_2ZnSn(Se_{0.55}S_{0.45})_4$ the presence of ZnS was detected (peak at 351 cm^{-1}) and in the spectrum of $Cu_2ZnSn(Se_{0.26}S_{0.74})_4$ peaks of ZnSe (peaks at 205 cm^{-1} and 251.5 cm^{-1}) and ZnS (peak at 351 cm^{-1}) were observed. In the spectrum of CZTS, a ZnS peak at 355 cm^{-1} was observed. Small deviations of the peak positions of the secondary phases in the solid solutions can also result from the formation of solid solutions of binary compounds.

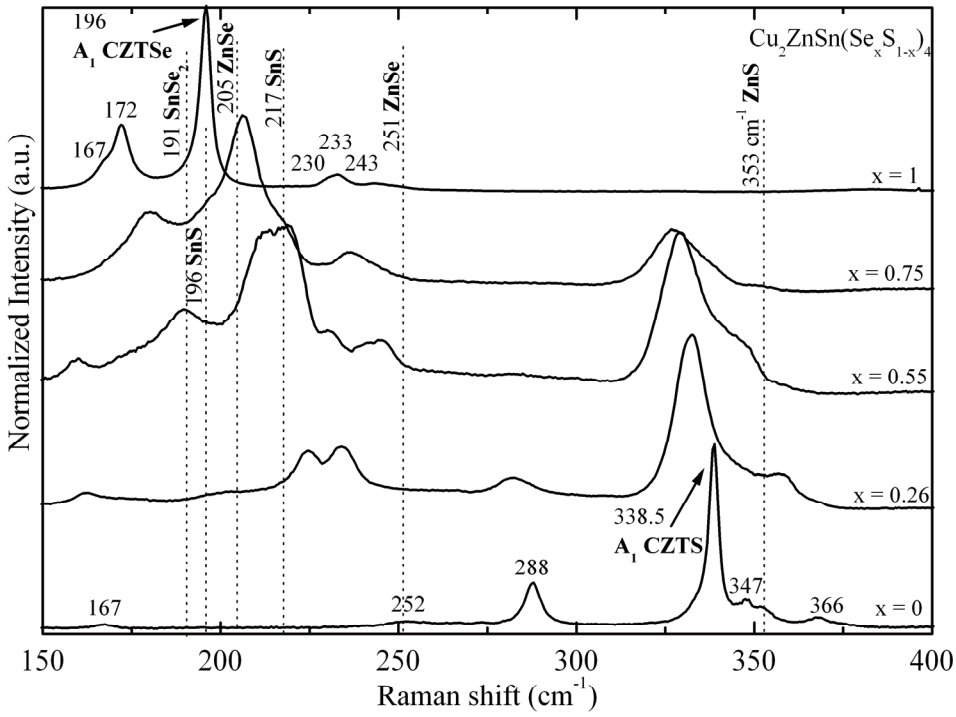

Figure 18. Room-temperature Raman spectra of $Cu_2ZnSn(Se_xS_{1-x})_4$ solid solutions with different Se/S concentration ratios.

The Raman peaks of $Cu_2ZnSn(Se_xS_{1-x})_4$ solid solutions broaden with the increasing sulphur content, giving the largest widths of the peaks for $Cu_2ZnSn(Se_{0.55}S_{0.45})_4$. This trend is correlated with the increasing structural disorder due to the random distribution of S and Se atoms in the lattice that leads to fluctuations in the masses and force constants in the neighborhood.

Both of the A_1 Raman modes of CZTSe and CZTS followed the two-mode behaviour throughout the entire alloy concentration range. Figure 19 presents the shift of the two A_1 modes with S concentration. As can be seen, the shift is larger for CZTSe. The force constants are responsible for the trends in the frequencies of the A_1 modes.

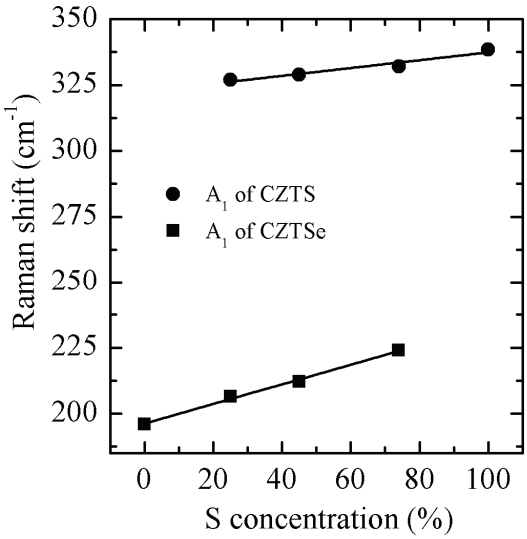

Figure 19. CZTS and CZTSe A_1 Raman mode frequency dependencies on the sulphur concentration in $Cu_2ZnSn(Se_xS_{1-x})_4$ solid solutions.

3.7. Photoluminescence spectra of the $Cu_2ZnSn(Se_xS_{1-x})_4$ solid solutions

Normalized PL spectra of the $Cu_2ZnSn(Se_xS_{1-x})_4$ solid solutions with different Se/S concentration ratios measured at T = 10 K are presented in Figure 20. Each spectrum (except for the one corresponding to Cu_2ZnSnS_4 that is fitted with two asymmetric PL bands) consists of one asymmetric PL band. The PL bands shift towards higher energies (see Figure 21) and become more asymmetric with the increasing sulphur concentration. The shift of the PL emission towards higher energies is in compliance with the EQE results that show bandgap widening with sulphur concentration [75]. Broadening of the PL bands with increasing sulphur concentration is also observed. The PL spectra are analyzed according to the theory of heavily doped semiconductors [54].

Excitation power dependent and temperature dependent PL measurements of the solid solutions indicate that the PL spectra of $Cu_2ZnSn(Se_xS_{1-x})_4$ are dominated by a BT- or BI- type recombination. In the excitation power dependencies a large blue-shift with a magnitude of about 15 meV per decade was detected. In addition, a linear dependence of the *lnI(T)* versus *1000/T* at higher temperatures was detected for all samples, except for the $Cu_2ZnSn(Se_{0.75}S_{0.25})_4$ that shows non-linear *lnI(T)* versus *1000/T* dependence at higher temperatures. The latter sample also gave smaller thermal activation energy of the acceptor states compared to the other samples. In the case of one of the end members

(Cu_2ZnSnS_4), the origin of the lower energy PL band is not clear since no detailed analysis of this PL band could have been performed due to its low intensity.

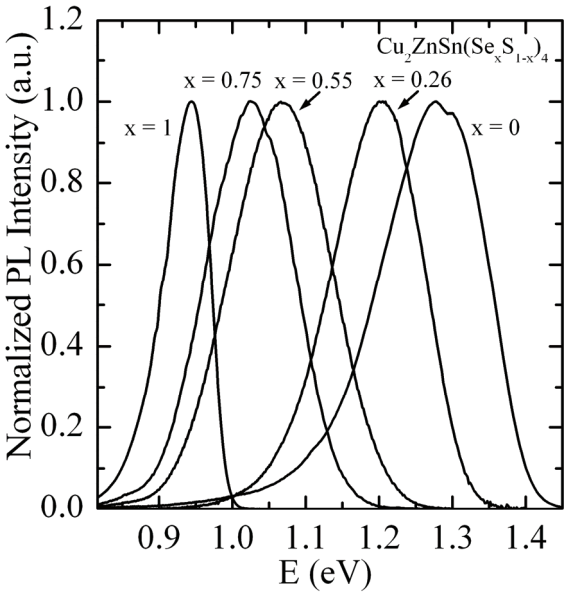

Figure 20. Normalized low-temperature PL spectra of the $Cu_2ZnSn(Se_xS_{1-x})_4$ solid solutions with different Se/S concentration ratios.

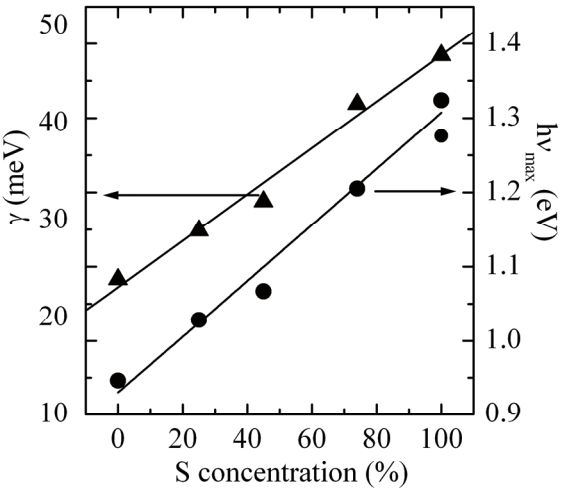

Figure 21. Approximately linear dependence of the PL band position and the average depth of spatial potential fluctuations γ on the sulphur concentration in $Cu_2ZnSn(Se_xS_{1-x})_4$ solid solutions.

The low-energy side of the PL band of the end members of the $Cu_2ZnSn(Se_xS_{1-x})_4$ solid solutions exhibit an exponential decay while the other members can be described by the Gaussian shape. This is an indication of the presence of deeper fluctuations within the samples containing both sulphur and selenium. The average amplitude of the potential fluctuations (see Figure 21) in the solid solutions were determined from the exponential and Gaussian spectral dependencies (3.5.1). As can be seen from Figure 21, γ increases with sulphur concentration in the solid solutions, being highest for CZTS. Analyzing the corresponding Raman spectra one would expect that γ is smaller in CZTS and CZTSe than in the solid solutions because of the lower defect concentration. It has been found by Raulot *et al.* [43] that all selenium and sulphur compounds have a Cu vacancy formation energy close to the $CuInSe_2$, $CuGaSe_2$ and $CuInS_2$, $CuGaS_2$ values, respectively. The sulphur compounds have a V_{Cu} formation energy about 0.5 eV larger than the selenides [43]. Therefore, one would expect a lower concentration of copper vacancies in CZTS compared with CZTSe, resulting also in a smaller γ. One possible explanation of the obtained opposite result (Figure 21) is the complexity of the phase diagrams of CZTSe and CZTS. The domain of a homogeneous material in the case of CZTS seems to be very narrow compared to CZTSe, resulting therefore in a more probable formation of other phases during the growth of the powder [76,77]. Despite the fact that γ is expected to increase due to the increasing defect concentration, we propose that in this case larger potential fluctuations are related to the presence of a defect phase or defect region that has a larger defect concentration and therefore also a higher γ value. At the same time these high γ values can be the result of compositional fluctuations where some crystal regions have different bandgap energy than others. The same behaviour was observed in $CuGa_3Se_5$ crystals [I]. The different bandgap energy can be caused by the different crystal structure in the case of solid solutions. It was shown, for example, that the band gap energy of kesterite-CZTS is about 0.12 eV larger than that of stannite-CZTS [37] and both structures are possible in solid solutions. The relative concentration of the defect phase increases with the sulphur concentration due to the weaker tolerance to deviations from stoichiometry in the case of CZTS. Due to the similarity of the PL properties of CZTS and the proposed defect phase one would assume that this phase has very similar properties to CZTS. Here we can see an analogy to the properties of ternary chalcopyrites where the formation of the so-called ordered defect compounds has been detected [2]. However, this assumption needs further investigation.

3.7.1. Photoluminescence spectra of $Cu_2ZnSnSe_4$ monograins

The room-temperature Raman spectra of two as-grown CZTSe monograin powders and an annealed monograin powder are presented in Figure 22. In the spectra of as-grown CZTSe (Raman modes at 167 cm^{-1}, 173 cm^{-1}, 196 cm^{-1}, 231 cm^{-1}, 245 cm^{-1}), the presence of an additional Cu_2SnSe_3 phase was detected

(Raman peak at 180 cm^{-1}). The frequencies of the A_1 Raman modes of Cu_2SnSe_3 and CZTSe are 180 cm^{-1} and 196 cm^{-1}, respectively [50]. After vacuum annealing the presence of the Cu_2SnSe_3 phase (peak at 180 cm^{-1}) could no longer be detected. Figure 23 presents the SEM micrograph of the as-grown CZTSe monograin surface. The presence of the secondary phase on the surface is clearly seen.

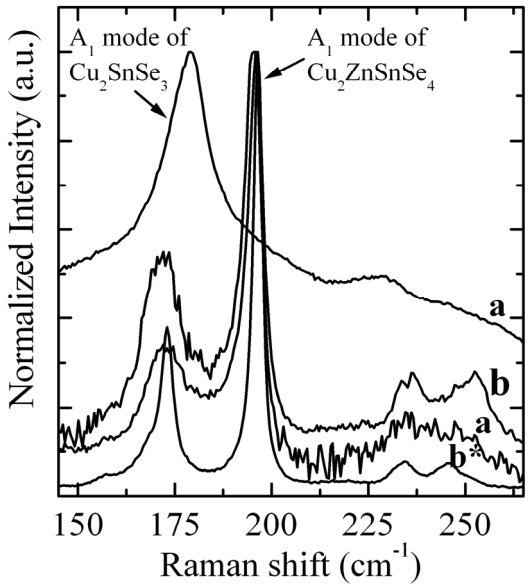

Figure 22. Normalized Raman spectra of the CZTSe monograins: a,b – as-grown CZTSe and b* – CZTSe after annealing. Two spectra taken from different points of the crystal surface of sample a are presented. As can be seen, the presence of the ternary Cu_2SnSe_3 phase was detected on the surface of as-grown CZTSe monograins (Raman mode at 180 cm^{-1}). This phase disappears after vacuum annealing.

The low-temperature (T = 10 K) photoluminescence spectra of the as-grown and annealed CZTSe monograins together with the spectra of Cu_2SnSe_3 crystals are presented in Figure 24 and the corresponding data are summarized in Table 4. The PL spectrum of one of the as-grown CZTSe monograins (a in Figure 24) consists of three Gaussian shaped PL bands at 0.765 eV, 0.86 eV and 0.95 eV. The other as-grown CZTSe spectrum (b in Figure 24) consists of one PL band at 0.81 eV and in the spectra of annealed CZTSe (b* in Figure 24) one asymmetric PL band at 0.946 eV was detected. Temperature and excitation power dependencies were used to identify the origin of the PL emisson of CZTSe monograins.

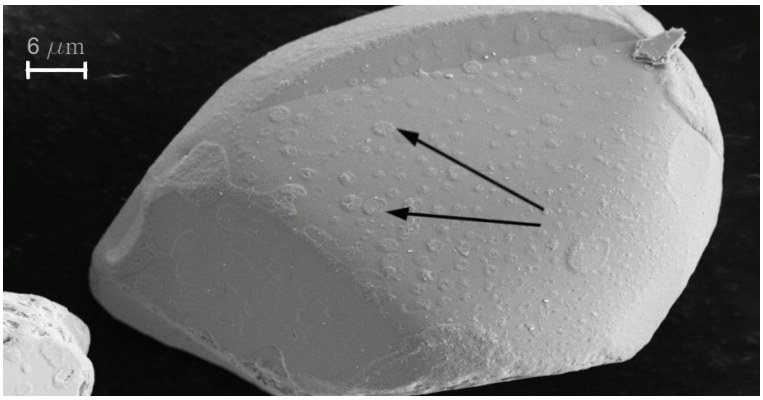

Figure 23. SEM micrograph of a CZTSe monograin. The presence of the Cu_2SnSe_3 phase forming small islands on the crystal surface (two of them are indicated by arrows) is clearly seen.

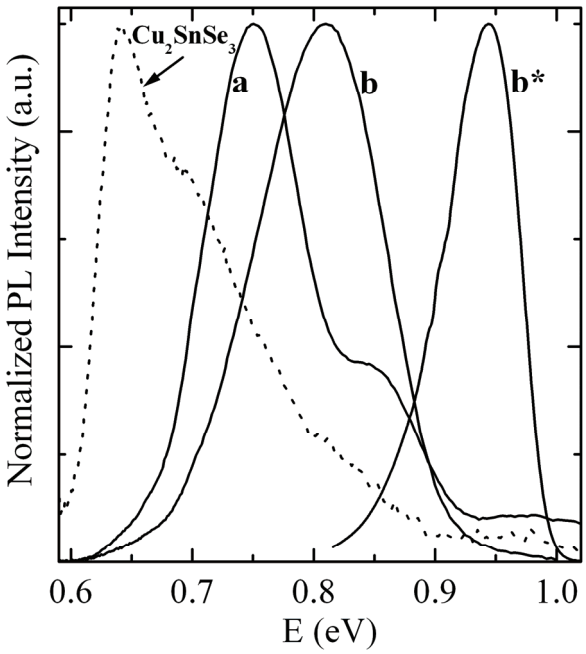

Figure 24. Comparison of the normalized low-temperature PL spectra of as-grown CZTSe (a,b) and annealed CZTSe (b*) monograins. The as-grown CZTSe monograin spectra (a) consists of three PL bands at 0.765 eV, 0.86 eV and 0.95 eV. The other as-grown CZTSe spectra (b) and the spectra of annealed CZTSe monograins (b*) consist of one PL band at 0.81 eV and 0.946 eV, respectively. PL spectra of Cu_2SnSe_3 crystals are shown for comparison with dotted line.

From the laser power dependencies of the PL spectra a blueshift with the magnitude of about 14 meV per decade was detected for the PL bands at 0.765 eV, 0.810 eV and 0.946 eV while the PL band at 0.86 eV shows no shift with excitation power. The blueshift of the PL bands can be taken as an evidence of the DAP recombination. However, the sligthly asymmetrical shape of the PL bands and rather large blueshift with the increasing laser power indicate the presence of spatial potential fluctuations in the material [54]. These fluctuations are small in sample a that shows PL bands with the Gaussian shape. The average depth of the fluctuations in samples b and b* was determined from the shape of the low-energy side of the PL bands and was found to be around 25 meV. This matches the value obtained from the temperature dependence of EQE curves of CZTSe MGL layer solar cells [51].

Table 4. Summary of the results obtained from the PL analysis of CZTSe monograins

PL band position	Recombination mechanism	Thermal activation energy (meV)	Origin	Sample
0.946 eV	BI	69 ± 4	CZTSe	annealed CZTSe [Zn]/[Sn] = 0.96, sample b*
0.860 eV	BB	-	Cu_2SnSe_3	as-grown CZTSe [Zn]/[Sn] = 1.03, sample a
0.810 eV	BI	44 ± 5	Cu_2SnSe_3	as-grown CZTSe [Zn]/[Sn] = 0.96, sample b
0.765 eV	DAP	26 ± 6	Cu_2SnSe_3	as-grown CZTSe [Zn]/[Sn] = 1.03, sample a

The thermal activation energies were determined from the Arrhenius plot (Figure 25). Since for the PL bands at 0.765 eV, 0.810 eV and 0.946 eV were found linear *lnI(T)* versus *1000/T* dependence at high temperatures that is common to the BI-transition [54], we used theoretical expression for discrete energy levels (3.4.1) to fit the experimental data. Thermal activation energies 26 ± 6 meV, 44 ± 5 meV and 69 ± 4 meV were obtained for the PL bands at 0.765 eV, 0.810 eV and 0.946 eV, respectively. The Arrhenius plot of the PL band at 0.860 eV did not show linear dependence at high temperatures, so the thermal activation energy for this recombination process could not be found. This band vanishes very slowly with temperature, being detectable even at room-temperature. It also shifts towards higher energies with an increasing temperature with the magnitude of 5 meV per 100 K. The laser power and temperature dependencies of the PL band at 0.860 eV

indicate that this emission results from the BB recombination. Therefore, the bandgap energy of the corresponding phase in the as-grown CZTSe sample must be around 0.86 eV at T = 10 K. We attribute the bandgap energy of 0.86 eV to the secondary Cu_2SnSe_3 phase detected by Raman spectroscopy in as-grown monograins. This conclusion is explained in more detail below.

The PL emission at 0.765 eV shows very fast quenching with temperature, the thermal activation energy being E_T = 26 ± 6 meV. Considering also the blueshift with the increasing laser power, we attribute this emission to the DAP recombination. This low activation energy is probably the ionization energy of a donor defect that should be a lower defect in a p-type material. We cannot distinguish the vanishing of the free-to-bound emission in this sample that should follow the ionization of a donor defect, therefore we cannot estimate the ionization energy of a corresponding acceptor. However, in the absence of remarkable potential fluctuations in sample a, it can be estimated considering that the energy of the emitted photon in a DAP transition is given by:

$$h\nu = E_g - E_A - E_D + e^2/(4\pi\varepsilon_0\varepsilon R), \qquad (3.7.1.1.)$$

where E_g is the bandgap energy, E_A and E_D are the acceptor and donor binding energies, respectively, and the last member is the Coulomb energy. Taking into account that the BB band allows us to estimate the bandgap energy of Cu_2SnSe_3 phase that was found to be around 0.86 eV, we obtain the acceptor activation energy of around 70 meV. From the thermal quenching of the PL band at 0.810 eV,

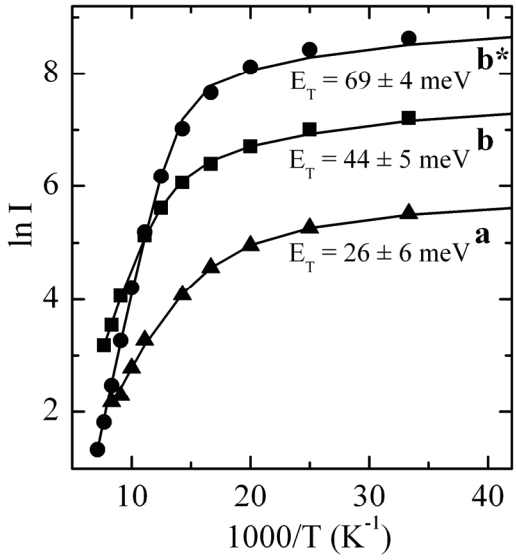

Figure 25. Arrhenius plot derived from the temperature dependencies of the PL spectra of CZTSe monograins. Thermal activation energies 26 ± 6 meV, 44 ± 5 meV and 69 ± 4 meV were obtained for the PL bands at 0.765 eV, 0.810 eV and 0.946 eV, respectively.

that was obtained from another as-grown monograin powder (sample b), we obtained an activation energy of 44 ± 5 meV. This emission results from the BI - recombination and may involve the same acceptor defect forming the donor-acceptor pair. The small difference in activation energies is due to the rough guess of the bandgap energy.

On the basis of the high energy PL band analysis at 0.946 eV that dominates the spectra of the annealed CZTSe monograin powder (sample b*) and is also present in the spectra of one of the as-grown powders, we found that this emission results from the BI–recombination and involves an acceptor defect with the ionization energy of E_T= 69 ± 4 meV. The results of the analysis of this PL band are inconsistent with the results obtained from the analysis of the other PL bands detected in these monograins. Considering the presence of the secondary phase of Cu_2SnSe_3 in the as-grown CZTSe monograins, we suggest that the lower energy PL bands at 0.765 eV, 0.810 eV and 0.860 eV to this additional phase that according to literature has a bandgap energy of 0.843 eV at room temperature [78]. For comparison we grew separately Cu_2SnSe_3 crystals and their PL spectrum is presented in Figure 24 with a dotted line. As can be seen from Figure 24, the lower energy bands detected in CZTSe monograins lie in the same spectral region. Vacuum annealing seems to remove the additional phase and the emission at 0.946 eV can be attributed to CZTSe. The results of the PL analysis of CZTSe monograins are summarized in Table 4.

According to the theory of heavily doped semiconductors [54] at low temperatures the BI-band`s maximum is located at $h\nu_{\max} = E_g - I_a$. In the case of BI transition, the effect of fluctuations to the bandgap energy is not remarkable. The resulting bandgap energy of CZTSe is found to be around 1.02 eV at T = 10 K. The obtained approximate bandgap energy of CZTSe is lower than the one reported in the literature, as was mentioned in the introduction. Yet, the studies of $Cu_2ZnSn(Se_{x-1}S_x)_4$ solid solutions indicate that the bandgap energy is decreasing with the Se concentration and allow us to consider the obtained bandgap energy of $Cu_2ZnSnSe_4$ to be correct. Also, the results of EQE measurements made for solar cells made from these CZTSe monograin powders confirm this result [51,75]. More recently Ahn *et al.* [79] have investigated the discrepancies of the reported bandgap values of CZTSe and proposed that the possible overestimation of the E_g is caused by the existence of ZnSe in the coevaporated films.

CONCLUSIONS

ODCs of the Cu-Ga-Se system

1. The A_1 Raman modes of $CuGa_3Se_5$, $CuGa_5Se_8$ and $CuGaSe_2$ were detected at 159 cm^{-1}, 166 cm^{-1} and 185 cm^{-1}, respectively. The broadening of the Raman modes with the increasing Ga concentration was observed and assigned to the increasing defect concentration in the films.

2. In the Raman spectra of $CuGa_5Se_8$ twelve peaks were detected and assigned for the first time.

3. The PL properties of $CuGa_3Se_5$ crystals were studied in connection with spatial compositional and potential fluctuations. In the low-temperature (T = 10 K) PL spectrum of $CuGa_3Se_5$ an asymmetrical PL band at 1.76 eV resulting from the BT-recombination was detected. The average activation energy of the acceptor states 45 meV and the average depth of the band edge fluctuations 70 meV were estimated.

4. The PL analysis of $CuGa_5Se_8$ also shows the presence of spatial potential fluctuations. In the low-temperature PL spectra of $CuGa_5Se_8$ single crystal and polycrystalline film, one broad asymmetric PL band at 1.788 eV and 1.765 eV, respectively, was observed. According to PL data, the emission is due to the BT- and BI-recombination in single crystals and polycrystalline film, respectively. The thermal activation energy of the acceptor states 40 ± 8 meV and 168 ± 5 meV for single crystal and polycrystalline $CuGa_5Se_8$, respectively, was found. The corresponding average amplitudes of the fluctuations were $\gamma = 62 \pm 4$ meV and $\gamma = 113 \pm 7$ meV.

Kesterites

1. The frequencies of the Raman modes of the $Cu_2ZnSn(Se_xS_{1-x})_4$ monograins were determined and the bimodal behaviour of the A_1 modes of $Cu_2ZnSnSe_4$ and Cu_2ZnSnS_4 was established.

2. From the Raman spectra of the $Cu_2ZnSn(Se_xS_{1-x})_4$ solid solutions, minor traces of additional binary phases such as ZnSe, ZnS, $SnSe_2$, SnS were found. The broadening of the Raman peaks with an increasing sulphur content was observed. It was assigned to an increasing structural disorder due to the random distribution of S and Se atoms in the lattice that leads to fluctuations in the masses and force constants in the neighbourhood. From the samples studied, the largest widths of the peaks were detected for $Cu_2ZnSn(Se_{0.55}S_{0.45})_4$.

3. From the PL analysis the widening of the bandgap of the $Cu_2ZnSn(Se_xS_{1-x})_4$ solid solutions with an increasing sulphur concentration was observed, indicating that CZTSe must have a lower bandgap energy than CZTS. The BI-recombination was detected as the main radiative recombination channel in the $Cu_2ZnSn(Se_xS_{1-x})_4$ monograins.

4. The average depth of the spatial potential fluctuations present in the $Cu_2ZnSn(Se_xS_{1-x})_4$ solid solutions was estimated and was found to increase with

sulphur concentration. The average depth 25 meV of the spatial potential fluctuations in CZTSe was found.

5. The bandgap energy of CZTSe determined from the PL analysis was found to be around 1.02 eV at T = 10 K.

ACKNOWLEDGEMENTS

I would like to express my deepest gratitude to my supervisor Prof. Jüri Krustok for his support, encouragement and helpful discussions over the years.

I would also like to thank Prof. Enn Mellikov for giving me the opportunity to join the research group at the Chair of Semiconductor Materials Technology.

I am very thankful to all my friendly colleagues in the Chair of Semiconductor Materials Technology, especially to Dr. Andri Jagomägi for helpful discussions and PhD students Mati Danilson and Taavi Raadik for helping me with the experiments. I wish to thank Dr. Jaan Raudoja and PhD student Kristi Timmo from our laboratory, Dr. Ernest Arushanov from the Institute of Applied Physics in Moldova, Dr. Ivan Bodnar from the Belarussian State University of Informatics and Radioelectronics in Belarus, and Dr. Jürgen Albert from Helmholtz Zentrum Berlin for sample preparation. I am also thankful to Dr. Olga Volobujeva for the SEM and EDS analysis.

I am very thankful to Prof. Susanne Siebentritt from University of Luxembourg, Prof. Malgorzata Igalson from Warsaw University of Technology, and Prof. Maximo Leon from Universidad Autonoma de Madrid for their pleasant and fruitful collaboration during this work.

Financial support from Estonian Science Foundation grants G-5149, G-6554, G6160, G-8282, INTAS grant no. 03-51-6314, the target financing by HTM (Estonia) No. SF0140099s08, The World Federation of Scientists National Scholarship Programme, and Estonian Doctoral School of Materials Science and Materials Technology is greatfully acknowledged.

My warmest gratitude belongs to my family.

Tallinn, October 2010

Maarja Grossberg

ABSTRACT

Optical Properties of Multinary Semiconductor Compounds for Photovoltaic Applications

This thesis is focused on the photoluminescence (PL) and Raman studies of ordered defect compounds (ODCs) $CuGa_3Se_5$ and $CuGa_5Se_8$, and kesterite $Cu_2ZnSn(Se_xS_{1-x})_4$ solid solutions with x = 1, 0.75, 0.55, 0.26 and 0. These compounds are promising materials for photovoltaic applications due to their optimal direct bandgap and high absorption coefficient. However, their performance as absorber materials depends crucially on their electrical and optical properties. To identify defect related recombination mechanisms in these compounds, we used PL that is a very sensitive method for studying defects in semiconductors. It was found that the PL spectra of both ODCs and kesterite compounds can be characterized with the model of highly doped and compensated semiconductors. In addition, the vibrational properties of $CuGa_5Se_8$ and $Cu_2ZnSn(Se_xS_{1-x})_4$ solid solutions were investigated by Raman spectroscopy.

The compositional dependence of the Raman spectra of polycrystalline Cu-Ga-Se films was studied. The A_1 Raman modes of $CuGa_3Se_5$, $CuGa_5Se_8$ and $CuGaSe_2$ were detected at 159 cm^{-1}, 166 cm^{-1} and 185 cm^{-1}, respectively. The broadening of the Raman modes with the increasing Ga concentration was observed and assigned to the increasing defect concentration in the films. In the Raman spectra of $CuGa_5Se_8$ twelve peaks were detected and assigned for the first time.

The PL properties of $CuGa_3Se_5$ crystals were studied in connection with spatial compositional and potential fluctuations. The presence of compositional fluctuations in the crystals was confirmed by the EDS analysis. In the low-temperature (T = 10 K) PL spectrum of $CuGa_3Se_5$ an asymmetrical PL band at 1.76 eV resulting from the BT-recombination was detected. The average activation energy of acceptor states 45 meV and the average depth of the band edge fluctuations 70 meV were estimated.

The PL analysis of $CuGa_5Se_8$ also shows the presence of spatial potential fluctuations. In the low-temperature PL spectra of $CuGa_5Se_8$ single crystal and polycrystalline film, one broad asymmetric PL band at 1.788 eV and 1.765 eV, respectively, was observed. According to PL data, the emission is due to the BT- and BI-recombination in single crystals and polycrystalline film, respectively. The thermal activation energy of acceptor states 40 ± 8 meV and 168 ± 5 meV for a single crystal and polycrystalline $CuGa_5Se_8$, respectively, was found. The corresponding average amplitudes of the fluctuations were γ = 62 ± 4 meV and γ = 113 ± 7 meV.

For the first time, the frequencies of the Raman modes of the $Cu_2ZnSn(Se_xS_{1-x})_4$ monograins were determined and the bimodal behaviour of the A_1 modes of $Cu_2ZnSnSe_4$ and Cu_2ZnSnS_4 was established. From the Raman spectra

of the $Cu_2ZnSn(Se_xS_{1-x})_4$ solid solutions minor traces of additional binary phases such as ZnSe, ZnS, $SnSe_2$, SnS were found. In the compositional dependence of the Raman spectra of the solid solutions the broadening of the peaks with the increasing sulphur content was observed. It was assigned to the increasing structural disorder due to the random distribution of S and Se atoms in the lattice that leads to fluctuations in the masses and force constants in the neighborhood. The largest widths of the peaks were detected for $Cu_2ZnSn(Se_{0.55}S_{0.45})_4$.

PL studies of the $Cu_2ZnSn(Se_xS_{1-x})_4$ solid solutions showed the widening of the bandgap with the increasing sulphur concentration, indicating that CZTSe must have lower bandgap energy than CZTS. According to the temperature and laser power dependencies of the PL spectra, the radiative recombination in the $Cu_2ZnSn(Se_xS_{1-x})_4$ solid solutions was suggested to result from the BI-recombination. The average depth of the spatial potential fluctuations 25 meV in CZTSe was estimated and it was found to increase with sulphur concentration. We also determined the low-temperature (T = 10 K) bandgap value of CZTSe around 1.02 eV. This value is close to the bandgap energy predicted by theoretical calculations but has not been obtained from experiments till now. At the time of writing this thesis, other groups have obtained similar results.

KOKKUVÕTE

Päikesepatareides kasutatavate mitmikpooljuhtühendite optilised omadused

Antud töö eesmärgiks oli uurida korrastatud defektstruktuuriga ühendite $CuGa_3Se_5$ ja $CuGa_5Se_8$ ning kesteriitsete ühendite $Cu_2ZnSn(Se_xS_{1-x})_4$ (x = 1, 0.75, 0.55, 0.26, 0) fotoluminestsentskiirgust ja Ramani hajumist. Suure neeldumiskoefitsiendi ja optimaalse otsese keelutsooni laiuse tõttu leiavad need materjalid kasutamist päikesepatareide absorberkihina. On selge, et absorbermaterjali elektrilised ja optilised omadused mõjutavad oluliselt päikesepatarei efektiivsust, mistõttu on oluline kindlaks teha materjalides leiduvad rekombinatsioonikanalid. Üheks tundlikumaks meetodiks defektide uurimisel on fotoluminestsents. Eksperimentide tulemused näitasid, et korrastatud defektstruktuuriga ühendite ja kesteriitsete tahkete lahuste fotoluminestsentsi spektreid saab kirjeldada tugevalt legeeritud ja kompenseeritud pooljuhtide mudeli abil. Kasutades Ramani spektroskoopiat, uurisime ka $CuGa_5Se_8$ ja $Cu_2ZnSn(Se_xS_{1-x})_4$ tahkete lahuste võnkespektreid.

Cu-Ga-Se polükristalsete kilede Ramani hajumise spektritest määrasime $CuGa_3Se_5$, $CuGa_5Se_8$ ja $CuGaSe_2$ A_1 Ramani moodid vastavalt 159 cm^{-1}, 166 cm^{-1} ja 185 cm^{-1} juures. Lisaks selgus, et Ga kontsentratsiooni kasvades Ramani piigid laienevad, mis on ilmselt tingitud defektide kontsentratsiooni suurenemisest kiledes. Kuna kirjanduses leidub vaid üks $CuGa_5Se_8$ Ramani hajumise spekter, uurisime seda ühendit lähemalt. Eksperimendist selgus, et $CuGa_5Se_8$ Ramani hajumise spekter koosnes kaheteistkümnest piigist, mille omistasime esmakordselt vastavatele kristallvõre võnkumistele.

$CuGa_3Se_5$ kristallide luminestsentskiirguse spektreid uurisime lähtudes tugevalt legeeritud pooljuhtide teooriast ja ka koostise fluktuatsioonidest. Koostise fluktuatsioonid avaldusid ka EDS analüüsis. $CuGa_3Se_5$ fotoluminestsentsi spekter temperatuuril 10 K koosnes ühest asümmetrilisest ribast 1.76 eV juures (T = 10 K), mille omistasime BT-rekombinatsioonile (*BT- band-to-tail i.k.*). Keskmiseks aktseptori aktivatsioonienergiaks saime ligikaudu 45 meV ning keelutsooni fluktuatsioonide keskmine sügavus oli ligikaudu 70 meV.

Ka $CuGa_5Se_8$ fotoluminestsentsi analüüs viitab ruumiliste potentsiaali fluktuatsioonide olemasolule kristallides. Madalatemperatuurne (T = 10 K) spekter kooneb ühest laiast asümmeetrilisest ribast 1.788 eV juures $CuGa_5Se_8$ monokristalli korral ja 1.765 eV juures $CuGa_5Se_8$ polükristalse kile korral. Luminestsentsi analüüsist selgus, et kiirgus pärineb BT- või BI-rekobinatsioonist (*BI – band-to-impurity i.k.)*. Leidsime, et aktseptorite termiline aktivatsioonienergia $CuGa_5Se_8$ monokristallis ja polükristalses kiles on vastavalt 40 ± 8 meV ja 168 ± 5 meV. Keskmisteks fluktuatsioonide sügavusteks saime vastavalt γ = 62 ± 4 meV ja γ = 113 ± 7 meV.

Kasutades Ramani spektroskoopiat, uurisime esmakordselt $Cu_2ZnSn(Se_xS_{1-x})_4$ monoterade võnkespektreid. Leidsime, et $Cu_2ZnSnSe_4$ (CZTSe) ja Cu_2ZnSnS_4 (CZTS) A_1 Ramani moodid on bimodaalsed. Lisaks tegime spektritest kindlaks binaarsete faaside nagu ZnSe, ZnS, $SnSe_2$, SnS vähese sisalduse $Cu_2ZnSn(Se_xS_{1-x})_4$ tahketes lahustes. Ramani hajumise spektrite sõltuvus koostisest näitas piikide poollaiuse suurenemist väävli sisalduse kasvades. See on ilmselt tingitud väävli ja seleeni aatomite juhuslikust jaotusest võres, mis põhjustab masside ja jõukonstantide fluktuatsioone ning võre kasvava struktuurilise korrapäratuse. Ramani piikide laius on maksimaalne $Cu_2ZnSn(Se_{0.55}S_{0.45})_4$ tahkes lahuses.

$Cu_2ZnSn(Se_xS_{1-x})_4$ tahkete lahuste fotoluminestsentsi analüüs näitas keelutsooni laienemist väävli sisalduse kasvades. Seega peab CZTSe keelutsoon olema väiksem kui CZTS-il. Fotoluminestsentsspektrite sõltuvustest temperatuurist ja ergastusvõimsusest leidsime, et põhiliseks rekombinatsiooni mehhanismiks $Cu_2ZnSn(Se_xS_{1-x})_4$ monoterades on ka BI-rekombinatsioon. Leidsime, et ruumiliste potentsiaali fluktuatsioonide keskmine sügavus $Cu_2ZnSn(Se_xS_{1-x})_4$ tahketes lahustes kasvab väävli kontsentratsiooni suurenedes. Ruumiliste potentsiaali fluktuatsioonide keskmiseks sügavuseks CZTSe-s saime 25 meV. Määrasime ka CZTSe keelutsooni laiuse E_g = 1.02 eV temperatuuril 10 K. See väärtus on sarnane teoreetiliselt arvutatud CZTSe keelutsooni laiusega. Eksperimentaalselt pole seni veel keegi teoreetilisele väärtusele sarnast tulemust saanud. Praeguseks on ilmunud ka teiste uurimisgruppide töid, kus on saadud meiega sarnaseid tulemusi.

REFERENCES

1) M. Powalla, P. Jackson, E. Lotter, D. Hariskos, S. Paetel, R. Würz, R. Menner, W. Wischmann, *Thin Solid Films (in press)*.
2) S. B. Zhang, S. H. Wei, A. Zunger, H. K. Yoshida, *Phys. Rev. B* 57 (1998) 9642.
3) J. Kessler, D. Schmid, R. Schafler, H. W. Schock, S. Menezes, *Proc. 23rd IEEE Photovoltaic Conference (Louisville) (New York: IEEE)* (1993) 549.
4) H. Z. Xiao, L. Yang Chung, A. Rockett, *J. Appl. Phys*. 76 (1994) 1503.
5) A. Meeder, L. Weinhardt, R. Stresing, D. Fuertes Marron, R. Würz, S. M. Babu, Th. Schedel-Niedrig, M. Ch. Lux-Steiner, C. Heske, E. Umbach, *J. Phys. Chem. Solids* 64 (2003) 1553.
6) R. Würz, M. Rusu, Th. Schedel-Niedrig, M. Ch. Lux-Steiner, H. Bluhm, M. Hävecker, E. Kleimenov, A. Knop-Gericke, R. Schlögl, *Surface Science* 580 (2005) 80.
7) A. Jasenek, U. Rau, V. Nadenau, D. Theiss, H. W. Schock, *Thin Solid Films* 361-362 (2000) 415-419.
8) S.M. Wasim, C. Rincon, G. Marin, J. M. Delgado, *Appl. Phys. Letters* 77 (2000) 94.
9) C. Rincon, S. M. Wasim, G. Marin, *Appl. Phys. Letters* 80 (2002) 998.
10) C. Rincon, S. M. Wasim, G. Marin, *J. Phys.: Condens. Matter* 14 (2002) 997.
11) S. M. Wasim, C. Rincon, G. Marin, *Phys. stat. sol. (a)* 194 (2002) 244.
12) S. H. Wei, S. B. Zhang, *J. Phys. Chem. Solids* 66 (2005) 1994.
13) J.E. Jaffe, A. Zunger, *Phys. Rev. B* 29 (1984) 1882.
14) S. Chichibu, T. Mizutani, K. Murakami, T. Shioda, T. Kurafuji, H. Nakanishi, S. Niki, P.J. Fons, A. Yamada, *J. Appl. Phys*. 83 (1998) 3678.
15) T. Negami, N. Kohara, M. Nishitani, T. Wada, T. Hirao, *Appl. Phys. Lett.* 67 (1995) 825.
16) G. Marin, C. Rincon, S.M. Wasim, G. Sanchez Perez, I. Molina, *J. Alloys and Comp.* 283 (1999) 1.
17) C. Rincon, S.M. Wasim, G. Marin, I. Molina, *J. Appl. Phys.* 93 (2003) 780.
18) G. Marin, R. Marquez, R. Guevara, S.M. Wasim, J.M. Delgado, C. Rincon, G. Sanchez Perez, I. Molina, P. Bocaranda, *Jpn. J. Appl. Phys.* 39 (2000) 44.
19) M. Leon, S. Levcenko, A. Nateprov, A. Nicorici, J. M. Merino, R. Serna, E. Arushanov, *J. Phys. D* 40 (2007) 740.
20) L. Duran, S.M. Wasim, C.A. Durante Rincon, E. Hernandez, C. Rincon, J.M. Delgado, J. Castro, J. Contreras, *phys. stat. sol. (a)* 199 (2003) 220.
21) G. Marin, S.M. Wasim, C. Rincon, G. Sanchez Perez, P. Bocaranda, I. Molina, R. Guevara, J.M. Delgado, *J. Appl. Phys.* 95 (2004) 8280.
22) C. Rincon, S. M. Wasim, G. Marin, J. M. Delgado, J. R. Huntzinger, A. Zwick, J. Galibert, *Appl. Phys. Letters* 73 (1998) 441.

23) C. Rincon, S.M. Wasim, G. Marin, E. Hernandez, G. Sanchez Perez, J. Galibert, *J. Appl. Phys*. 87 (2000) 2293.
24) F. Guastavino, K. Zeaiter, L. Djellal, Yanuar, D. Bayaa, M. Abdelali, C. Llinares, *Solid State Phenomena* 67-68 (1999) 427.
25) J. Krustok, H. Collan, M. Yakushev, K. Hjelt, *Physica Scripta* T79 (1999) 179.
26) J. Krustok, J. Raudoja, M. Yakushev, R.D. Pilkington, H. Collan, *Phys. stat. sol.* (a) 173 (1999) 483.
27) A. Jagomägi, J. Krustok, J. Raudoja, M. Grossberg, M. Danilson, M. Yakushev, *Physica B* 337 (2003) 369.
28) S. M. Wasim. G. Marin, C. Rincon, P. Bocaranda, G. Sanchez Perez, *J. Phys. Chem. Solids* 61 (2000) 669.
29) Chuan-Ming Xu, Wen-Hao Huang, Jun Xu, Xiao-Jie Yang, Jian Zuo, Xiao-Liang Xu, Hong-Tu Liu, *J. Phys. Condens. Matter* 16 (2004) 4149.
30) N.S. Orlova, I.V. Bodnar, T.L. Kushner, *Cryst. Res. Technol*. 38 (2003) 125.
31) N.S. Orlova, I.V. Bodnar, T.L. Kushner, *J. Phys. Chem. Solids* 64 (2003) 1895.
32) M. Leon, R. Serna, S. Levcenko, A. Nateprov, A. Nicorici, J.M. Merino, E. Arushanov, *phys. stat. sol (a)* 203 (2006) 2913.
33) S.R. Hall, J.T. Szymanski, J.M. Stewart, *Can. Mineral.* 16 (1978) 131.
34) T. M. Friedlmeier, H. Dittrich, H. W. Schock, *1997 Inst. Phys. Conf. Ser. No. 152, Proc. 11th ICTMC (Salford)* 345.
35) H. Matsushita, T. Maeda, A. Katsui, T. Takizawa, *J. Cryst. Growth* 208 (2000) 416.
36) I.D. Olekseyuk, L.D. Gulay, I.V. Dydchak, L.V. Piskach, O.V. Parasyuk, O.V. Marchuk, *J. Alloys Compounds* 340 (2002) 141.
37) S. Chen, X.G. Gong, A. Walsh, S.H. Wei, *Appl. Phys. Lett.* 94 (2009) 041903.
38) H. Katagiri, K. Saitoh, T. Washio, *Sol. Energy Mater. Sol. Cells* 65 (2001) 141.
39) T.K. Todorov, K.B. Reuter, D.B. Mitzi, *Adv. Mater.* 22 (2010) E156.
40) G. Suresh Babu, Y.B. Kishore Kumar, P.Uday Bhaskar, V. Sundara Raja, *Semicond. Sci. Technol*. 23 (2008) 085023.
41) A. Nagoya, R. Asahi, *Phys. Rev. B* 81 (2010) 113202.
42) H. Katagiri, N. Ishigaki, T. Ishida, *Jpn. J. Appl. Phys*. 40 (2001)500.
43) J.M. Raulot, C. Domain, J.F. Guillemoles, *J. Phys. Chem. Solids* 66 (2005) 2019.
44) K. Tanaka, Y. Miyamoto, H. Uchiki, K. Nakazawa, H. Araki, *phys. stat. sol. (a)* 203 (2006) 2891.
45) Y. Miyamoto, K. Tanaka, M. Oonuki, N. Moritake, H. Uchiki, *Jpn. J. Appl. Phys.* 47 (2008) 596.
46) K. Hönes, E. Zscherpel, J. Scragg, S. Siebentritt, *Physica B* 404 (2009) 4949.

47) K. Oishi, G. Saito, K. Ebina, M. Nagahashi, K. Jimbo, W.S. Maw, H. Katagiri, M. Yamazaki, H. Araki, A. Takeuchi, *Thin Solid Films* 517 (2008) 1449.
48) P.M.P. Salome, P.A. Fernandes, A.F. da Cunha J.P. Leitao, J. Malaquias, A. Weber, J.C. Gonzalez, M.I.N. da Silva, *Sol. Energy Mater. Sol. Cells* 94 (2010) 2176.
49) H. Yasuda, E. Sekiya, T. Maeda, H. Matsushita, A. Katsui, *J. Adv. Sci*. 11 (1999) 42.
50) M. Altosaar, J. Raudoja, K. Timmo, M. Danilson, M. Grossberg, J. Krustok, E. Mellikov, *phys. stat. sol (a)* 205 (2008) 167.
51) J. Krustok, R. Josepson, T. Raadik, M. Danilson, *Physica B* 405 (2010) 3186.
52) A. Bauknecht, S. Siebentritt, J. Albert, M.Ch. Lux-Steiner, *J. Appl. Phys*. 89 (2001) 4391.
53) H. B. Bebb, E.W. Williams, *Semiconductors and Semimetals*, Vol 8 Transport and Optical Phenomena (1972) pp. 181- 420.
54) A.P. Levanyuk, V.V. Osipov, *Sov. Phys. Usp.* 24 (1981) 187.
55) B.I. Shklovskii, A.L. Efros, *„Electronic properties of doped semiconductors'', Springer, Berlin* (1984).
56) A.P. Levanyuk, V.V. Osipov, *Sov. Phys. Semicond*. 7 (1973) 721.
57) V.V. Osipov, T.I. Soboleva, M.G. Foigel, *Sov. Phys. Semicond*. 11 (1977) 752.
58) G.D. Holah, J.S. Webb, H. Montgomery, *Solid State Phys.* C 7 (1974) 3875.
59) A.M. Mintairov, N.A. Sadehikov, T. Sauncy, M. Holtz, G.A. Seryogin, S.A. Nikishin, H. Temkin, *Phys. Rev. B* 59 (1999) 15197.
60) I.V. Bodnar, G.F. Smirnova, A.G. Koroza, A.P. Chernyakova, *phys. stat. sol. B* 158 (1990) 469.
61) J.F. Chang, S.S. Mitra, *Phys. Rev*. 172 (1968) 924.
62) H. Neumann, *Helv. Phys. Acta* 58 (1985) 337.
63) F.J. Ramirez, C. Rincon, *Solid State Commun.* 84 (1992) 551.
64) S. Roy, P. Guha, S.N. Kundu, H. Hanzawa, S. Chaudhuri, A.K. Pal, *Mater. Chem. Phys.*73 (2002) 24.
65) C.M. Xu, X.L. Xu, J. Xu, X.J. Yang, J. Zuo, X.M. Dang, Y. Feng, W.H. Huang, H.T. Liu, *Chin. J. Semicond*. 24 (2003) 1057.
66) E.P. Petrov, *J. Quant. Spec. Radiat. Transf.* 103 (2007) 272.
67) J. Krustok, A. Jagomägi, M. Grossberg, J. Raudoja, M. Danilson, *Solar Energy Mater. Solar Cells* 90 (2006) 1973.
68) J. Krustok, H. Collan, K. Hjelt, *J. Appl. Phys.* 81 (1997) 1442.
69) G. Marin, J.M. Delgado, S.M. Wasim, C. Rincon, G. Sanchez Perez, A.E. Mora, P. Bocaranda, J.A. Henao, *J. Appl. Phys.* 87 (2000) 7814.
70) S. Siebentritt, N. Papathanasiou, M.Ch. Lux-Steiner, *Physica B* 376-377 (2006) 831.

71) G. Perna, M. Lastella, M. Ambrico, V. Capozzi, *Appl. Phys. A* 83 (2006) 127.
72) 13. G. Lucovsky, J. C. Mikkelsen, Jr., W. Y. Liang, R. M. White, R. M. Martin, *Phys. Rev. B* 14 (1976) 1663.
73) Young-Moon Yu, M.-H. Hyun, S. Nam, D. Lee, O. Byungsung, K.- S. Lee, Pyeong Yeol Yu, Yong Dae Choi*, J. Appl. Phys*. 91 (2002) 9429.
74) H. R. Chandrasekhar, R.G. Humphreys, U. Zwick, M. Cardona, *Phys. Rev. B* 15 (1977) 2177.
75) K. Timmo, M. Altosaar, J. Raudoja, K. Muska, M. Pilvet, M. Kauk, T. Varema, M. Danilson, O. Volobujeva, E. Mellikov, *Solar Energy Mater. Solar Cells* 94 (2010) 1889.
76) I.D. Olekseyuk, I.V. Dudchak, L.V. Piskach, *J. Alloys and Compounds* 368 (2004) 135.
77) I.V. Dudchak, L.V. Piskach, *J. Alloys and Compounds* 351 (2003) 145.
78) G. Marcano, C. Rincon, L.M. de Chalbaud, D.B. Bracho, G. Sanchez Perez, *J. Appl. Phys.* 90 (2001) 1847.
79) S. Ahn, S. Jung, J. Gwak, A. Cho, K. Shin, K. Yoon, D. Park, H. Cheong, J. H. Yun, *Appl. Phys. Lett*. 97 (2010) 021905.

APPENDIX A

PAPER I

M. Grossberg, J. Krustok, A. Jagomägi, M. Leon, E. Arushanov, A. Nateprov, I. Bodnar. Investigation of potential and compositional fluctuations in $CuGa_3Se_5$ crystals using photoluminescence spectroscopy. *Thin Solid Films*, 515 (2007) 6204-6207.

Available online at www.sciencedirect.com
ScienceDirect
Thin Solid Films 515 (2007) 6204–6207
www.elsevier.com/locate/tsf

Investigation of potential and compositional fluctuations in $CuGa_3Se_5$ crystals using photoluminescence spectroscopy

M. Grossberg [a,*], J. Krustok [a], A. Jagomägi [a], M. Leon [b], E. Arushanov [c], A. Nateprov [c], I. Bodnar [d]

[a] Tallinn University of Technology, Ehitajate tee 5, 19086 Tallinn, Estonia
[b] Departamento de Fisica Aplicada, Facultad de Ciencias, C-XII, Universidad Autonoma de Madrid, 28049, Madrid, Spain
[c] Institute of Applied Physics, Academie 5, MD-2028 Chisinau, Republic of Moldova
[d] Department of Chemistry, Belarussian State University of Informatics and Radioelectronics, P. Brovka str. 6, 220027 Minsk, Belarus

Available online 16 January 2007

Abstract

We studied the photoluminescence (PL) properties of the ordered defect compound $CuGa_3Se_5$. Different single crystals were grown by the vertical Bridgman method and by the solid phase crystallization method. Their crystal structure and cell parameters were determined by X-ray diffraction. The PL spectra were recorded at $T=10$–300 K. Also, laser power dependences were studied. We found an asymmetric PL band at 1.76 eV. PL band shifts towards higher energies with increasing laser power. The shape and properties of this band assure the presence of potential and compositional fluctuations. The influence of both fluctuations on the PL properties of $CuGa_3Se_5$ is studied and the radiative recombination processes are explained.

PACS: 78.55.Hx; 71.55.Ht; 61.72.Ji; 78.30.A
Keywords: $CuGa_3Se_5$; Chalcopyrite crystals; Photoluminescence; Ordered defect compounds; Potential fluctuations

1. Introduction

$CuGaSe_2$ and the related I–III–VI_2 chalcopyrite compounds are of great interest due to their potential in photovoltaic and nonlinear optical applications. Another attractive property is their tolerance to large range of anion-to-cation off stoichiometry, manifested by the existence of an ordered defect compounds (ODC) with large variations in their Cu/Ga/Se ratio [1]. These ODCs, like $CuGa_3Se_5$ and $CuGa_5Se_8$, generally possess wider bandgap and the formation of ternary Cu–Ga–Se compounds with varying bandgaps enables the formation of heterojunctions used in the design of high-performance electronic and optoelectronic devices. The bandgap energy of $CuGa_3Se_5$ for bulk samples at room temperature is 1.754 eV and for thin films 1.855 eV [2].

Rincon et al. [3] have measured the PL spectrum of $CuGa_3Se_5$ that consists of one broad band $h\nu_{max}=1.63$ eV ($T=15$ K) that is proposed to result from donor–acceptor pair recombination. Guastavino et al. [4] have measured the PL spectrum of $CuGa_3Se_5$ that consists of one broad asymmetric edge emission band at $h\nu_{max}=1.6$ eV ($T=4.2$ K) and one deeper band at $h\nu_{max}\sim1.2$ eV ($T=4.2$ K). The broadness of the PL bands (150–200 meV) was interpreted also by donor–acceptor pair transitions.

At the same time, the asymmetric shape of the PL band in ternary chalcopyrites is often caused by the band tails induced by potential fluctuations due to the high concentration of intrinsic defects [5–7]. Furthermore, compositional fluctuations also affect the shape of PL bands by creating the fluctuations of the bandgap energy. In this paper, we study the photoluminescence (PL) properties of $CuGa_3Se_5$ in connection with compositional and potential fluctuations.

2. Experimental

The $CuGa_3Se_5$ crystals were grown by the solid phase crystallization (SPC) method and vertical Bridgman method.

* Corresponding author. Tel.: +372 6203210; fax: +372 6203367.
E-mail address: mgross@staff.ttu.ee (M. Grossberg).

0040-6090/$ - see front matter © 2007 Elsevier B.V. All rights reserved.
doi:10.1016/j.tsf.2006.12.068

For the SPC growth, the stoichiometric amounts of Cu (99.999% of purity), Ga (99.9999%) and Se (99.999%) (~20 g total) were placed together in quartz ampoule with an inner surface coated by carbon. Ampoule was evacuated up to 10^2 Pa and sealed. For synthesis, one-zone vertical resistance furnace was used. Ampoule with Cu, Ga, and Se was heated up to 550–600 °C and kept at this temperature for 24 h. Then, the temperature was raised with the rate of 50 K/h up to 950 °C. This temperature is about 30 °C lower than the melting point temperature of $CuGa_3Se_5$ (T_m=1359 K [8]). Ampoule was held at this temperature for 10 days before cooling. An ingot consisting of a few single crystal blocks of $CuGa_3Se_5$ was obtained.

For the Bridgman growth, crystals with given composition grown by the two-temperature method were used. The details of the growth can be found in Ref. [8].

For the structural characterization, X-ray diffraction (XRD) patterns, recorded by the Siemens D 500 diffractometer were used. The composition of the crystals was determined by energy-dispersive X-ray analysis (EDAX) performed on the Leo Supra 35 SEM. PL measurements were done using closed-cycle He cryostat (T=8–300 K) and He–Cd laser (441.6 nm) as an excitation source.

3. Results and discussion

3.1. Structural analysis

The phases and crystallographic structure of the crystals were determined by X-ray diffraction. Rietveld method was used for the derivation of crystal structure information from powder XRD data. The X-ray analysis demonstrated the single phase of the tetragonal chalcopyrite-related structure of $CuGa_3Se_5$. The Rietveld evaluation produced unit-cell parameters a=0.54874 nm, and c=1.10049 nm for $CuGa_3Se_5$ crystal grown by the SPC method and a=0.54803 nm, and c=1.09734 nm for the crystal grown by the vertical Bridgman method. These values are close to data a=0.544995(8) nm, and c=1.0946(3) nm reported in Ref. [9].

3.2. Composition analysis

The studies of the crystals' composition were done by energy-dispersive X-ray analysis (EDAX). The chemical composition was measured in several points of crystals and the presence of compositional fluctuations was detected, being larger for the $CuGa_3Se_5$ samples grown by the SPC method, see Fig. 1.

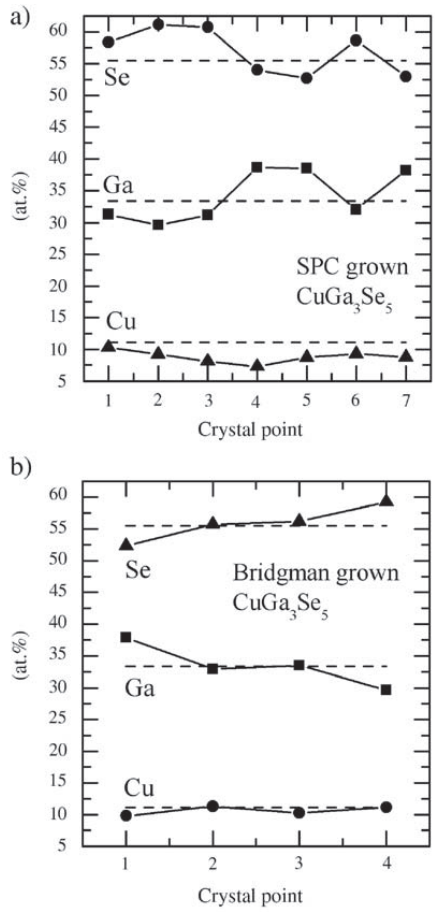

Fig. 1. Chemical composition measured in several points of $CuGa_3Se_5$ crystals grown by the SPC method (a) and by the vertical Bridgman method (b). The dashed line represents the chemical composition of $CuGa_3Se_5$ (Cu:Ga:Se=11.11:33.33:55.55 at.%).

3.3. Photoluminescence results

In heavily doped semiconductors Coulomb potential fluctuations are induced due to the random distribution of unscreened charged defects. These potential fluctuations will lead to a local perturbation of the band structure, thus broadening the defect level distribution and forming band tails [10,11]. Radiative recombination in heavily doped crystal is therefore governed by the recombination of carriers localized in spatially separated potential wells originating from Coulomb potential fluctuations. The presence of compositional fluctuations causes additional broadening of the PL bands due to the variation of the bandgap energy, see Fig. 2.

In this study, we found a broad (full width at half maximum (FWHM) ~200 meV) asymmetric PL band at 1.76 eV. It has an exponential slope on the low-energy side and steeper Gaussian incline on the high-energy side. This type of asymmetric PL bands was found in many ternaries [5–7,13]. Fig. 3 shows normalised spectra of the asymmetric PL band for SPC grown $CuGa_3Se_5$, measured from different points of the crystal. The maximum energy difference of the corresponding peak positions is ~60 meV. This difference may be taken as the approximate value of the bandgap energy fluctuations. The mean amplitude of the Coulomb potential fluctuations γ_0 is the average energetic difference between the hole energy in the Coulomb potential fluctuation minimum and maximum, see Fig. 2. The average

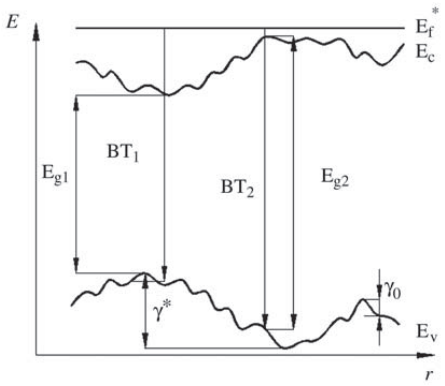

Fig. 2. BT recombination model in $CuGa_3Se_5$ in the presence of potential- and compositional fluctuations. BT_1 and BT_2 emissions originate from different parts of the crystal with different bandgap energy (E_{g1} vs E_{g2}).

amplitude of band edge fluctuations γ^* in the presence of potential and compositional fluctuations is the mean difference of the energy of holes in the valence band fluctuation minimum and maximum. The slope of the low-energy side of the PL band is determined by the density of states in the valence band and therefore depends on the amplitude of both fluctuations. Thus, the values of the mean amplitude of the band edge fluctuations γ^* can be derived form the slope of the low-energy side of the PL band [5,6,10]. The compositional fluctuations also affect the half-width of the PL band. The values of the mean amplitude of the band edge fluctuations γ^* and the FWHM of the BT-band for several chalcopyrite compounds are shown in Table 1. The average value of γ^* of the crystals investigated in this study has been determined from the exponential slope of the low-energy side of the PL band (see Fig. 2) and was about 70 meV, and 90 meV for Bridgman, and SPC grown $CuGa_3Se_5$, respectively. These rather high values of γ^* and FWHM support the idea of the coexistence of potential and compositional fluctuations in these samples.

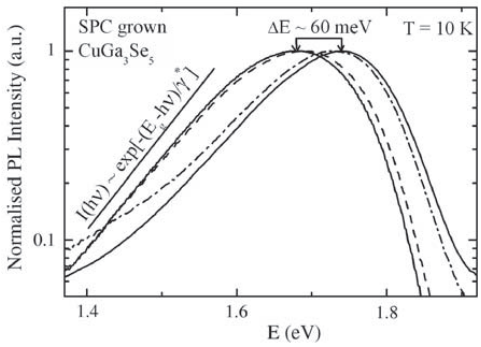

Fig. 3. Normalised spectra of the 1.76 eV PL band for SPC grown $CuGa_3Se_5$, measured from different spots of the crystal. The energy difference of the peak positions is ~60 meV. The exponential slope of the low-energy side of the BT-band gives the average depth of the band edge fluctuations γ^*.

Table 1
Values of the average amplitude of the band edge fluctuations γ^*, calculated from the low-energy slope of the PL band, and FWHM of the BT-band for several chalcopyrite compounds

Compound	γ^* (meV)	FWHM (meV)	References
$CuGaSe_2$	17.6	50	[6]
$CuIn_{0.5}Ga_{0.5}Se_2$	17.0	49	[5]
$AgGaTe_2$	4.5	16	[13]
$CuInSe_2$	24.1	51	Our data
$CuGa_3Se_5$ (Bridgman)	58.1–72.8	170–178	Present work
$CuGa_3Se_5$ (SPC)	71.4–94.5	188–220	Present work

Excitation power and temperature dependent photoluminescence measurements indicate that our spectra are dominated by the BT-type recombination that involves free electron and a hole that is localized in the valence band tail. Due to their small effective mass ($m_e^* \approx 0.08 m_e$), almost all electrons are free. Due to band edge fluctuations, at low temperatures, holes in the valence band can not be considered as free like in the undisturbed crystal with flat bands (graphical illustration and theoretical discussion of this kind of configuration are presented in Refs. [7] and [10]). Holes are localized in the valence band potential wells and form so-called pseudo-acceptor states. The activation energy of the thermal quenching of the BT-band allows us to evaluate the average depth of these pseudo-acceptor states. From Arrhenius plot of thermal quenching of the PL bands, we obtained thermal activation energies 38± 12 meV, and 53±17 meV for Bridgman, and SPC crystals, respectively. Although, the $\ln I(T)$ versus $1000/T$ dependence is very similar to the theoretical dependence for discrete energy levels [12], it is clear that in the case of BT-type recombination, the fitting is not completely valid due to continuous tail states. However, the average activation energy of pseudo-acceptor states can be estimated to be approximately 45 meV.

In Fig. 4, the temperature dependence of the peak position of the 1.76 eV PL band is shown along with the bandgap energy E_g of $CuGa_3Se_5$ [2]. The observed shift of the peak position energy

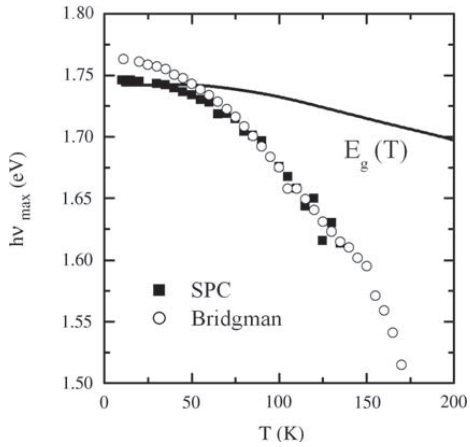

Fig. 4. Temperature dependence of the peak position of the 1.76 eV PL band and the bandgap energy E_g [2] of $CuGa_3Se_5$.

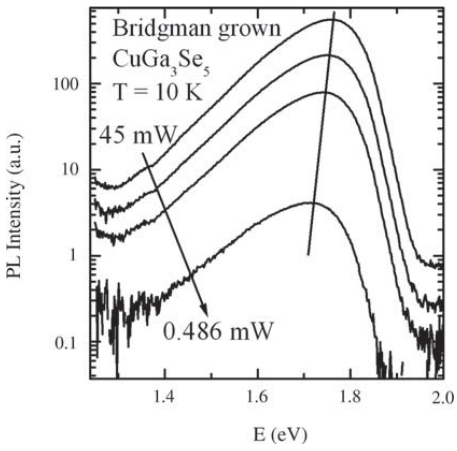

Fig. 5. The laser power dependence of PL spectrum of the $CuGa_3Se_5$ crystal grown by the vertical Bridgman method. The observed PL band shifts to higher energies with increasing excitation intensity. The magnitude of the shift is about 19 meV per decade.

exceeds the temperature dependence of the bandgap energy. This feature is predicted by the theory of heavily doped semiconductors [6,10]. According to the theory, when holes, localized in the valence band tail are freed at higher temperatures, BB-transition, that involves a free electron and a free hole, dominates the spectra. However BB-band may not appear in the presence of large compositional fluctuations, because higher thermal energy is needed to liberate holes. In our case, the thermal energy is enough to redistribute the holes between the potential wells and therefore BB-band was not detected.

The excitation power dependence of the PL peak at 1.76 eV is shown in Fig. 5. The blue shift of the BT-band with the magnitude of about 19 meV per decade was detected. This confirms that the observed emission results from BT recombination together with the bandgap fluctuations [6,10].

The detailed theoretical discussion of these results is beyond the scope of this paper and will be presented in the near future.

4. Conclusions

The photoluminescence properties of the ordered defect compound $CuGa_3Se_5$ have been studied. Broad asymmetric PL band at 1.76 eV, resulting from BT-type recombination, has been detected. The shape and the properties of this PL band were explained assuming the coexistence of compositional fluctuations and the potential fluctuations due to high concentration of charged defects. The energy-dispersive X-ray analysis confirmed the variation of composition in the samples.

Acknowledgement

This work was supported by INTAS grant nr. 03-51-6314 and by the Estonian Science Foundation grant G-6554.

References

[1] S.B. Zhang, S.H. Wei, A. Zunger, Phys. Rev. B 57 (1998) 9642.
[2] G. Marin, C. Rincon, S.M. Wasim, G. Sanchez Perez, I. Molina, J. Alloys Compd. 283 (1999) 1.
[3] C. Rincon, S.M. Wasim, G. Marin, E. Hernandez, G. Sanchez Perez, J. Galibert, J. Appl. Phys. 87 (2000) 2293.
[4] F. Guastavino, K. Zeaiter, L. Djellal, Yanuar, D. Bayaa, M. Abdelali, C. Llinares, Solid State Phenom. 67–68 (1999) 427.
[5] J. Krustok, H. Collan, M. Yakushev, K. Hjelt, Phys. Scr. T79 (1999) 179.
[6] J. Krustok, J. Raudoja, M. Yakushev, R.D. Pilkington, H. Collan, Phys. Status Solidi 173 (1999) 483.
[7] A. Jagomägi, J. Krustok, J. Raudoja, M. Grossberg, M. Danilson, M. Yakushev, Physica B 337 (2003) 369.
[8] N.S. Orlova, I.V. Bodnar, T.L. Kushner, J. Phys. Chem. Solids 64 (2003) 1895.
[9] S.M. Wasim, C. Rincon, G. Marin, R. Marquez, G. Sanchez Perez, R. Guevara, J.M. Delgado, L. Nieves, Mater. Res. Soc. Symp. Proc. 668 (2001) H1.2.1.
[10] A.P. Levanyuk, V.V. Osipov, Sov. Phys., Usp. 133 (1981) 443.
[11] B.I. Shklovskij, A.L. Efros, Electronic Properties of Doped Semiconductors, Springer, Berlin, 1984.
[12] J. Krustok, H. Collan, K. Hjelt, J. Appl. Phys. 81 (1997) 1442.
[13] J. Krustok, A. Jagomägi, M. Grossberg, J. Raudoja, M. Danilson, Solar Energy Mater. Solar Cells 90 (2006) 1973.

PAPER II

M. Grossberg, J. Krustok, I. Bodnar, S. Siebentritt, J. Albert. Photoluminescence and Raman spectra of the ordered vacancy compound $CuGa_5Se_8$. *Physica B : Condenced Matter* 403 (2008) 184-189.

Available online at www.sciencedirect.com
ScienceDirect
Physica B 403 (2008) 184–189
PHYSICA B
www.elsevier.com/locate/physb

Photoluminescence and Raman spectra of the ordered vacancy compound $CuGa_5Se_8$

M. Grossberg[a,*], J. Krustok[a], I. Bodnar[b], S. Siebentritt[c], J. Albert[d]

[a]*Tallinn University of Technology, Ehitajate tee 5, 19086 Tallinn, Estonia*
[b]*Department of Chemistry, Belarussian State University of Informatics and Radioelectronics, P. Brovka str. 6, 220027 Minsk, Belarus*
[c]*Université du Luxembourg, 162a avenue de la Faïencerie, L-1511, Luxembourg*
[d]*Hahn-Meitner Institut, Glienicker Straße 100, 14109 Berlin, Germany*

Received 10 July 2007; received in revised form 16 August 2007; accepted 22 August 2007

Abstract

We studied the photoluminescence (PL) and Raman properties of the ordered defect compound $CuGa_5Se_8$. Twelve peaks were detected from the room-temperature Raman spectra with the A_1 mode around 160 cm^{-1}. Due to the stress in the polycrystalline thin film the corresponding frequencies of the Raman modes of a $CuGa_5Se_8$ single crystal were slightly shifted. One broad asymmetric PL band at 1.788 and 1.765 eV was observed at 10 K in the PL spectra of $CuGa_5Se_8$ single crystal and polycrystalline layer, respectively. The temperature and laser power dependencies of the PL spectra were also studied. The shape and properties of the PL band assure the presence of potential fluctuations and the analyses of the PL data suggest that the emission is due to band-to-tail (BT) or band-to-impurity (BI) recombination.

PACS: 71.20.Nr; 78.55.−M; 78.30.−J

Keywords: $CuGa_5Se_8$; Chalcopyrite crystals; Raman spectroscopy; Photoluminescence; Ordered defect compounds; Potential fluctuations

1. Introduction

One of the reasons why ternary chalcopyrite compounds are interesting is their toleration of a large range of anion to cation off-stoichiometry that leads to the existence of a number of ordered defect compounds [1]. It is reported that solar cells with the efficiency around 19% have been produced [2] using thin films based on $CuIn(Ga)Se_2$. The ordered defect compound $CuIn_3Se_5$ that precipitates as a secondary phase on the thin film surface of In-rich $CuInSe_2$ [3] is expected to improve the efficiency of such cells. Apart form $CuIn_3Se_5$, other In-rich phases like $CuIn_5Se_8$ and Ga-rich phases $CuGa_3Se_5$ and $CuGa_5Se_8$ have been reported [4,5] in the Cu_2Se–In_2Se_3 and Cu_2Se–Ga_2Se_3 quasi-binary systems, respectively. These compounds are called ordered vacancy compunds (OVCs), because vacancies are expected to orderly occupy particular crystallographic sites in their crystal structure to satisfy the four electrons per site rule [6]. They are also referred to as ordered defect compounds (ODCs) since Zhang et al. [1] have explained the existence and stability of these compounds with the presence of $(In_{Cu}^{2+} + 2V_{Cu}^{-1})$ donor–acceptor defect pairs (DADPs) that have very low formation energies.

In this paper we present the results of Raman and photoluminescence studies of $CuGa_5Se_8$. To our knowledge, very little work on the physical properties of $CuGa_5Se_8$ appear in the literature and there are no photoluminescence studies of $CuGa_5Se_8$ published. The temperature dependence of the energy gap in bulk samples of $CuGa_5Se_8$ have been reported by Marin et al. [5]. It was found that the bandgap energy varies from 1.917 to 1.811 eV in the temperature range between 10 and 300 K. Xu et al. [7] have investigated Raman spectra of $Cu(In_{1-x}Ga_x)_5Se_8$ thin films with varying x. To our knowledge, this is the only Raman spectrum of $CuGa_5Se_8$

*Corresponding author. Tel.: +372 6203210; fax: +372 6203367.
E-mail address: mgross@staff.ttu.ee (M. Grossberg).

0921-4526/$ - see front matter © 2007 Elsevier B.V. All rights reserved.
doi:10.1016/j.physb.2007.08.098

in the literature. From room-temperature Raman measurements they found seven peaks at 78, 93, 107, 160, 259 and 289 cm^{-1}, the peak at 160 cm^{-1} being the dominant A_1 mode of $CuGa_5Se_8$. However, no fitting of the spectra have been performed and no more detailed identification or assignment of the observed peaks has been made. Orlova et al. [8,9] have investigated the structural parameters, the axial thermal expansion coefficients and the characteristic Debye temperature of the $CuGa_5Se_8$ single crystals by using X-ray diffraction method. The unit cell parameters $a = 0.54682$ nm and $c = 1.09116$ nm were determined. It was also found that $CuGa_5Se_8$ has very close to $CuGa_3Se_5$ value of thermal expansion coefficient. There is also only a small difference in the crystal lattice parameters of these compounds. These properties of OVC compounds are essential for obtaining the high-quality epitaxial layers, for forming heterojunctions and for producing solar cells based on these ternary compounds. Leon et al. [10] have studied $CuGa_5Se_8$ by spectroscopic ellipsometry and determined the dielectric-function-related optical constants, such as the complex refractive index, extinction coefficient, absorption coefficient and normal-incidence reflectivity.

In order to understand the role of the ordered vacancies, we studied the photoluminescence and Raman spectra of $CuGa_5Se_8$ polycrystalline thin films and single crystals. To identify the observed Raman modes, the data obtained are compared with Raman spectra of $CuGa_5Se_8$ thin films reported in the literature [7].

2. Experimental methods

The MOCVD grown $CuGa_5Se_8$ polycrystalline thin films and single crystals grown by the vertical Bridgman method used in the present study exhibit compositions very close to its ideal value of 1:5:8 as measured by energy dispersive X-ray spectroscopy (EDX). The $CuGa_5Se_8$ thin films are grown in an Aixtron AIX200 MOCVD reactor on GaAs substrates. Cyclopentadienyl–copper, triethyl–gallium and ditertiary-butyl–selenide were used as Cu-, Ga- and Se-precursor, respectively. The growth process was derived from the process for $CuGaSe_2$ [11]. The growth temperature 570 °C was used and the reactor pressure was kept at 50 mbar. The processing time was 4 h. The dependence of the composition ratio on the partial pressure ratio was not linear. From the SEM images the polycrystallinity of the films was detected. The $CuGa_5Se_8$ single crystals were grown by the horizontal Bridgman method. The directed crystallization of the melt was performed by cooling of the furnace of the hot-zone up to ~1170 K at a rate of ~2 K h^{-1}. For more growth details of see Ref. [9].

The photoluminescence and room-temperature Raman spectra were recorded by using a Horiba's LabRam HR high resolution spectrometer equipped with a multichannel detection system in the backscattering configuration. In micro-Raman measurements, the incident laser light with the wavelength of 532 nm can be focused on the sample within a spot of 1 μm in diameter and the spectral resolution of the spectrometer is about 0.5 cm^{-1}. For photoluminescence measurements, the samples were mounted in the closed-cycle He cryostat and cooled down to 10 K. The 441.6 nm He–Cd laser line was used for photoluminescence excitation.

3. Experimental results and discussion

3.1. Raman results

The chalcopyrite crystal $A^IB^{III}C_2^{VI}$, with space group $I\bar{4}2d$, has eight atoms per primitive cell. $CuGa_5Se_8$ crystallizes in a chalcopyrite-related structure. To our knowledge, the space group of $CuGa_5Se_8$ has not yet been published. Marin et al. [6] made an assumption that $CuGa_5Se_8$ crystallizes in space group $P\bar{4}2m$ like $AgIn_5Se_8$. The unit cell parameters of $CuGa_5Se_8$ are very close to the unit cell parameters of $CuGaSe_2$. So it is expected that its vibrational spectra is very similar to the chalcopyrite one. Its vibrational spectrum consists of 24 zone-center vibrational modes:

$$1A_1 + 2A_2 + 3B_1 + 4B_2 + 7E,$$

where the E-modes are doubly degenerated. These modes are classified into three acoustic ($B_2 + E$) and 21 optical modes ($1A_1 + 2A_2 + 3B_1 + 3B_2 + 6E$). Except for two silent modes ($2A_2$), there are 22 Raman active modes:

$$1A_1 + 3B_1 + 3B_2(LO) + 3B_2(TO) + 6E(LO) + 6E(TO).$$

Correct assignment of the lattice vibrations is of great importance for a fundamental understanding of the structural properties of chalcopyrites. However, this is not always an easy task, because of the difficulties in growing high quality bulk crystals, the great variety of defects in the chalcopyrite materials and its dependence on a deviation from stoichiometry.

The Raman spectrum of the MOCVD grown $CuGa_5Se_8$ layer with the fitting result are shown in Fig. 1. The Bridgman grown $CuGa_5Se_8$ single crystal showed very

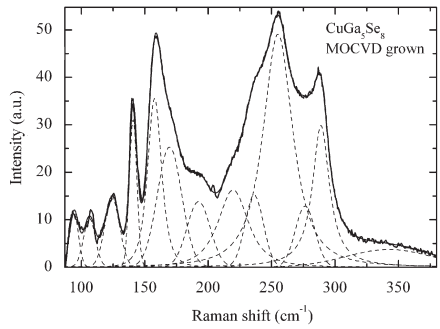

Fig. 1. The room-temperature Raman spectra of MOCVD grown $CuGa_5Se_8$ polycrystalline layer and the result of fitting. Twelve peaks were detected from the spectra. The peak at 93 cm^{-1} is due to the cut-off of the filter and is not taken into account.

similar spectrum. Because of the slightly asymmetric shape of Raman peaks, each peak was fitted using Pearson VII function [12]. Twelve peaks were detected from these spectra. For comparison, Raman peak positions and possible mode assignments, as discussed in the following are listed in Table 1. It is seen from the table, that the A_1 peak at $161\,cm^{-1}$ of a $CuGa_5Se_8$ single crystal is shifted to higher wavenumbers by $3\,cm^{-1}$ compared to the A_1 peak position at $158\,cm^{-1}$ of a $CuGa_5Se_8$ polycrystalline thin film. Negative and positive shifts attributed to the stress in the polycrystalline films can also be observed for other Raman modes.

According to the simplified version of Keating's model, the frequency of the A_1 mode v that results from the motion of the Se atom with the cations remaining at rest, is given by [13]

$$v \approx \sqrt{\frac{k}{M_{Se}}}, \tag{1}$$

where k is a force constant related to the cations–anion bond-stretching forces and M_{Se} is the mass of the Se atom. The vacancies present in OVCs tend to reduce the stretching forces, and thereby the corresponding vibrational frequencies. Since in first approximation the vibrational frequencies in chalcopyrites depend mainly on the interaction of the nearest neighbor atoms and taking also into account that only one vacancy exists for each four Se atoms in the OVC [1], it can be assumed that for the A_1 mode k is reduced by 25% as compared to its value in the normal chalcopyrite. Under this assumption, we can calculate the approximate value of the A_1 mode frequency v' of $CuGa_5Se_8$:

$$v' \approx \sqrt{\frac{0.75k}{M_{Se}}} \approx 0.87v, \tag{2}$$

where v is the A_1 mode frequency in $CuGaSe_2$. The frequency of the A_1 mode for $CuGaSe_2$ at room temperature is $184\,cm^{-1}$ [14], giving us the frequency of $161\,cm^{-1}$ for the A_1 mode in $CuGa_5Se_8$. The observed Raman peaks at 161 and $158\,cm^{-1}$ of a $CuGa_5Se_8$ single crystal and polycrystalline thin film, respectively, are in very good agreement with the theoretically expected value. The A_1 Raman mode of $CuGa_5Se_8$ at $160\,cm^{-1}$ was also observed in Ref. [7].

The B_1 modes involve the motion of the cations. Since the presence of ordered vacancies on Se sites is not expected to occur in these materials, the frequencies of these modes in OVC are expected to be very similar to that observed in $CuGaSe_2$ [15]. Thus, the mode at 117 and $124\,cm^{-1}$ in $CuGa_5Se_8$ single crystal and polycrystalline thin film, respectively, probably corresponds to the second-lowest frequency B_1 mode reported at $116\,cm^{-1}$ in $CuGaSe_2$ at 300 K [14]. The lowest frequency B_1 mode, whose corresponding values in $CuGaSe_2$ and $CuGa_3Se_5$ are 76 and $72\,cm^{-1}$ [16,17], respectively, is not observed in our spectrum due to the limitations of our experimental system. The highest frequency B_1 mode, which should be very weak because it corresponds to the motion of the cations in antiphase, is expected to be observed close to the A_1 peak. This mode has not yet been reported in $CuGa_3Se_5$ or $CuGa_5Se_8$ even at low temperatures.

The remaining modes should be assigned as B_2 and E modes that mostly correspond to the combined motion of all the atoms. Hence, by similar considerations given for the A_1 mode, it is expected that its frequencies are slightly lower than those observed in $CuGaSe_2$ [15]. Thus the peaks at around 255, 236, 220 and $192\,cm^{-1}$ in polycrystalline $CuGa_5Se_8$ and at 253, 235, 216 and $186\,cm^{-1}$ in a $CuGa_5Se_8$ single crystal, can be related to 273, 261, 239 and $199\,cm^{-1}$ in $CuGaSe_2$, respectively. The calculated

Table 1
Raman peak positions, obtained form the fitting, and possible mode assignments

Raman peak position (cm^{-1})					
MOCVD grown $CuGa_5Se_8$	Bridgman grown $CuGa_5Se_8$	$CuGaSe_2$, Ref. [14]	$CuGa_3Se_5$, Ref. [17]	$CuGa_5Se_8$, Ref. [7]	Possible origin
343	344	–	–	–	B_2+E
289	293	–	286	289	B_2+E
277	280	–	274	–	B_2
255	253	273	252	259	E
236	235	261	–	–	B_2 or E
220	216	239	220	–	E
–	–	–	200	–	E
192	186	199	187	–	B_2
170	168	–	–	–	B_2+E
158	161	184	166	160	A_1
141	142	–	142	–	E
124	117	116	–	–	B_1
106	99	96	105	107	E
–	–	–	90	93	B_1
–	–	–	72	78	B_1
–	–	60	64	–	B_2
–	–	–	48	–	E

ratio of each pair of corresponding frequencies in $CuGa_5Se_8$ and $CuGaSe_2$ ν'/ν varies from 0.90 to 0.94 which as also found for $CuGa_3Se_5$ Raman peaks in Ref. [15]. The peak at 141 cm^{-1} probably corresponds to E mode, reported at 142 cm^{-1} in $CuGa_3Se_5$ [17]. The peak around 289 cm^{-1} in $CuGa_5Se_8$ probably corresponds to a combination of the lowest-energy B_2 mode, which is expected to occur at around 53 cm^{-1}, and the E mode at 236 cm^{-1}. Similarly, the peak around 170 cm^{-1} in $CuGa_5Se_8$ probably corresponds to a combination of B and the E modes. Such combinations have also been observed in $CuGaSe_2$ and $CuGa_3Se_5$ [14,15].

We also observed the broadening of Raman peaks in $CuGa_5Se_8$ compared to $CuGaSe_2$. It is expected that high concentration of defects in OVCs leads to the formation of concentration fluctuations [7]. Such spatially extended effects caused by mixed defects and clusters can decrease the phonon lifetimes, which may be responsible for the broadening of Raman bands. This can be taken as an indication of a reduction in crystalline quality due to a large density of defects in $CuGa_5Se_8$.

3.2. Photoluminescence results

Only one broad asymmetric band at 1.788 and 1.765 eV was observed at 10 K in the PL spectra of Bridgman grown $CuGa_5Se_8$ single crystal and MOCVD grown polycrystalline layer, respectively (Fig. 2). PL band positions are at much lower energies compared to the bandgap energy of $CuGa_5Se_8$ ($E_g = 1.811$ eV at 300 K and $E_g(0) \approx 1.917$ eV [6]). Similar spectrum was obtained for $CuGa_3Se_5$ [18]. The asymmetric shape and the position of the PL band suggest that there are Coulomb potential fluctuations induced due to the random distribution of unscreened charged defects present in our samples. These potential fluctuations will lead to a local perturbation of the band structure, thus broadening the defect level distribution and forming band tails [18,19]. Radiative recombination in such crystals is

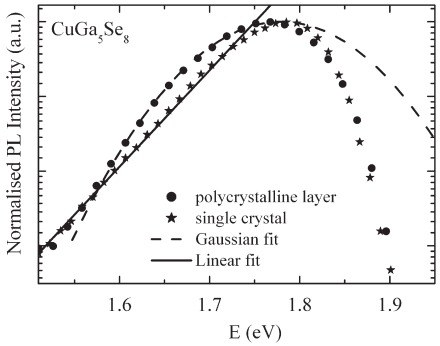

Fig. 2. Normalized PL spectra of polycrystalline and single crystal $CuGa_5Se_8$ at 10 K. The lines represent the fittings of the low-energy side of the PL bands. The polycrystalline and single crystal $CuGa_5Se_8$ showed Gaussian and exponential spectral dependence of the low-energy tail of emission, respectively.

therefore governed by the recombination of carriers localized in spatially separated potential wells originating from Coulomb potential fluctuations. The analysis of the PL data suggests that the emission is due to band-to-tail (BT) or band-to-impurity (BI) recombination, because both emissions show very similar behavior [20].

Siebentritt et al. [21] have analyzed the shape of the band tails in case of fluctuating potentials using two different models. According to them, the low-energy tail of PL emissions can be described by a Gaussian or an exponential spectral dependence. This based on the more general theoretical analysis of the density of states function by Osipov and Levanyuk [22]. The low-energy sides of the PL band of the $CuGa_5Se_8$ samples analyzed in the present paper showed Gaussian shape and exponential decay for the polycrystal and single crystal, respectively. It is an indication of the presence of deeper fluctuations with the Gaussian shape density of states function in polycrystal while the density of states function in the band tails of a single crystal has an exponential distribution. Deeper potential fluctuations in $CuGa_5Se_8$ polycrystal also explain the shift of the PL band position towards lower energies compared to the single crystal. Like in Ref. [21], the average amplitudes of the fluctuations $\gamma = 62$ and 113 meV for the $CuGa_5Se_8$ single crystal and polycrystal, respectively, were determined from the exponential and Gaussian spectral dependencies, respectively [22]:

$$I(E) \sim \exp\left(-\frac{E}{\gamma}\right) \quad \text{or} \quad I(E) \sim \exp\left(-\frac{(E-E_0)^2}{2\gamma^2}\right), \tag{3}$$

where E_0 is assumed to represent an average emission energy in the case of fluctuating potentials.

Excitation power and temperature dependent (Figs. 3 and 4) photoluminescence measurements indicate that our spectra are dominated by the BT-type recombination that involves free electron and a hole that is localized in the valence band tail [22]. Although other models can be used, we follow in our discussion here the arguments and the nomenclature used there. Due to their small effective mass, almost all electrons are free. Holes are localized in the valence band potential wells and form so-called pseudo-acceptor states. The activation energy of the thermal quenching of the PL band allows us to evaluate the average depth of these pseudo-acceptor states. From Arrhenius plot of thermal quenching of the PL band (Fig. 3), we obtained an estimation of thermal activation energy of pseudo-acceptor states 40 ± 8 and 168 ± 5 meV for single crystal and polycrystalline $CuGa_5Se_8$, respectively. The $ln\, I(T)$ versus $1000/T$ dependence was fitted with theoretical expression for discrete energy levels proposed in [23]

$$\Phi(T) = \frac{\Phi_0}{1 + \alpha_1 T^{3/2} + \alpha_2 T^{3/2} \exp(-E_T/kT)}, \tag{4}$$

where Φ is integrated intensity, α_1 and α_2 are the process rate parameters and E_T is the thermal activation energy. Despite the similarity between the experimental and theoretical dependencies, it is clear that in the case of BT

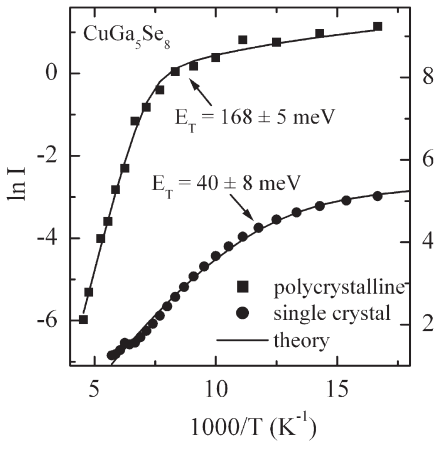

Fig. 3. Arrhenius graph of $CuGa_5Se_8$ single crystal and polycrystalline layer obtained from the temperature dependence of the PL spectra. Solid lines represent the fitting of the experimental data with the theoretical expression (4). Thermal activation energies of 168 and 40 meV were obtained for polycrystalline and single crystal $CuGa_5Se_8$, respectively.

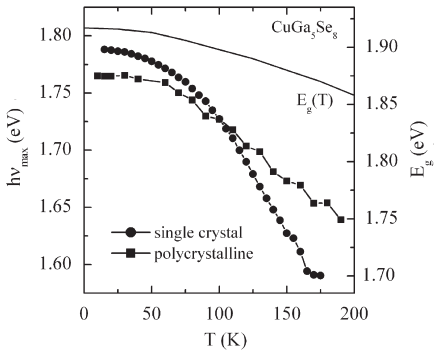

Fig. 4. Temperature dependence of the PL band peak position. Solid line represents the temperature dependence of the bandgap energy E_g of $CuGa_5Se_8$ [6].

type recombination, the fitting is not completely valid due to continuous tail states.

Higher thermal activation energy in $CuGa_5Se_8$ polycrystalline film is probably related to the coexistence of BT- and BI-type recombination in the sample, the latter being related to a deeper acceptor level. The Gaussian shape of the low-energy tail of PL emission supports this idea.

In Fig. 4 the temperature dependence of the PL band peak position along with the bandgap energy E_g of $CuGa_5Se_8$ [6] is shown. The peak position energy decreasing rate exceeds the bandgap energy decreasing rate with temperature. This feature is predicted by the theory of heavily doped semiconductors [22] and was also observed in $CuGa_3Se_5$ [18]. More detailed analysis of the temperature dependence of PL band position in case of heavily doped materials can be found in Refs. [19,20].

From the excitation power dependence, the blue shift of the PL band with the magnitude of about 15 and 23 meV per decade for $CuGa_5Se_8$ single crystal and polycrystalline layer, respectively, was detected. This again confirms that the observed emission results from BT or BI recombination [22]. The observed shift is larger for the sample with deeper potential fluctuations, as predicted by the theory.

4. Conclusions

The Raman and PL properties of the ordered vacancy compound $CuGa_5Se_8$ have been studied. Twelve peaks were detected from the room-temperature Raman spectra with the A_1 mode around 160 cm^{-1}. One broad asymmetric PL band at 1.788 and 1.765 eV was observed at 10 K in the PL spectra of $CuGa_5Se_8$ single crystal and polycrystalline layer, respectively. The analyses of the PL data suggest that the emission is due to BT- or BI-type recombination, indicating the presence of potential fluctuations due to high concentration of charged defects.

Acknowledgments

This work was supported by INTAS Grant no. 03-51-6314 and by the Estonian Science Foundation Grant G-6554.

References

[1] S.B. Zhang, S.H. Wei, A. Zunger, H. Katayama-Yoshida, Phys. Rev. B 57 (1998) 9642.
[2] M.A. Contreras, B. Egaas, K. Ramanathan, J. Hiltner, A. Swartzlander, F. Hasoon, R. Noufi, Proc. Photovoltaic Res. Appl. 7 (1999) 311.
[3] D. Schmid, M. Ruckh, F. Grunwald, H.W. Schock, J. Appl. Phys. 73 (1993) 2902.
[4] S.H. Wei, S.B. Zhang, A. Zunger, Appl. Phys. Lett. 72 (1998) 3199.
[5] G. Marin, S.M. Wasim, C. Rincon, G. Sanchez Perez, P. Bocaranda, I. Molina, R. Guevara, J.M. Delgado, Appl. Phys. 95 (2004) 8280.
[6] G. Marin, J.M. Delgado, S.M. Wasim, C. Rincon, G. Sanchez Perez, A.E. Mora, P. Bocaranda, J.A. Henao, J. Appl. Phys. 87 (2000) 7814.
[7] C.-M. Xu, W.-H. Huang, J. Xu, X.-J. Yang, J. Zuo, X.-L. Xu, H.-T. Liu, J. Phys. Condens. Matter 16 (2004) 4149.
[8] N.S. Orlova, I.V. Bodnar, T.L. Kushner, Cryst. Res. Technol. 38 (2003) 125.
[9] N.S. Orlova, I.V. Bodnar, T.L. Kushner, J. Phys. Chem. Solids 64 (2003) 1895.
[10] M. Leon, R. Serna, S. Levcenko, A. Nateprov, A. Nicorici, J.M. Merino, E. Arushanov, Phys. Stat. Sol (A) 203 (2006) 2913.
[11] A. Bauknecht, S. Siebentritt, J. Albert, M.C. Lux-Steiner, J. Appl. Phys. 89 (2001) 4391.
[12] E.P. Petrov, J. Quant. Spectrosc. Radiat. Transfer 103 (2007) 272.
[13] H. Neumann, Helv. Phys. Acta 58 (1985) 337.
[14] F.J. Ramirez, C. Rincon, Solid State Commun. 84 (1992) 551.
[15] C. Rincon, S.M. Wasim, G. Marin, J.M. Delgado, J.R. Huntzinger, A. Zwick, J. Galibert, Appl. Phys. Lett. 73 (1998) 441.
[16] J. Gonzalez, J.C. Chervin, Jpn. J. Appl. Phys. 32 (Suppl.) (1993) 575.
[17] C. Rincon, S.M. Wasim, G. Marin, E. Hernandez, G. Sanchez Perez, J. Galibert, J. Appl. Phys. 87 (2000) 2293.
[18] M. Grossberg, J. Krustok, A. Jagomägi, M. Leon, E. Arushanov, A. Nateprov, I. Bodnar, Thin Solid Films 515 (2007) 6204.

[19] J. Krustok, H. Collan, M. Yakushev, K. Hjelt, Phys. Scripta (T) 79 (1999) 179.
[20] A. Jagomägi, J. Krustok, J. Raudoja, M. Grossberg, M. Danilson, M. Yakushev, Physica B 337 (2003) 369.
[21] S. Siebentritt, N. Papathanasiou, M.Ch. Lux-Steiner, Physica B 376–377 (2006) 831.
[22] A.P. Levanyuk, V.V. Osipov, Sov. Phys. Usp. 24 (1981) 187.
[23] J. Krustok, H. Collan, K. Hjelt, J. Appl. Phys. 81 (1997) 1442.

PAPER III

M. Grossberg, J. Krustok, S. Siebentritt, J. Albert. Compositional dependence of Raman scattering and photoluminescence emission in Cu-Ga-Se films grown by MOCVD, *Physica B: Condenced Matter* 404 (14-15) (2009) 1984-1988.

Physica B 404 (2009) 1984–1988

Contents lists available at ScienceDirect

Physica B

journal homepage: www.elsevier.com/locate/physb

Compositional dependence of Raman scattering and photoluminescence emission in Cu–Ga–Se films grown by MOCVD

M. Grossberg [a,*], J. Krustok [a], S. Siebentritt [b], J. Albert [c]

[a] Tallinn University of Technology, Ehitajate tee 5, 19086 Tallinn, Estonia
[b] Université du Luxembourg, 162a avenue de la Faïencerie, L-1511 Luxembourg
[c] Helmholtz Centre Berlin, Glienicker Straße 100, 14109 Berlin, Germany

ARTICLE INFO

Article history:
Received 2 February 2009
Received in revised form
25 February 2009
Accepted 20 March 2009

PACS:
78.30.Hv
78.55.Hx
61.72.Sd

Keywords:
Chalcopyrite crystals
Raman spectroscopy
Photoluminescence
Ordered defect compounds
Potential fluctuations

ABSTRACT

This paper presents Raman scattering and photoluminescence (PL) analysis of polycrystalline Cu–Ga–Se films grown epitaxially on the GaAs substrate. In the compositional dependence of the Raman spectra of the $CuGaSe_2$ films, the appearance of the ordered vacancy compounds (OVCs) $CuGa_3Se_5$ and $CuGa_5Se_8$ was observed. The dominating A_1 Raman modes were detected at 185, 166 and 159 cm^{-1}, respectively. The PL bands of $CuGaSe_2$, $CuGa_3Se_5$ and $CuGa_5Se_8$ at $T = 10$ K were detected at 1.615, 1.72 and 1.76 eV, respectively. The dominating PL emission channel is the band-to-tail (BT) type recombination.

1. Introduction

The wide bandgap ternary chalcopyrite compound $CuGaSe_2$ is a promising material for optoelectronic devices. In this paper we will present the results of compositional dependent Raman and photoluminescence (PL) studies on ternary chalcopyrite semiconductor $CuGaSe_2$ in an attempt to investigate the effect of the Ga addition on its structural and optical properties. It is known that ternary chalcopyrite compounds tolerate large range of anion to cation off-stoichiometry that leads to the existence of a number of ordered defect compounds (ODCs) [1]. Ga-rich phases $CuGa_3Se_5$ and $CuGa_5Se_8$ have been reported [2,3] in the Cu_2Se–Ga_2Se_3 quasi-binary system. These compounds are called ordered defect compounds since Zhang et al. [1] have explained the existence and stability of such compounds in the related Cu–In–Se system with the presence of $(In_{Cu}^{2+} + 2V_{Cu}^{-1})$ donor–acceptor defect pairs (DADPs) that have very low formation energies. These compounds are also referred to as ordered vacancy compounds (OVCs), because vacancies are expected to orderly occupy particular crystallographic sites in their crystal structure to satisfy the four electrons per site rule [4]. It is expected that the ordered defect compound $CuIn_3Se_5$ that precipitates as a secondary phase on the thin film surface of In-rich $CuInSe_2$ will improve the efficiency of $CuInSe_2$ based solar cells [5]. It is important to understand the effect of the ordered arrays of defects on the electrical and optical properties of opto-electronical devices, when one considers these compounds for photovoltaic applications.

There are several papers published about the Raman and PL properies of $CuGaSe_2$ [6–8]. However, little information can be found in the literature about the PL and Raman properties of OVCs in Cu–Ga–Se system. We have investigated the low-temperature PL properties of $CuGa_3Se_5$ single crystals and found one PL band at 1.76 eV resulting from band-to-tail (BT) type recombination [9], indicating the presence of potential and compositional fluctuations in the crystals. Rincon et al. [2] have investigated photoluminescence, infrared reflectivity and Raman spectra of $CuGa_3Se_5$. They found that the main PL emission at 1.63 eV is due to the donor–acceptor pair (DAP) recombination and estimated the donor and acceptor activation energies 15 and 300 meV, respectively. However, the asymmetric shape and the large blueshift of the PL band with increasing excitation intensity are in contradiction with the DAP recombination theory. We believe

* Corresponding author. Tel.: +372 620 3210; fax: +372 620 3367.
E-mail address: mgross@staff.ttu.ee (M. Grossberg).

0921-4526/$ - see front matter © 2009 Elsevier B.V. All rights reserved.
doi:10.1016/j.physb.2009.03.027

that the observed emission is related to the recombination involving the band tails as it was found in Ref. [9] for another PL band with similar properties in $CuGa_3Se_5$. They also combined the analysis of IR and Raman spectra and assigned the corresponding vibrational modes of $CuGa_3Se_5$. The most intense peak at 166 cm^{-1} was assigned to the A_1 mode. From the X-ray data, it has been established that $CuGa_3Se_5$ has a chalcopyrite-related structure that belongs to the space group $P\bar{4}2c$ and has unit cell parameters $a = 0.54995(8)$ nm and $c = 1.0946(3)$ nm [10].

To our knowledge, very little work on the optical properties of $CuGa_5Se_8$ appear in the literature and there is only one PL study of $CuGa_5Se_8$ published. We have investigated the PL properties of $CuGa_5Se_8$ [11] and found broad asymmetric bands at 1.788 and 1.765 eV at 10 K in the PL spectra of $CuGa_5Se_8$ single crystal and polycrystalline layer, respectively. The analyses of the PL data suggest that the emission is due to BT- or BI-type (band-to impurity) recombination, indicating the presence of potential fluctuations due to high concentration of charged defects. The temperature dependence of the energy gap in bulk samples of $CuGa_5Se_8$ have been reported by Marin et al. [12]. Xu et al. [2] have found seven peaks from room temperature Raman spectra of $CuGa_5Se_8$, the peak at 160 cm^{-1} being the dominant A_1 mode. Orlova et al. [13,14] have determined the unit cell parameters of $CuGa_5Se_8$ single crystals by using X-ray diffraction method: $a = 0.54682$ nm and $c = 1.09116$ nm. It was also found that $CuGa_5Se_8$ and $CuGa_3Se_5$ have very close values of thermal expansion coefficients and crystal lattice parameters. These properties of OVC compounds are essential for forming heterojunctions and for producing solar cells based on these ternary compounds.

2. Experimental methods

The Cu–Ga–Se thin films were grown in an Aixtron AIX200 MOCVD reactor on GaAs substrates. Cyclopentadienyl-copper, triethyl-gallium and ditertiary-butyl-selenide were used as Cu-, Ga- and Se-precursor, respectively. The growth process was derived from the process for $CuGaSe_2$ [7]. The growth temperature 570 °C was used and the reactor pressure was kept at 50 mbar during the processing time of 4 h. The dependence of the composition ratio on the partial pressure ratio was not linear. The ratio of Cu and Ga elemental compositions [Cu]/[Ga] varied from 1 to 0.19, as was determined by energy dispersive X-ray spectroscopy (EDX). Scanning electron microscopy (SEM) images of the samples showed the surface roughness and polycrystallinity of the Ga-rich films.

The room temperature Raman spectra were recorded by using a Horiba's LabRam HR high resolution spectrometer equipped with a multichannel detection system in the backscattering configuration. In micro-Raman measurements, the incident laser light with the wavelength of 532 nm is focused on the sample within a spot of 10 μm in diameter and the spectral resolution of the spectrometer is about 1.5 cm^{-1}. For PL measurements, the samples were mounted in the He cryostat and cooled down to 10 K. The 514 nm Ar^+ laser line was used for PL excitation.

3. Experimental results and discussion

3.1. Raman results

The chalcopyrite crystal $A^{I}B^{III}C_2^{VI}$ has eight atoms per primitive cell. Its vibrational spectrum consists of 24 zone-center vibrational modes:

$$1A_1 + 2A_2 + 3B_1 + 4B_2 + 7E,$$

where the E-modes are doubly degenerated. These modes are classified into 3 acoustic (B_2+E) and 21 optical modes ($1A_1$+$2A_2$+$3B_1$+$3B_2$+6E). Except for two silent modes ($2A_2$), there are 22 Raman active modes:

$$1A_1 + 3B_1 + 3B_2(LO) + 3B_2(TO) + 6E(LO) + 6E(TO).$$

A_1 mode is usually dominating the Raman spectra, because it involves only displacements of the anions with the cations remaining at rest [15]. The B_1 modes involve the motion of the cations and the B_2 and E modes correspond to the combined motion of all the atoms. The frequencies of the Raman modes are influenced by the great variety of defects in the chalcopyrite materials and deviation from stoichiometry. Therefore, for fundamental understanding of the structural properties of chalcopyrites, it is important to investigate their vibrational properties.

The compositional dependence of the room temperature Raman spectra of Cu–Ga–Se films is shown in Fig. 1. The appearance of $CuGa_3Se_5$ and $CuGa_5Se_8$ phases in the spectra of

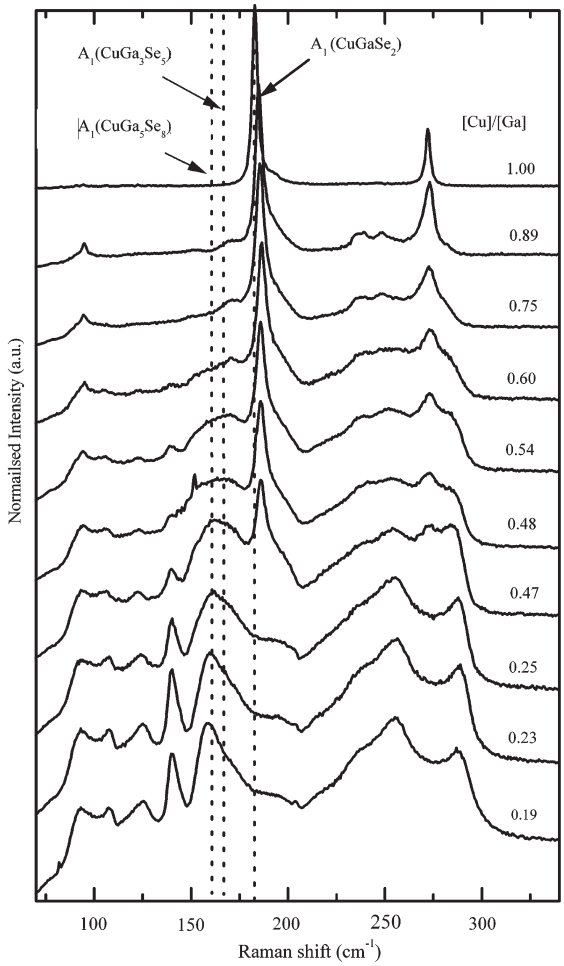

Fig. 1. Room temperature Raman spectra of Cu–Ga–Se films with different [Cu]/[Ga] ratios. The Raman peaks at 185, 166 and 159 cm^{-1} correspond to A_1 mode of $CuGaSe_2$, $CuGa_3Se_5$ and $CuGa_5Se_8$, respectively.

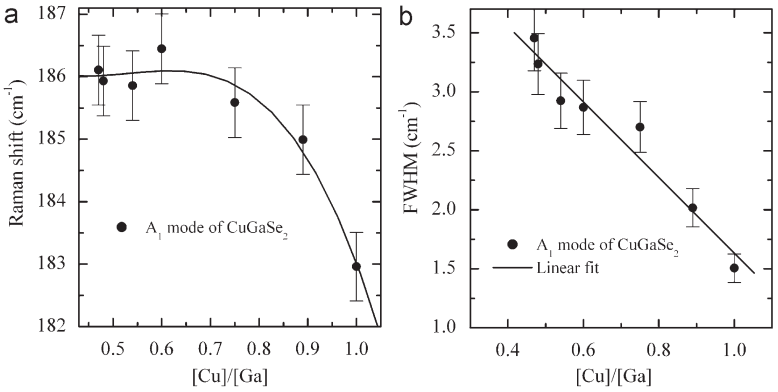

Fig. 2. Compositional dependence of the peak position of the A_1 Raman mode of $CuGaSe_2$ (a) and its FWHM (b).

$CuGaSe_2$ films is visible with decreasing [Cu]/[Ga] ratio. The dominating A_1 Raman peaks were detected at 185, 166 and 159 cm^{-1} for $CuGaSe_2$, $CuGa_3Se_5$ and $CuGa_5Se_8$, respectively. The presence of binary phases in the films was not detected from the spectra.

According to the simplified version of Keating's model [15], the frequency of the A_1 mode ν is given by $\nu \approx \sqrt{k/M_{Se}}$, where M_{Se} is the mass of the Se atom and k being the force constant related to the cation–anion bond-stretching forces. Due to the presence of the vacancy in the OVC the stretching forces are relaxed, thus reducing slightly the corresponding vibrational frequencies compared to chalcopyrites with 1:1:2 stoichiometry. Since in first approximation the vibrational frequencies in chalcopyrites depend mainly on the nearest neighbor atoms interaction [15] and taking also into account that one vacancy exists for each four and five Se atoms in $CuGa_5Se_8$ and $CuGa_3Se_5$, respectively, it was proposed in Ref. [16] that for the A_1 mode k is reduced by 25% and 20% for $CuGa_5Se_8$ and $CuGa_3Se_5$, respectively, as compared to its value in the normal chalcopyrites. Under this assumption, frequencies $\nu' \approx \sqrt{0.75k/M_{Se}} \approx 0.87\nu$ and $\nu' \approx \sqrt{0.8k/M_{Se}} \approx 0.89\nu$ of this mode, where ν is the frequency in the normal chalcopyrites, is to be expected for $CuGa_5Se_8$ and $CuGa_3Se_5$, respectively. The frequency of the A_1 mode for $CuGaSe_2$ at room temperature is 184 cm^{-1} [17], giving us the frequencies of 164 and 161 cm^{-1} for the A_1 mode in $CuGa_3Se_5$ and $CuGa_5Se_8$, respectively. The recorded A_1 mode frequencies were 185, 166 and 159 cm^{-1} for $CuGaSe_2$, $CuGa_3Se_5$ and $CuGa_5Se_8$, respectively. The obtained wavenumbers are in very good agreement with the theoretically expected values.

The A_1 mode frequency of $GuGaSe_2$ shows nonlinear shift to higher wavenumbers with the decrease of Cu content up to [Cu]/[Ga] = 0.47 (Fig. 2a). From the Raman spectra of films with lower [Cu]/[Ga] ratios only the presence of $CuGa_5Se_8$ phase was detected. Apart from the frequency, also the full width at half maximum (FWHM) of the A_1 Raman band of $CuGaSe_2$ (Fig. 2b) and all other modes is broadening with the increase of Ga content. Similar behavior has been observed in $CuIn_{1-x}Ga_xSe_2$ [18], $Cu(In_{1-x}Ga_x)_5Se_8$ [3] and $Cu(In_{1-x}Ga_x)_3Se_5$ [19] films. Differences in the degree of disorder and increasing defect concentration are believed to be responsible for the observed changes in Raman mode width as a function of the [Cu]/[Ga] ratio. Therefore, the broadening of the Raman bands can be an indication of a large defect density in the OVC's. The PL results presented below also show the increasing defect concentration with increase in Ga concentration.

The Raman modes of $CuGaSe_2$, $CuGa_3Se_5$ and $CuGa_5Se_8$ were also discussed in more detail in Refs. [2,11,17].

3.2. Photoluminescence results

According to Zhang et al. [1], the creation of periodic V_{Cu} reduces the Se p–Cu d interband repulsion in the OVC's, as compared to $CuInSe_2$. This effect lowers the valence band maximum of $CuIn_3Se_5$ and $CuIn_5Se_8$. This phenomenon has been observed also in $CuGaSe_2$ [20]. Although the defect pair $(III_{Cu}^{2+}+2V_{Cu}^{-})$ also lowers the conduction band minimum, the first effect predominates, because the p–d repulsion is very strong in the selenides of the OVC's [21]. Therefore the bandgap of OVC's is wider and the PL emission is observed at higher energies. The available published values of the room temperature bandgap energies of $CuGaSe_2$, $CuGa_3Se_5$ and $CuGa_5Se_8$ thin films and polycrystalline bulk samples are 1.64–1.70 eV [22,23], 1.74–1.87 eV [10,24–28] and 1.78–1.97 eV [12,22,27–29], respectively. The wide range of bandgap energies is, besides different crystallinity of the materials, probably related to the presence of Urbach's tail in the optical absorption spectra, making the precise bandgap determination somewhat complicated.

Fig. 3 shows low-temperature PL spectra of Cu–Ga–Se films with different [Cu]/[Ga] ratios, ranging from $0.19 \leqslant$ [Cu]/[Ga] $\leqslant 1.00$. The observed PL properties as a function of [Cu]/[Ga] ratio can be summarized as follows:

1. [Cu]/[Ga] = 1: Stoichiometric $CuGaSe_2$ film shows PL peak at 1.615 eV. It was proposed in Ref. [6] that PL band at 1.617 eV originates from the band-tail recombination.
2. $0.6 \leqslant$ [Cu]/[Ga] $\leqslant 1$: The PL spectra of Cu-poor $CuGaSe_2$ films show single broad emission band with an asymmetric line-shape. It has an exponential slope on the low-energy side and steeper Gaussian incline on the high-energy side. With increasing Ga content the emission band broadens and shows redshift. This behavior indicates that due to high concentration of native defects resulting from the off-stoichiometry of the films, there are potential fluctuations present in these Cu-poor films as has been observed before. It was proposed in Ref. [7] that this emission results from so-called quasi-DAP transition. The theory of radiative recombination mechanisms in case of Coulomb potential fluctuations can be found in Ref. [30].
3. $0.47 \leqslant$ [Cu]/[Ga] $\leqslant 0.54$: New band at around 1.72 eV appears in the PL spectra. This band originates from the $CuGa_3Se_5$ phase.

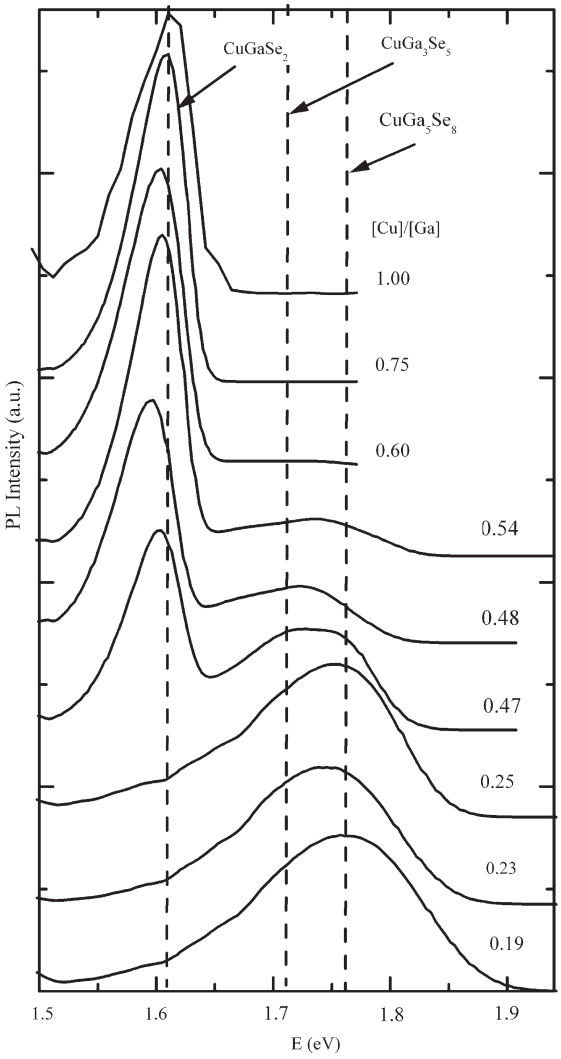

Fig. 3. Compositional dependence of PL spectra of Cu–Ga–Se films at 10 K. The PL bands of $CuGaSe_2$, $CuGa_3Se_5$ and $CuGa_5Se_8$ were detected at 1.615, 1.72 and 1.76 eV, respectively. Predicted peak positions for different phases are indicated by dashed lines.

Unfortunately we were unable to grow pure $CuGa_3Se_5$ films. Similarly to the PL band from Cu-poor $CuGaSe_2$, the band at 1.72 eV results from radiative recombination governed by the recombination of carriers localized in spatially separated potential wells originating from Coulomb potential fluctuations. The PL properties of $CuGa_3Se_5$ are discussed in more detail in Ref. [9], where it is proposed that this emission results from the BT -type recombination. The film with $[Cu]/[Ga] = 0.47$ shows a shoulder around 1.76 eV that originates from the $CuGa_5Se_8$ phase. The corresponding Raman spectra also show the coexistence of $CuGaSe_2$ and related ordered defect phases $CuGa_3Se_5$ and $CuGa_5Se_8$.

4. $0.19 \leqslant [Cu]/[Ga] \leqslant 0.25$: The $CuGaSe_2$ phase is no longer present in the samples as can also be seen from the Raman spectra of the films with these compositions. The Ga-rich films show only broad asymmetric emission from $CuGa_5Se_8$ that results similarly to the emission of $CuGa_3Se_5$ films from BT- or BI-type recombination as was proposed in Ref. [11], where more detailed discussion the PL properties of $CuGa_5Se_8$ can be found.

4. Conclusions

In conclusion, the compositional dependence of the Raman and PL properties of polycrystalline Cu–Ga–Se films was studied. The appearance of the OVCs $CuGa_3Se_5$ and $CuGa_5Se_8$ was observed in the Raman and PL spectra of $CuGaSe_2$ films with increasing Ga concentration. The A_1 Raman modes were detected at 185, 166 and 159 cm^{-1}, respectively. The broadening of the Raman modes with increasing Ga concentration was detected and it was assigned to the increasing defect concentration in the films. The PL bands of $CuGaSe_2$, $CuGa_3Se_5$ and $CuGa_5Se_8$ were detected at 1.615, 1.72 and 1.76 eV, respectively, at 10 K. The photoluminescence analysis showed the presence of potential fluctuations in the Cu–Ga–Se films.

Acknowledgments

This work was supported by INTAS Grant no. 03-51-6314 and by the Estonian Science Foundation Grants G-6554. The support of the World Federation of Scientists National Scholarship Programme is gratefully acknowledged.

References

[1] S.B. Zhang, S.H. Wei, A. Zunger, H. Katayama-Yoshida, Phys. Rev. B 57 (1998) 9642.
[2] C. Rincon, S.M. Wasim, G. Marin, E. Hernandez, G. Sanchez Perez, J. Galibert, J. Appl. Phys. 87 (2000) 2293.
[3] C.M. Xu, W.H. Huang, J. Xu, X.J. Yang, J. Zuo, X.L. Xu, H.T. Liu, J. Phys. Condens. Matter 16 (2004) 4149.
[4] G. Marin, J.M. Delgado, S.M. Wasim, C. Rincon, G. Sanchez Perez, A.E. Mora, P. Bocaranda, J.A. Henao, J. Appl. Phys. 87 (2000) 7814.
[5] D. Schmid, M. Ruckh, F. Grunwald, H.W. Schock, J. Appl. Phys. 73 (1993) 2902.
[6] J. Krustok, J. Raudoja, M. Yakushev, R.D. Pilkington, H. Collan, Phys. Stat. Sol. (a) 173 (1999) 483.
[7] A. Bauknecht, S. Siebentritt, J. Albert, M.Ch. Lux-Steiner, J. Appl. Phys. 89 (2001) 4391.
[8] D. Papadimitriou, N. Esser, C. Xue, Phys. Stat. Sol. (b) 242 (2005) 2633.
[9] M. Grossberg, J. Krustok, A. Jagomägi, M. Leon, E. Arushanov, A. Nateprov, I. Bodnar, Thin Solid Films 515 (2007) 6204.
[10] G. Marin, S. Tauleigne, S.M. Wasim, R. Guevara, J.M. Delgado, C. Rincon, A.E. Mora, G. Sanchez Perez, MRS Bull. 33 (1998) 1057.
[11] M. Grossberg, J. Krustok, I. Bodnar, S. Siebentritt, J. Albert, Physica B 403 (2008) 184.
[12] G. Marin, S.M. Wasim, C. Rincon, G. Sanchez Perez, P. Bocaranda, I. Molina, R. Guevara, J.M. Delgado, J. Appl. Phys. 95 (2004) 8280.
[13] N.S. Orlova, I.V. Bodnar, T.L. Kushner, Cryst. Res. Technol. 38 (2003) 125.
[14] N.S. Orlova, I.V. Bodnar, T.L. Kushner, J. Phys. Chem. Solids 64 (2003) 1895.
[15] H. Neumann, Helv. Phys. Acta 58 (1985) 337.
[16] C. Rincon, S.M. Wasim, G. Marin, J.M. Delgado, J.R. Huntzinger, A. Zwick, J. Galibert, J. Appl. Phys. Lett. 73 (1998) 441.
[17] F.J. Ramirez, C. Rincon, Solid State Commun. 84 (1992) 551.
[18] S. Roy, P. Guha, S.N. Kundu, H. Hanzawa, S. Chaudhuri, A.K. Pal, Mater. Chem. Phys. 73 (2002) 24.
[19] C.M. Xu, X.L. Xu, J. Xu, X.J. Yang, J. Zuo, X.M. Dang, Y. Feng, W.H. Huang, H.T. Liu, Chin. J. Semicond. 24 (2003) 1057.
[20] S.M. Wasim, C. Rincon, G. Marin, R. Marquez, G. Sanchez Perez, R. Guevara, J.M. Delgado, L. Nieves, Mat. Res. Soc. Symp. Proc. 668 (2001) H1.2.1.
[21] J.E. Jaffe, A. Zunger, Phys. Rev. B 29 (1984) 1882.
[22] S.M. Wasim, C. Rincon, G. Marin, J.M. Delgado, Appl. Phys. Lett. 77 (2000) 94.
[23] S. Chichibu, T. Mizutani, K. Murakami, T. Shioda, T. Kurafuji, H. Nakanishi, S. Niki, P.J. Fons, A. Yamada, J. Appl. Phys. 83 (1998) 3678.
[24] T. Negami, N. Kohara, M. Nishitani, T. Wada, T. Hirao, Appl. Phys. Lett. 67 (1995) 825.

[25] G. Marin, C. Rincon, S.M. Wasim, G. Sanchez Perez, I. Molina, J. Alloys Compd. 283 (1999) 1.
[26] C. Rincon, S.M. Wasim, G. Marin, I. Molina, J. Appl. Phys. 93 (2003) 780.
[27] G. Marin, R. Marquez, R. Guevara, S.M. Wasim, J.M. Delgado, C. Rincon, G. Sanchez Perez, I. Molina, P. Bocaranda, Jpn. J. Appl. Phys. 39 (2000) 44.
[28] M. Leon, S. Levcenko, A. Nateprov, A. Nicorici, J.M. Merino, R. Serna, E. Arushanov, J. Phys. D 40 (2007) 740.
[29] L. Duran, S.M. Wasim, C.A. Durante Rincon, E. Hernandez, C. Rincon, J.M. Delgado, J. Castro, J. Contreras, Phys. Stat. Sol. (a) 199 (2003) 220.
[30] A.P. Levanyuk, V.V. Osipov, Sov. Phys. Usp. 24 (1981) 187.

PAPER IV

M. Grossberg, J. Krustok, K. Timmo, M. Altosaar. Radiative recombination in $Cu_2ZnSnSe_4$ monograins studied by photoluminescence spectroscopy, *Thin Solid Films* 517 (2009) 2489-2492.

Thin Solid Films 517 (2009) 2489–2492

Contents lists available at ScienceDirect

Thin Solid Films

journal homepage: www.elsevier.com/locate/tsf

Radiative recombination in $Cu_2ZnSnSe_4$ monograins studied by photoluminescence spectroscopy

M. Grossberg *, J. Krustok, K. Timmo, M. Altosaar

Tallinn University of Technology, Ehitajate tee 5, 19086 Tallinn, Estonia

ARTICLE INFO

Available online 8 November 2008

Keywords:
$Cu_2ZnSnSe_4$
Photoluminescence
Raman spectroscopy

ABSTRACT

In this study we investigated the optical properties of $Cu_2ZnSnSe_4$ monograin powders that were synthesized from binary compounds in the liquid phase of flux material (KI) in evacuated quartz ampoules. The monograin powder had p-type conductivity. Radiative recombination processes in $Cu_2ZnSnSe_4$ monograins were studied using photoluminescence spectroscopy. The detected low-temperature (T=10 K) photoluminescence band at 0.946 eV results from band-to-impurity recombination in $Cu_2ZnSnSe_4$. The ionization energy of the corresponding acceptor defect was found to be 69±4 meV. Additional photoluminescence bands detected at 0.765 eV, 0.810 eV and 0.860 eV are proposed to result from Cu_2SnSe_3 phase whose presence in the as-grown monograins was detected by Raman spectroscopy and SEM analysis. Considering photoluminescence results, it is proposed that the optical bandgap energy of $Cu_2ZnSnSe_4$ is around 1.02 eV at 10 K.

1. Introduction

Lately, quaternary semiconductors $Cu_2ZnSnSe_4$, Cu_2ZnSnS_4, $Cu_2CdSnSe_4$ have attracted lot of attention as possible absorber materials for solar cells. These materials have optimal direct bandgap for solar energy conversion and high absorption coefficient ($>10^4$ cm^{-1}) [1]. They are believed to be suitable alternatives for $CuInSe_2$ absorbers that contain expensive In.

There are some difficulties in determining the bandgap energy of $Cu_2ZnSnSe_4$ (CZTSe) due to the formation of secondary phases in low temperature growth. Matsushita et al. [2] have determined the bandgap value of 1.44 eV for CZTSe from optical absorption measurements. Yasuda et al. [3] obtained bandgap energy of 1.40 eV for CZTSe. On the other hand, Raulot et al. [4] have performed *ab initio* calculation of electronic structure of CZTSe and found bandgap around 0.8 eV. In our previous paper [5], it was proposed based on the quantum efficiency curves of the CZTSe monograin layer solar cells that CZTSe has lower bandgap energy than proposed by the authors mentioned above. According to the additional quantum efficiency and photoluminescence measurements, the bandgap energy of CZTSe is expected to be in the vicinity of 1 eV.

Only a little information about the defect structure of $Cu_2ZnSnSe_4$ can be found in the literature. Raulot et al. [4] have studied the defect formation energies of CZTSe. The lowest formation energy was found for V_{Cu} that can be considered as dominating defect in CZTSe. We have previously published photoluminescence (PL) spectrum of CZTSe that consisted of one PL band at 0.85 eV [5], however the detailed analysis was not made. In this paper, we study the defect structure of $Cu_2ZnSnSe_4$ using photoluminescence spectroscopy.

2. Experimental

The $Cu_2ZnSnSe_4$ monograins were synthesized from CuSe, ZnSe and SnSe precursors in molten KI at 720 °C. More details about the synthesis can be found in Ref. [5]. The obtained material consisted of around 100 μm grain size powder crystals with tetragonal shape and rounded grain edges. The chemical composition of monograin powders was determined by the energy dispersive X-ray spectroscopy (EDS). The monograins had p-type conductivity. In order to increase the quality of the monograins, vacuum annealing was performed to the crystals. Comparison of the PL properties of the two as-grown (samples a and b with different compositions) and annealed CZTSe (sample b*) monograins is discussed (see the compositional details of the samples in Table 1).

The room temperature Raman spectra were recorded by using a Horiba's LabRam HR high resolution spectrometer equipped with a multichannel CCD detection system in the backscattering configuration. In micro-Raman measurements, the incident laser light with the wavelength of 532 nm can be focused on the sample within a spot of 10 μm in diameter. For PL measurements, the samples were mounted in the closed-cycle He cryostat and cooled down to 10 K. The 441 nm He–Cd laser line was used for PL excitation.

3. Results and discussion

The room-temperature Raman spectra of two as-grown CZTSe monograin powders and an annealed monograin powder are presented in

* Corresponding author. Tel.: +372 6203210; fax: +372 6203367.
E-mail address: mgross@staff.ttu.ee (M. Grossberg).

0040-6090/$ – see front matter © 2008 Elsevier B.V. All rights reserved.
doi:10.1016/j.tsf.2008.11.024

Table 1
Summary of the results obtained from the PL analysis of CZTSe monograins

PL band position	Recombination mechanism	Thermal activation energy (meV)	Origin	Sample
0.946 eV	BI	69±4	CZTSe	Annealed CZTSe [Zn]/[Sn] = 0.96, sample b*
0.860 eV	BB	–	Cu_2SnSe_3	as-grown CZTSe [Zn]/[Sn] = 1.03, sample a
0.810 eV	BI	44±5	Cu_2SnSe_3	as-grown CZTSe [Zn]/[Sn] = 0.96, sample b
0.765 eV	DAP	26±6	Cu_2SnSe_3	as-grown CZTSe [Zn]/[Sn] = 1.03, sample a

Fig. 1. In the spectra of as-grown CZTSe (Raman modes at 167 cm^{-1}, 173 cm^{-1}, 196 cm^{-1}, 231 cm^{-1}, and 245 cm^{-1}) the presence of additional Cu_2SnSe_3 phase was detected (Raman peak at 180 cm^{-1}). The frequencies of the A_1 Raman modes of Cu_2SnSe_3 and CZTSe are 180 cm^{-1} and 196 cm^{-1}, respectively [5]. After vacuum annealing the presence of the Cu_2SnSe_3 phase (peak at 180 cm^{-1}) could no longer be detected.

Fig. 2. presents SEM micrograph of the as-grown CZTSe monograin surface. The presence of secondary phase on the surface is clearly seen. The secondary phases being observed in CZTSe in other studies include CuSe, ZnSe and Cu_2SnSe_3 [6]. Magorian-Friedlmeier et al. [7] studied the formation of $Cu_2ZnSnSe_4$ by evaporation of reactants from elemental and binary sources with varying metallic ratios. It was found that only in the case of Zn deficiency a ternary compound Cu_2SnSe_3, has been formed. No other ternary compounds were found. It was also found in Ref. [8] that for a synthesis process in which the metallic elements are well intermixed in the ratio [Cu]:[Zn]:[Sn] = 2:1:1 the compound Cu_2SnSe_3 might form in addition to $Cu_2ZnSnSe_4$ since [Cu]:[Sn] = 2:1.

The low-temperature (T = 10 K) photoluminescence spectra of the as-grown and annealed CZTSe monograins together with the spectra of Cu_2SnSe_3 crystals are presented in Fig. 3 and corresponding data are summarised in Table 1. The PL spectrum of one of the as-grown CZTSe monograins (a in Fig. 3) consists of three Gaussian shaped PL bands at 0.765 eV, 0.86 eV and 0.95 eV. The other as-grown CZTSe spectrum (b in Fig. 3) consists of one PL band at 0.81 eV and in the spectra of annealed CZTSe (b* in Fig. 3) one PL band at 0.946 eV was detected. Temperature and excitation power dependencies were used to identify the origin of the PL emission of CZTSe monograins.

From the laser power dependencies of the PL spectra a blueshift with the magnitude of about 14 meV per decade was detected for the PL bands at 0.765 eV, 0.810 eV and 0.946 eV while the PL band at 0.86 eV shows no shift with excitation power. The blueshift of the PL bands can be taken as an evidence of donor–acceptor pair (DAP) recombination. However, the slightly asymmetrical shape of the PL bands and rather large blueshift with increasing laser power indicate the presence of Coulomb potential fluctuations in the material [9,10]. These fluctuations are small in sample a that shows PL bands with Gaussian shape. These potential fluctuations will lead to a local perturbation of the band structure, thus broadening the defect level distribution and forming band tails. These fluctuations are often detected in multinary compounds [9–11]. In a p-type material and in case of small effective mass of electrons, the radiative recombination can therefore mainly arise from four different channels: band-to-tail recombination (BT), that comprises a free electron and a hole that is localised in the valence band tail; band-to-band recombination (BB), that involves a free electron and a free hole, band-to-impurity (BI) recombination that involves an acceptor state that is deep enough not to overlap with the valence band tail, and donor–acceptor pair recombination that involves an acceptor and a donor state that are deep enough not to overlap with the corresponding band tails. The average depth of the fluctuations in samples b and b* was determined from the shape of the low-energy side of the PL bands (see details in Ref. [9]) and was found to be around 25 meV.

In order to determine the thermal activation energies of the recombination processes in CZTSe the temperature dependencies of the PL

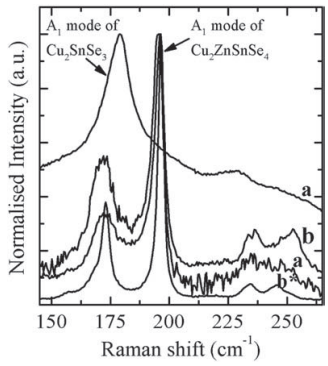

Fig. 1. Normalised Raman spectra of the surface of the CZTSe monograins: a, b — as-grown CZTSe and b* — CZTSe after annealing. Two spectra taken from different points of the crystal surface of sample a are presented. As can be seen, the presence of ternary Cu_2SnSe_3 phase was detected on the surface of as-grown CZTSe monograins (Raman mode at 180 cm^{-1}). This phase disappears after vacuum annealing.

spectra were measured. The temperature dependence of the PL spectrum of annealed CZTSe monograin powder is presented in Fig. 4. The thermal activation energies were determined from the Arrhenius plot (Fig. 5.). Since for the PL bands at 0.765 eV, 0.810 eV and 0.946 eV we found linear $\ln I(T)$ versus $1000/T$ dependence at high temperatures, that is common to BI-transition [9], we used theoretical expression for discrete energy levels proposed in Ref. [12] to fit the experimental data:

$$\Phi(T) = \frac{\Phi_0}{1 + \alpha_1 T^{3/2} + \alpha_2 T^{3/2} \exp(-E_T/kT)}, \quad (1)$$

where Φ is integrated intensity, α_1 and α_2 are the process rate parameters and E_T is the thermal activation energy. Thermal activation energies 26±6 meV, 44±5 meV and 69±4 meV were obtained for the PL bands at 0.765 eV, 0.810 eV and 0.946 eV, respectively. The Arrhenius plot of the PL band at 0.860 eV did not show linear dependence at high temperatures, so the thermal activation energy for this recombination process could not be found. This band vanishes very slowly with temperature, being detectable even at room-temperature. It also shifts towards higher energies with increasing temperature with the magnitude of 5 meV per 100 K. The laser power and temperature dependencies of the PL band at 0.860 eV indicate that this emission results from band-to-band (BB) recombination. Therefore, the bandgap energy of the corresponding phase in as-grown CZTSe sample must be around 0.86 eV at T = 10 K. We attribute the bandgap energy of 0.86 eV to the secondary Cu_2SnSe_3 phase detected by Raman spectroscopy in as-grown monograins. This conclusion is explained in more detail below.

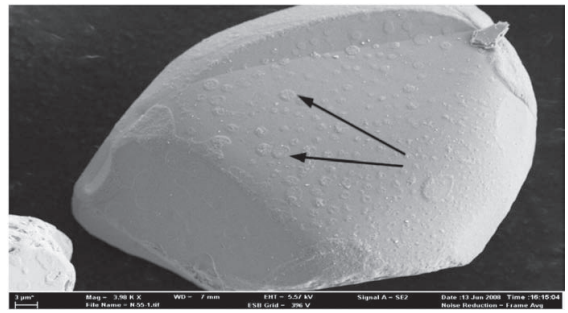

Fig. 2. SEM micrograph of a CZTSe monograin. The presence of Cu_2SnSe_3 phase forming small islands on the crystal surface (two of them are indicated by arrows) is clearly seen.

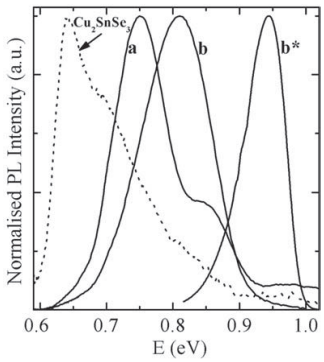

Fig. 3. Comparison of the normalised low-temperature PL spectra of as-grown CZTSe (a, b) and annealed CZTSe (b*) monograins. The as-grown CZTSe monograin spectra (a) consists of three PL bands at 0.765 eV, 0.86 eV and 0.95 eV. The other as-grown CZTSe spectra (b) and the spectra of annealed CZTSe monograins (b*) consist of one PL band at 0.81 eV and 0.946 eV, respectively. PL spectra of Cu_2SnSe_3 crystals are shown for comparison with dotted line.

The PL emission at 0.765 eV shows very fast quenching with temperature, the thermal activation energy being E_T=26±6 meV. Considering also the blueshift with increasing laser power, we attribute this emission to donor–acceptor pair recombination. This low activation energy is probably the ionization energy of a donor defect that should be lower defect in a p-type material. We cannot distinguish the vanishing of the free-to-bound emission in this sample, what should follow the ionization of a donor defect, therefore we cannot estimate the ionization energy of a corresponding acceptor. However, in the absence of remarkable potential fluctuations in sample a, it can be estimated considering that the energy of the emitted photon in a DAP transition is given by:

$$h\nu = E_g - E_A - E_D + e^2/(4\pi\varepsilon_0\varepsilon R), \quad (2)$$

where E_g is the bandgap energy, E_A and E_D are the acceptor and donor binding energies, respectively, and the last member is Coulomb energy. Taking into account that the BB band allows us to estimate the bandgap energy of Cu_2SnSe_3 phase, that was found to be around

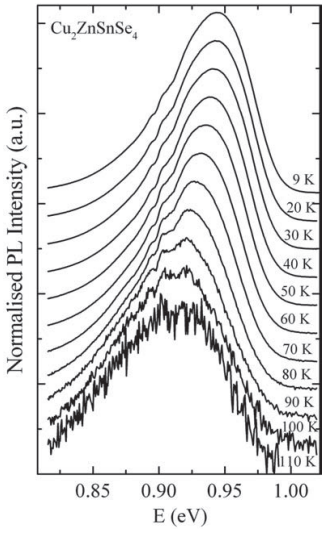

Fig. 4. Temperature dependence of the PL spectra of annealed CZTSe monograins (sample b*), measured in the temperature range of 9 K to 110 K.

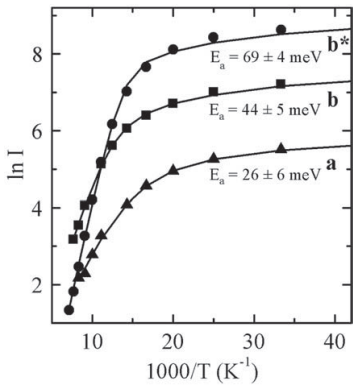

Fig. 5. Arrhenius plot derived from the temperature dependencies of the PL spectra of CZTSe monograins. Thermal activation energies 26±6 meV, 44±5 meV and 69±4 meV were obtained for the PL bands at 0.765 eV, 0.810 eV and 0.946 eV, respectively. Eq. (1) was used for fitting the experimental data.

0.86 eV, we obtain the acceptor activation energy of around 70 meV. From the thermal quenching of the PL band at 0.810 eV, that was obtained from another as-grown monograin powder (sample b), we obtained activation energy of 44±5 meV. This emission results from BI-recombination and may involve the same acceptor defect forming the donor–acceptor pair. The small difference in activation energies is due to the rough guess of the bandgap energy.

Analysing the high energy PL band at 0.946 eV that dominates the spectra of annealed CZTSe monograin powder (sample b*) and is also present in the spectra of one of the as-grown powders, we find that this emission results from the BI-recombination and involves an acceptor defect with ionization energy of E_T=69±4 meV. The results of the analysis of this PL band are inconsistent with the results obtained from the analysis of the other PL bands detected in these monograins. Considering the presence of the secondary phase of Cu_2SnSe_3 in the as-grown CZTSe monograins, we propose that the lower energy PL bands at 0.765 eV, 0.810 eV and 0.860 eV to this additional phase that according to literature has a bandgap energy of 0.843 eV at room temperature [13]. This has to be investigated in more detail in further studies. For comparison we grew separately Cu_2SnSe_3 crystals and their PL spectrum is presented in Fig. 3 with dotted line. As can be seen from Fig. 3, the lower energy bands detected in CZTSe monograins lie in the same spectral region. Vacuum annealing seems to remove the additional phase and the emission at 0.946 eV can be attributed to CZTSe. The results of the PL analysis of CZTSe monograins are summarised in Table 1.

The theory of heavily doped semiconductors [9] proves that at low temperatures the BI-bands' maximum is located at $h\nu_{max}=E_g-I_a$, where I_a is the defect ionization energy. In case of BI transition, the effect of fluctuations to the bandgap energy is not remarkable. The resulting bandgap energy of CZTSe is found to be around 1.02 eV at T=10 K. The obtained approximate bandgap energy of CZTSe is lower than the one reported in the literature as was mentioned in the introduction. However, it is reported that Cu_2ZnSnS_4 has bandgap energy of around 1.5 eV [14]. Our studies of $Cu_2ZnSn(Se_{x-1}S_x)_4$ solid solutions (to be published) indicate that the bandgap energy is decreasing with Se concentration and allow us to consider the obtained bandgap energy of $Cu_2ZnSnSe_4$ to be correct. Also the results of quantum efficiency measurements made for solar cells made from these CZTSe monograin powders confirm this result [5].

4. Conclusions

The photoluminescence properties of as-grown and vacuum annealed $Cu_2ZnSnSe_4$ monograin powders were studied. PL bands at 0.765 eV, 0.810 eV and 0.860 eV found in as-grown monograins were

proposed to arise from the additional phase Cu_2SnSe_3 whose presence in the monograins was detected by Raman spectroscopy and SEM/EDS analysis. After vacuum annealing of the CZTSe powder, pure CZTSe was obtained and the resulting PL emission at 0.946 eV was attributed to an acceptor defect with ionization energy of $E_T = 69 \pm 4$ meV. According to the PL results, it is proposed that the bandgap energy of CZTSe at $T = 10$ K is around 1.02 eV.

Acknowledgments

This work was supported by the Estonian Science Foundation grants G-6554 and G-6160. The support of the World Federation of Scientists National Scholarship Programme is gratefully acknowledged.

References

[1] K. Ito, T. Nakazawa, Jpn. J. Appl. Phys. 27 (1988) 2094.
[2] H. Matsushita, T. Maeda, A. Katsui, T. Takizawa, J. Cryst. Growth 208 (2000) 416.
[3] H. Yasuda, E. Sekiya, T. Maeda, H. Matsushita, A. Katsui, J. Adv. Sci. 11 (1999) 42.
[4] J.M. Raulot, C. Domain, J.F. Guillemoles, J. Phys. Chem. Solids 66 (2005) 2019.
[5] M. Altosaar, J. Raudoja, K. Timmo, M. Danilson, M. Grossberg, J. Krustok, E. Mellikov, Phys. Stat. Sol (a) 205 (2008) 167.
[6] T.M. Friedlmeier, H. Dittrich, H.W. Schock, Institute of Physics Conference Series No. 152: Proceeding of 11th International Conference on Ternary and Multinary Compounds, 1997, p. 345, Salford.
[7] Th. Magorian-Friedlmeier, N. Wieser, Th. Walter, H. Dittrich, H.W. Schock, Proc. 14th Europ. Photovolt. Sol. En. Conf., Barcelona, Spain, 1997, p. 1242.
[8] F. Hegert, R. Hock, Thin Solid Films 515 (2007) 5953.
[9] A.P. Levanyuk, V.V. Osipov, Sov. Phys. Usp. 24 (1981) 187.
[10] J. Krustok, H. Collan, M. Yakushev, K. Hjelt, Phys. Scr. T79 (1999) 179.
[11] A. Jagomägi, J. Krustok, J. Raudoja, M. Grossberg, M. Danilson, M. Yakushev, Physica B 337 (2003) 369.
[12] J. Krustok, H. Collan, K. Hjelt, J. Appl. Phys. 81 (1997) 1442.
[13] G. Marcano, C. Rincon, L.M. de Chalbaud, D.B. Bracho, G. Sanchez Perez, J. Appl. Phys. 90 (2001) 1847.
[14] K. Tanaka, Y. Miyamoto, H. Uchiki, K. Nakazawa, H. Araki, Phys. Stat. Sol. (a) 203 (2006) 2891.

PAPER V

M. Grossberg, J. Krustok, J. Raudoja, K. Timmo, M. Altosaar, T. Raadik. Photoluminescence and Raman study of $Cu_2ZnSn(Se_xS_{1-x})_4$ monograins for photovoltaic applications, *Thin Solid Films* (in press)

Photoluminescence and Raman study of $Cu_2ZnSn(Se_xS_{1-x})_4$ monograins for photovoltaic applications.

M. Grossberg[1], J. Krustok, J. Raudoja, K.Timmo, M. Altosaar, T. Raadik
Tallinn University of Technology, Ehitajate tee 5, 19086 Tallinn, Estonia.

Abstract

The quaternary semiconductors $Cu_2ZnSnSe_4$ and Cu_2ZnSnS_4 have attracted a lot of attention as possible absorber materials for solar cells due to their direct bandgap and high absorption coefficient (>10^4 cm^{-1}). In this study we investigate the optical properties of $Cu_2ZnSn(Se_xS_{1-x})_4$ monograin powders that were synthesized from binary compounds in the liquid phase of potassium iodide (KI) flux materials in evacuated quartz ampoules. Radiative recombination processes in $Cu_2ZnSn(Se_xS_{1-x})_4$ monograins were studied by using low-temperature photoluminescence (PL) spectroscopy. A continuous shift from 1.3 eV to 0.95 eV of the PL emission peak position with increasing Se concentration was observed indicating the narrowing of the bandgap of the solid solutions. Recombination mechanisms responsible for the PL emission are discussed. Vibrational properties of $Cu_2ZnSn(Se_xS_{1-x})_4$ monograins were studied by using micro-Raman spectroscopy. The frequencies of the optical modes in the given materials were detected and the bimodal behaviour of the A_1 Raman modes of $Cu_2ZnSnSe_4$ and Cu_2ZnSnS_4 is established.

Keywords: $Cu_2ZnSnSe_4$; Cu_2ZnSnS_4, Photoluminescence; Raman spectroscopy

1. Introduction.

Lately, the quaternary semiconductors $Cu_2ZnSnSe_4$ (CZTSe), Cu_2ZnSnS_4 (CZTS), $Cu_2CdSnSe_4$ have attracted a lot of attention as possible absorber materials for solar cells. These materials have an optimal direct bandgap for solar energy conversion and high absorption coefficients (>10^4 cm^{-1}) [1]. They are believed to be suitable alternatives for $CuInSe_2$ (CIS) and $Cu(InGa)Se_2$ (CIGS) absorbers since their elemental components are abundant in the Earth`s crust.

Only little information about the defect structure of $Cu_2ZnSnSe_4$ and Cu_2ZnSnS_4 can be found in the literature. Raulot et al. [2] have studied the energies of defect formation of CZTSe by ab initio electronic structure calculations. The lowest energy of formation was found for V_{Cu} that can be considered as dominating defect in CZTSe. We have previously published a photoluminescence (PL) analysis of CZTSe monograins [3] where PL emission at 0.946 eV was attributed to an acceptor defect with an ionization energy of E_T=69 ± 4 meV. Tanaka et al. [4] have determined donor-acceptor pair recombination with a thermal activation energy of 48 meV and a PL band gap of around 1.3 eV in S-poor CZTS single crystals grown by the iodine transport method. More recently, Hönes et al [5] have proposed a defect related recombination model for CZTS involving shallow defect levels – two shallow acceptor states 10 ± 5 meV and 30 ± 5 meV above the valence band and a donor state 5 ± 3 meV below the conduction band.

[1] Corresponding author : mgross@staff.ttu.ee, tel: +3726203210, fax: +3726203367

The band gap energy of CZTS is reported to be from 1.40 – 1.45 eV [5, 6] to 1.51 eV [7]. For CZTSe, quite different bandgaps have been reported. Mostly, it is proposed that the band gap energy lies between 1.4 eV and 1.56 eV [8,9]. However, it was suggested by us that the band gap energy of CZTSe is about 1.02 eV according to our PL analysis [3]. Based on *ab initio* calculations Raulot et al. [2] have found a bandgap of around 0.9 eV for CZTSe.

In this paper, we study the changes in Raman spectra of the $Cu_2ZnSn(Se_xS_{1-x})_4$ solid solutions with varying sulphur to selenium concentration ratio and changes in defect structure using photoluminescence spectroscopy.

2. Experimental details.

The $Cu_2ZnSn(Se_xS_{1-x})_4$ solid solutions were synthesized from CuSe(S), ZnSe(S) and SnSe(S) precursors in molten KI. More details about the synthesis can be found in [10]. The obtained material consisted of single crystalline particles with diameters of around 100 μm with tetragonal shape and rounded grain edges. The chemical composition of the monograin powders was determined by energy dispersive x-ray spectroscopy (EDS) (see Table 1). X-ray diffraction (XRD) measurements confirmed the formation of solid solutions. The monograins had p-type conductivity.

Table 1. Compositions of the studied solid solutions as determined by EDS

x	[Cu]/([Zn]+[Sn])	[Zn]/[Sn]
1	0.88	1.03
0.75	0.93	0.99
0.55	0.97	0.98
0.26	0.95	0.98
0	0.95	0.98

Room temperature Raman spectra were recorded by using a Horiba`s LabRam HR high resolution spectrometer equipped with a multichannel CCD detection system in backscattering configuration. In micro-Raman measurements, the incident laser light with a wavelength of 532 nm can be focused on the sample within a spot of 10 μm in diameter. For PL measurements, the samples were mounted in a closed-cycle He cryostat and cooled down to 10 K. The 441 nm He-Cd laser line was used for PL excitation.

3. Results and discussion.

3.1. Raman analysis.

The dependence of the Raman spectra on the composition of the $Cu_2ZnSn(Se_xS_{1-x})_4$ solid solutions with x values of 1, 0.75, 0.55, 0.26 and 0, are presented in figure 1. The A_1 Raman mode frequencies of CZTSe and CZTS (indicated by arrows in figure 1) are 196 cm^{-1} and 338.5 cm^{-1}, respectively. The A_1 modes are pure anion modes which correspond to vibrations of sulfur and selenium atoms surrounded by motionless neighboring atoms [11]. A linear shift of the A_1 Raman modes of CZTS and CZTSe towards higher wavenumbers with increasing sulphur concentration in $Cu_2ZnSn(Se_xS_{1-x})_4$ is demonstrated in figure 2. The other Raman peaks of CZTSe were detected at 167, 172, 230, 233, 243 cm^{-1} and the Raman peaks of CZTS at 167, 252, 288, 347, 366 cm^{-1} (labeled with numbers in figure 1). The lattice vibrational properties of these solid solutions have not been discussed so far.

All Raman spectra of the studied $Cu_2ZnSn(Se_xS_{1-x})_4$ solid solutions show peaks of some secondary (mostly binary) phases (positions of the peaks are indicated by dotted lines in

figure 1). However, the Raman peaks corresponding to additional phases have very low intensities in comparison with the CZTSe or CZTS peak intensities. All Raman spectra were fitted using Lorentzian functions to resolve the peaks. In the Raman spectrum of CZTSe the presence of ZnSe (peak at 249 cm^{-1}) was detected and also a $SnSe_2$ phase might be present (peak at 191 cm^{-1}). The corresponding Raman frequencies of ZnSe and $SnSe_2$ reported in the literature are 252 cm^{-1} [12] and 186 cm^{-1} [13], respectively. In $Cu_2ZnSn(Se_{0.75}S_{0.25})_4$ the presence of ZnS (peak at 353 cm^{-1}) and SnS (peaks at 196 cm^{-1} and 217 cm^{-1}) was detected. According to literature data, the corresonding Raman frequencies of ZnS and SnS are 353 cm^{-1} [14] and 192 cm^{-1} , 218 cm^{-1} [15], respectively. In the spectrum of $Cu_2ZnSn(Se_{0.55}S_{0.45})_4$ the presence of ZnS was detected (peak at 351 cm^{-1}) and in the spectrum of $Cu_2ZnSn(Se_{0.26}S_{0.74})_4$ peaks of ZnSe (peaks at 205 cm^{-1} and 251.5 cm^{-1}) and ZnS (peak at 351 cm^{-1}) were observed. In the spectrum of CZTS, a ZnS peak at 355 cm^{-1} was observed. Small deviations of peak positions of the secondary phases in the solid solutions can also be the result of a formation of solid solutions of binary compounds.

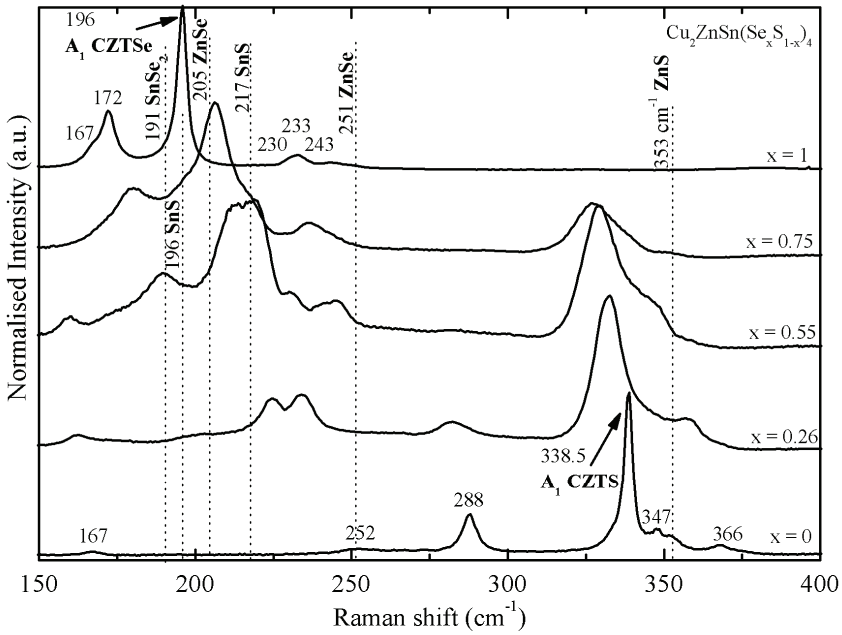

Figure 1. Room-temperature Raman spectra of $Cu_2ZnSn(Se_xS_{1-x})_4$ solid solutions with different Se/S concentration ratio. The A_1 modes of $Cu_2ZnSnSe_4$ and Cu_2ZnSnS_4 show bimodal behaviour.

The Raman peaks of $Cu_2ZnSn(Se_xS_{1-x})_4$ solid solutions broaden with increasing sulphur content, giving the largest widths of the peaks for $Cu_2ZnSn(Se_{0.55}S_{0.45})_4$. This trend is correlated with the increasing structural disorder due to the random distribution of S and Se atoms in the lattice that leads to fluctuations in the masses and force constants in the neighborhood.

Figure 2 presents the shift of the two A_1 modes with S concentration. As can be seen, the shift is larger for the CZTSe A_1 peak. This has also been observed in the case of $CuInS_{2x}Se_{2(1-x)}$ crystals [16]. The force constants are responsible for the trends in the frequencies of the A_1 mode. Both of the A_1 Raman modes of CZTSe and CZTS followed the two-mode behaviour throughout the entire alloy concentration range.

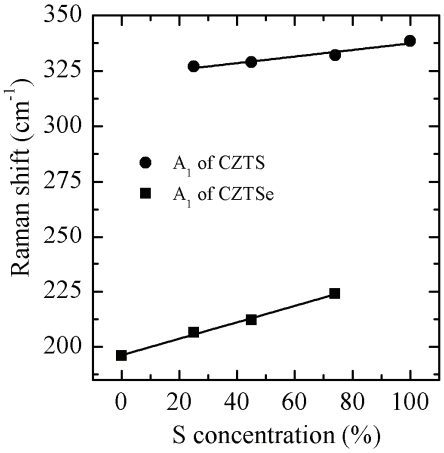

Figure 2. CZTS and CZTSe A_1 Raman mode frequency dependencies on the sulphur concentration in $Cu_2ZnSn(Se_xS_{1-x})_4$ solid solutions. The A_1 mode of both compounds shifts approximately linearly towards higher wavenumbers with increasing sulphur concentration.

3.2. Photoluminescence analysis.

Normalised photoluminescence spectra of the $Cu_2ZnSn(Se_xS_{1-x})_4$ solid solutions with different Se/S concentration ratios measured at T = 10 K are presented in Figure 3. Each spectrum (except for the one corresponding to Cu_2ZnSnS_4 that is fitted with two asymmetric PL bands) consists of one asymmetric PL band. The PL bands shift towards higher energies (see Figure 4) and become more asymmetric with increasing S concentration. Broadening of the PL bands with increasing S concentration is also observed. PL bands with such an asymmetric shape and behaviour are often observed in ternary chalcopyrites such as $CuInSe_2$ [17], $CuGaSe_2$ [18] and others that contain large concentrations of charged defects. One would expect similar results from quaternary compounds that are derived from the ternaries by substituting half of the group III element (In) by a group II element (Zn) and the other half by a group IV element (Sn).

In a semiconductor with a random distribution of high concentrations of charged donors and acceptors spatial fluctuations of the electrostatic potential are formed. These potential fluctuations will lead to a local perturbation of the band structure, thus broadening the defect level distribution and forming band tails [19]. Since the effective mass of an electron is much smaller than the effective mass of a hole in all direct-gap semiconductors, the electrons do not localize and the density of states near to the conduction band edge can be ignored. Radiative recombination in these “heavily doped” crystals is therefore often governed by the recombination of free electrons and holes localised in spatially separated potential wells originating from Coulomb potential fluctuations.

Excitation power dependent and temperature dependent PL measurements of the solid solutions performed in the present study indicate that the PL spectra of $Cu_2ZnSn(Se_xS_{1-x})_4$ are dominated by a band-to-impurity (BI) type recombination that involves free electron and a hole in the acceptor state that is deep enough not to overlap with the valence band tail. In the excitation power dependencies a large blue-shift with a magnitude of about 15 meV per decade was detected. In addition, a non-linear dependence of the *lnI(T)* versus *1000/T* at higher temperatures was detected. That is common behaviour of “heavily doped” semiconductors [17,18].

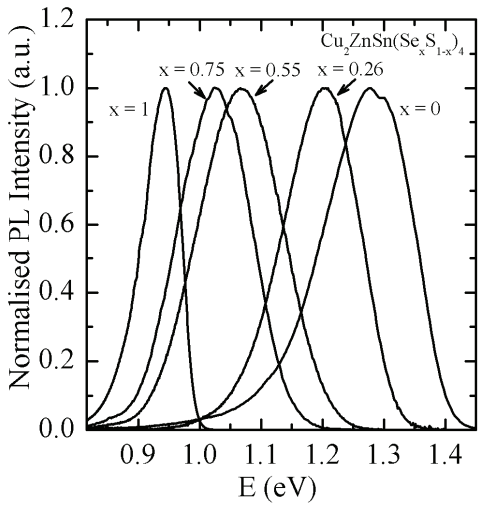

Figure 3. Normalised low-temperature photoluminescence spectra of the $Cu_2ZnSn(Se_xS_{1-x})_4$ solid solutions with different Se/S concentration ratios. A nearly linear shift of the PL emission towards higher energies with increasing S concentration was observed up to a total value of 0.4 eV.

In the case of one of the end members (Cu_2ZnSnS_4), the origin of the lower energy PL band is not clear since no detailed analysis of this PL band could have been performed due to its low intensity.

In the case of a material that contains a large concentration of charged defects an important aspect to consider is the average depth of the potential fluctuations γ that is the mean difference of the energy of holes in the valence band fluctuation minimum and maximum. These fluctuations are expected to reduce the efficiency of the corresponding solar cells [20]. The low-energy tail of the PL bands is correlated to the average depth of the potential fluctuations γ [19] and was therefore used to estimate it.

Siebentritt et al. [21] have analyzed the shape of the band tails in the case of fluctuating potentials for thin-film materials using two different models. According to them, the low-energy tail of asymmetrical PL bands can be described by a Gaussian or an exponential spectral dependence. This is based on the more general theoretical analysis of the density of states function by Osipov and Levanyuk [19].

The low-energy side of the PL band of the end members of the $Cu_2ZnSn(Se_xS_{1-x})_4$ solid solutions analyzed in the present paper exhibit an exponential decay while the other members can be described by the Gaussian shape. This is an indication of the presence of deeper fluctuations within the samples containing both sulphur and selenium. As in [21], the average amplitude of the potential fluctuations (see figure 4) in the solid solutions were determined from the exponential and Gaussian spectral dependencies, respectively [19]:

$$I(E) \sim \exp\left(-\frac{E}{\gamma}\right) \text{ or } I(E) \sim \exp\left(-\frac{(E-E_0)^2}{2\gamma^2}\right), \qquad (1)$$

where E_0 is assumed to represent an average emission energy in the case of fluctuating potentials. As can be seen from figure 4, γ increases with increasing S concentration in the solid solutions, being highest for CZTS. Analyzing the corresponding Raman spectra one would expect that γ is smaller in CZTS and CZTSe than in the solid solutions, because of the

lower defect concentration. It has been found by Raulot et al [2] that all selenium and sulphur compounds have a Cu vacancy formation energy close to the $CuInSe_2$, $CuGaSe_2$ and $CuInS_2$, $CuGaS_2$ values, respectively. The sulphur compounds have a V_{Cu} formation energy about 0.5 eV larger than the selenides [2]. Therefore one would expect a lower concentration of copper vacancies in CZTS compared with CZTSe resulting also in a smaller γ.

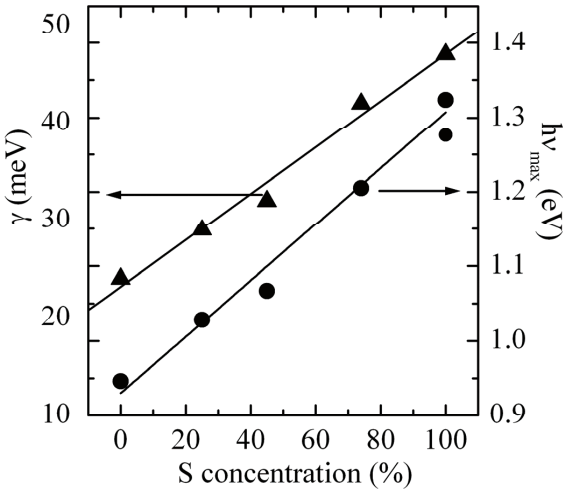

Figure 4. Approximately linear dependence of the PL band position and the average depth of potential fluctuations γ on the S concentration in $Cu_2ZnSn(Se_xS_{1-x})_4$ solid solutions.

One possible explanation of the obtained opposite result (figure 4) is the complexity of the phase diagrams of CZTSe and CZTS. The domain of a homogenous material in case of CZTS seems to be very narrow compared to CZTSe, resulting therefore in a more probable formation of other phases during the growth of the powder [22,23]. Despite the fact that γ is expected to increase due to the increasing defect concentration, we propose that in this case larger potential fluctuations are related to the presence of a defect phase or defect region that has a larger defect concentration and therefore also a higher γ value. At the same time these high γ values can be a result of compositional fluctuations, where some crystal regions have different band gap energy than others. The same behaviour was observed in $CuGa_3Se_5$ crystals [24]. The different band gap energy can be caused by different crystal structure in case of solid solutions. It was shown that, for example, that the band gap energy of kesterite-CZTS is about 0.12 eV larger than that of stannite-CZTS [25] and both structures are possible in solid solutions.The relative concentration of the defect phase increases with increasing S concentration due to the weaker tolerance to deviations from stoichiometry in the case of CZTS. Due to the similarity of the PL properties of CZTS and the proposed defect phase one would assume that this phase has very similar properties to CZTS. Here we can see an analogy to the properties of ternary chalcopyrites where the formation of so-called ordered defect compounds have been detected [26]. However, this assumption needs further investigation.

4. Conclusions.

We studied the optical properties of $Cu_2ZnSn(Se_xS_{1-x})_4$ monograin powders using PL and Raman spectroscopy. The bimodal behaviour and a shift towards higher frequencies of the A_1 Raman modes of CZTSe and CZTS with increasing S concentration was estabilised.

From PL analysis a widening of the bandgap of the solid solutions with increasing S concentration was observed. A BI recombination was detected as the main radiative recombination channel in the monograins. The average depth of the potential fluctuations present in the samples was estimated and was found to increase with increasing S concentration.

Acknowledgements.

This work was supported by the Estonian Science Foundation grant G-8282 and and by the target financing by HTM (Estonia) No. SF0140099s08. Support of the World Federation of Scientists National Scholarship Programme and EAS is gratefully acknowledged.

References

1. K. Ito, T. Nakazawa, Jpn. J. Appl. Phys. 27 (1988) 2094.
2. J.M. Raulot, C. Domain, J.F. Guillemoles, J. Phys. Chem. Solids 66 (2005) 2019.
3. M. Grossberg, J. Krustok, K.Timmo, M. Altosaar, Thin Solid Films 517 (2009) 2489.
4. K. Tanaka, Y. Miyamoto, H. Uchiki, K. Nakazawa, H. Araki, phys. stat. sol. (a) 203 (2006) 2891.
5. K. Hönes, E. Zscherpel, J. Scragg, S. Siebentritt, Physica B 404 (2009) 4949.
6. H. Katagiri, N. Ihigaki, T. Ishida, K. Saito, Jpn. J. Appl. Phys. 40 (2001) 500.
7. K. Ito, T. Nakazawa, Jpn. J. Appl. Phys. 27 (1988) 2094.
8. G. Suresh Babu, Y. B. Kishore Kumar, P. Uday Bhaskar, V. Sundara Raja, Semicond. Sci. Technol. 23 (2008) 1.
9. Rachmat Adhi Wibowo, Woo Seok Kim, Eun Soo Lee, Badrul Munir, Kyoo Ho Kim, J. Phys. Chem. Solids 68 (2007) 1908.
10. M. Altosaar, J. Raudoja, K. Timmo, M. Danilson, M. Grossberg, J. Krustok, E. Mellikov, phys. stat. sol. (a) 205 (2008) 167.
11. H. Neumann, Helv. Phys. Acta 58 (1985) 337.
12. G. Perna, M. Lastella, M. Ambrico, V. Capozzi, Appl. Phys. A 83 (2006) 127.
13. G. Lucovsky, J. C. Mikkelsen, Jr., W. Y. Liang, R. M. White, R. M. Martin, Phys. Rev. B 14 (1976) 1663.
14. Young-Moon Yu, M.-H. Hyun, S. Nam, D. Lee, O. Byungsung, K.- S. Lee, Pyeong Yeol Yu, Yong Dae Choi, J. Appl. Phys. 91 (2002) 9429.
15. H. R. Chandrasekhar, R.G. Humphreys, U. Zwick, M. Cardona, Phys. Rev. B 15 (1977) 2177.
16. R Bacewicz, W. Gebicki, J. Filipowicz, J. Phys. Condens. Matter 6 (1994) L777.
17. J. Krustok, H. Collan, M. Yakushev, K. Hjelt, Physica Scripta T79 (1999) 179.
18. J. Krustok, J. Raudoja, M. Yakushev, R. D. Pilkington, and H. Collan, phys. stat. sol. (a) 173 (1999) 483.
19. A.P. Levanyuk, V.V. Osipov, Sov. Phys. Usp. 24 (1981) 187.
20. J.H. Werner, J. Mattheis, U. Rau, Thin Solid Films 480-481 (2005) 399.
21. S. Siebentritt, N. Papathanasiou, M.Ch. Lux-Steiner, Physica B 376-377 (2006) 831.
22. I.D. Olekseyuk, I.V. Dudchak, L.V. Piskach, J. Alloys and Compounds 368 (2004) 135.
23. I.V. Dudchak, L.V. Piskach, J. Alloys and Compounds 351 (2003) 145.
24. M. Grossberg, J. Krustok, A. Jagomägi, M. Leon, E. Arushanov, A. Nateprov, I. Bodnar, Thin Solid Films 515 (2007) 6204.
25. S. Chen, X.G. Gong, A. Walsh, S.-H. Wei, Appl. Phys. Letters 94 (2009) 041903.
26. S.B. Zhang, S.H. Wei, A. Zunger, Phys. Rev. B 57 (1998) 9642.

APPENDIX B

ELULOOKIRJELDUS

Ees- ka perekonnanimi:	Maarja Grossberg
Sünniaeg ja -koht:	20.05.1981, Tallinn
E-post:	mgross@staff.ttu.ee
Hariduskäik	2005 – Tallinna Tehnikaülikool, Keemia- ja materjalitehnoloogia teaduskond, doktorantuur 2005 – Tallinna Tehnikaülikool, Keemia- ja materjalitehnoloogia teaduskond, magistrikraad 2003 – Tallinna Tehnikaülikool, Tehniline füüsika, bakalaureusekraad 1999 – Tallinna Tehnikagümnaasium, keskharidus
Teenistuskäik	2006 – Tallinna Tehnikaülikool, Materjaliteaduse instituut, teadur 2003 – 2005 Tallinna Tehnikaülikool, Materjaliteaduse instituut, insener 2002 – 2003 Tallinna Tehnikaülikool, Materjaliteaduse instituut, tehniline töötaja
Kaitstud lõputööd	,,Kalkopüriitse kolmikühendi $CuGaTe_2$ fotoluminestsentsi uuringud'', magistritöö, juhendaja prof. Jüri Krustok ,,Kalkopüriitse kolmikühendi $CuInTe_2$ fotoluminestsentsi uuringud'', bakalaureusetöö, juhendaja prof. Jüri Krustok
Täiendusõpe	okt. – dets. 2006 Hahn-Meitneri Instituut (Saksamaa), materjalide epitaksiaalkasvatus 21.08.2006 – 25.08.2006 European Union Centre of Excellence in PV Materials and Devices (Eesti), ,,YSSS-2006 on PV" jaan. – veeb. 2006 Universidad Autonoma de Madrid (Hispaania), röntgendifraktsiooni meetod 16.11.2005 – 19.11.2005 WITec GmbH (Saksamaa), konfokaalne Raman Spektroskoopia juuni – juuli 2004 Varssavi Tehnikaülikool (Poola), Päikesepatareide mahtuvuslikud ja optilised mõõtmismeetodid 13.10.2003 – 17.10.2003 Helsingi Tehnoloogiaülikool (Soome), fotopeegelduse meetod

CURRICULUM VITAE

First name and surname:	Maarja Grossberg
Date and place of birth:	20.05.1981, Tallinn
E-mail:	mgross@staff.ttu.ee

Education	2005 – Tallinn University of Technology, Faculty of Chemistry and Materials Technology, doctoral study 2005 – Tallinn University of Technology, Faculty of Chemistry and Materials Technology, Master of Science in Natural Sciences 2003 – Tallinn University of Technology, Faculty of Science, Bachelor of Science in Natural Sciences 1999 – Tallinn Technical Secondary School
Professional experience	2006 – Tallinn University of Technology, Department of Materials Science, researcher 2003 – 2005 Tallinn University of Technology, Department of Materials Science, engineer 2002 – 2003 Tallinn University of Technology, technical assistant
Defended dissertations	„Photoluminescence studies of ternary chalcopyrite compound $CuGaTe_2$", master thesis, supervisor Prof. Jüri Krustok „Photoluminescence studies of ternary chalcopyrite compound $CuInTe_2$", bachelor thesis, supervisor Prof. Jüri Krustok
Training courses	Oct. – Dec. 2006, Hahn-Meitner-Institut Berlin (Germany), epitaxial growth of materials 21.08.2006 – 25.08.2006, European Union Centre of Excellence in PV Materials and Devices, (Estonia), ''YSSS-2006 on PV" Jan. – Febr. 2006, Universidad Autonoma de Madrid (Spain), X-ray Diffraction method 16.11.2005 – 19.11.2005, WITec GmbH (Germany), Confocal Raman spectroscopy June – July 2004, Warsaw University of Technology (Poland), capacitance spectroscopy and optical studies of solar cells

13.10.2003 – 17.10.2003, Helsinki University of Technology (Finland), photoreflectance method

List of publications

1. **M. Grossberg**, J. Krustok, S. Siebentritt, J. Albert. Compositional dependence of Raman scattering and photoluminescence emission in Cu-Ga-Se films grown by MOCVD, Physica B: Condenced Matter 404(14-15) (2009) 1984-1988.
2. O. Volobujeva, J. Raudoja, E. Mellikov, **M. Grossberg,** S. Bereznev, R. Traksmaa. $Cu_2ZnSnSe_4$ films by selenization of Sn-Zn-Cu sequential films. J. of Phys. and Chem. of Solids 70(3-4) (2009) 567-570.
3. M. Krunks, T. Dedova, E. Kärber, V. Mikli, I. Oja Acik, **M. Grossberg**, A. Mere. Growth and electrical properties of ZnO nanorod arrays prepared by chemical spray pyrolysis, Physica B: Condenced Matter 404(22) (2009) 4422-4425.
4. **M. Grossberg**, J. Krustok, K. Timmo, M. Altosaar. Radiative recombination in $Cu_2ZnSnSe_4$ monograins studied by photoluminescence spectroscopy, Thin Solid Films 517 (2009) 2489-2492.
5. A. Bollero, **M. Grossberg**, B. Asenjo, M.T. Gutierrez. CuS-based thin films for architectural glazing applications produced by co-evaporation: morphology, optical and electrical properties, Surface and Coatings Technology 204 (2009) 593-600.
6. O. Volobujeva, M. Altosaar, J. Raudoja, E. Mellikov, **M. Grossberg**, L. Kaupmees, P. Barvinsch. SEM analysis and selenization of Cu-In alloy films produced by co-sputtering of metals, Solar Energy Materials and Solar Cells 93 (1) (2009) 11-14.
7. A. Bollero, **M. Grossberg**, T. Raadik, J.F. Trigo, J. Herrero, M.T. Gutierrez. Growth of Cu-rich/poor $CuInS_2$ thin films by the sequential modulated flux deposition technique, Thin Film Compound Semiconductor Photovoltaics 2009 MRS Spring Meeting (San Fransisco 13-17.04.2009) MRS Proceedings 2009, 1165-M02-06.
8. E. Mellikov, M. Altosaar, M. Krunks, J. Krustok, T. Varema, O. Volobujeva, **M. Grossberg**, L. Kaupmees, T. Dedova, K. Timmo, K. Ernits, J. Kois, I. Oja Acik, M. Danilson, S. Bereznev. Research in solar cell technologies at Tallinn University of Technology. Thin Solid Films 516 (2008) 7125-7134.
9. V. Valdna, **M. Grossberg**, J. Hiie, U. Kallavus, V. Mikli, R. Traksmaa, M. Viljus. Preparation and properties of CdTe Films on Mo/Glass substrates,

Thin Film Compound Semiconductor Photovoltaics 2009 MRS Spring Meeting (San Fransisco 13-17.04.2009) MRS Proceedings 2009, 1165-M08-24.

10. O. Volobujeva, E. Mellikov, J. Raudoja, **M. Grossberg**, S. Bereznev, M. Altosaar, R. Traksmaa. SEM analysis and selenization of Cu-Zn-Sn sequential films produced by evaporation of metals, Conference On Optoelectronic and Microelectronic Materials and Devices (COMMAD 2008) Proceedings (Sydney 28.07-01.08.2008) IEEE Publishing 2009, 257-260.
11. O. Volobujeva, J. Kois, R. Traksmaa, K. Muska, S. Bereznev, **M. Grossberg**, E. Mellikov. Influence of annealing conditions on the structural quality of $CuInSe_2$ thin films. Thin Solid Films 516 (2008) 7105-7109.
12. M. Kauk, M. Altosaar, J. Raudoja, K. Timmo, T. Varema, M. Danilson, **M. Grossberg**, E. Mellikov. The influence of doping with donor type impurities on the properties of $CuInSe_2$. phys. stat. sol. (c) 5, 609-611 (2008).
13. M. Altosaar, J. Raudoja, K. Timmo, M. Danilson, **M. Grossberg**, J. Krustok, E. Mellikov. $Cu_2Zn_{1-x}Cd_xSn(Se_{1-y}S_y)_4$ solid solutions as absorber materials for solar cells. phys. stat. sol. (a) 205, 167-170 (2008).
14. **M. Grossberg**, J. Krustok, I. Bodnar, S. Siebentritt, J. Albert. Photoluminescence and Raman spectra of the ordered vacancy compound $CuGa_5Se_8$. Physica B 403, 184-189 (2008).
15. T. Dedova, M. Krunks, **M. Grossberg**, O. Volobujeva, I. Oja Açik. A novel deposition method to grow ZnO nanorods: spray pyrolysis. Superlattices and Microstructures 42, 444- 450(2007).
16. P. Fochuk, R. Grill, Ye. Nykonyuk, J. Krustok, N. Armani, Z. Zakharuk, **M. Grossberg**, O. Panchuk. High Temperature Properties of CdTe Crystals, doped by Sb. IEEE Transactions on Nuclear Science, 54, 763-768 (2007).
17. **M. Grossberg**, J. Krustok, A. Jagomägi, M. Leon, E. Arushanov, A. Nateprov, I. Bodnar. Investigation of potential and compositional fluctuations in $CuGa_3Se_5$ crystals using photoluminescence spectroscopy. Thin Solid Films, 515, 6204-6207 (2007).
18. J. Krustok, **M. Grossberg**, A. Jagomägi, M. Danilson and J. Raudoja. Analysis of the edge emission of highly conductive $CuGaTe_2$. Thin Solid Films, 515, 6192-6195 (2007)
19. J. Krustok, A. Jagomägi, **M. Grossberg**, J. Raudoja, and M. Danilson. Photoluminescence properties of polycrystalline $AgGaTe_2$. Solar Energy Materials and Solar Cells. v. 90, No. 13, pp. 1973-1982 (2006).

20. M. Yakushev, Y. Feofanov, J. Krustok, **M. Grossberg**, A. Mudriy. Radiation hardness of $CuInSe_2$. Izv. Akad Nauk, ser. Fiz, v. 70, No 6, pp. 919-923 (2006).
21. A.Jagomägi, J.Krustok, **M.Grossberg**, M.Danilson, J.Raudoja. Deep defect related photoluminescence in heavily doped $GuGaTe_2$ crystals. phys. stat. sol. (a) v.203, No. 5, pp. 949-955 (2006).
22. K. Timmo, M. Altosaar, J. Raudoja, E. Mellikov, T. Varema, M. Danilson, **M. Grossberg**. The effect of sodium doping to $CuInSe_2$ monograin powder properties. Thin Solid Films, 515, 5887-5890 (2007).
23. M. Altosaar, J. Raudoja, K. Timmo, M. Danilson, **M. Grossberg**, M. Krunks, T. Varema, E. Mellikov. $Cu_2ZnSnSe_4$ monograin powders for solar cell application. Photovoltaic Energy Conversion, Conference Record of the 2006 IEEE 4th World Conference, 1, 468–470 (2006).
24. M. Kauk, M. Altosaar, J. Raudoja, K. Timmo, **M. Grossberg**, T. Varema, K. Ernits. Tailoring the composition and properties of $CuInSe_2$ materials for solar cell application. SPIE Proceedings vol. 5946, 224-229 (2005).
25. A. Jagomägi, J. Krustok, J. Raudoja, **M. Grossberg**, I. Oja, M. Krunks, and M. Danilson. Photoluminescence and Raman spectroscopy of polycrystalline $AgInTe_2$. Thin Solid Films v. 480-481, pp.246-249, 2005
26. M.Kauk, M. Altosaar, J. Raudoja, K. Timmo, **M. Grossberg**, T. Varema, E. Mellikov. Growth of $CuInSe_2$ monograin powders with different compositions. Mater. Res. Soc. Symp. Proc. Vol. 865, 2005 F 14.27.
27. M.Kauk, K.Ernits**, M. Grossberg**, J.Krustok, T. Varema, M.Altosaar, E.Mellikov. Chemical etching of $CuInSe_2$ absorber surface for monograin layer solar cell application. Proceeding of 20th European Photovoltaic Solar Energy Conference, 2006, 1811-1815
28. Jüri Krustok, Mati Danilson, Andri Jagomägi, **Maarja Grossberg**, Jaan Raudoja. Device characteristics of $CuInSe_2$ based solar cells. SPIE Proceedings vol. 5946, pp. 236-242, 2004
29. A. Jagomägi, J. Krustok, J. Raudoja**, M. Grossberg**, M. Danilson. Deep and edge photoluminescence emission of $CuInTe_2$. phys. stat. sol. (b), v.237, No 2, pp. R3-R5, 2003
30. A. Jagomägi, J. Krustok, J. Raudoja**, M. Grossberg**, M. Danilson, M. Yakushev. Photoluminescence studies of heavily doped $CuInTe_2$ crystals. Physica B v. 337, pp. 369-374, 2003

DISSERTATIONS DEFENDED AT TALLINN UNIVERSITY OF TECHNOLOGY ON *NATURAL AND EXACT SCIENCES*

1. **Olav Kongas**. Nonlinear dynamics in modeling cardiac arrhytmias. 1998.

2. **Kalju Vanatalu**. Optimization of processes of microbial biosynthesis of isotopically labeled biomolecules and their complexes. 1999.

3. **Ahto Buldas**. An algebraic approach to the structure of graphs. 1999.

4. **Monika Drews**. A metabolic study of insect cells in batch and continuous culture: application of chemostat and turbidostat to the production of recombinant proteins. 1999.

5. **Eola Valdre**. Endothelial-specific regulation of vessel formation: role of receptor tyrosine kinases. 2000.

6. **Kalju Lott**. Doping and defect thermodynamic equilibrium in ZnS. 2000.

7. **Reet Koljak**. Novel fatty acid dioxygenases from the corals *Plexaura homomalla* and *Gersemia fruticosa.* 2001.

8. **Anne Paju**. Asymmetric oxidation of prochiral and racemic ketones by using sharpless catalyst. 2001.

9. **Marko Vendelin**. Cardiac mechanoenergetics *in silico*. 2001.

10. **Pearu Peterson**. Multi-soliton interactions and the inverse problem of wave crest. 2001.

11. **Anne Menert**. Microcalorimetry of anaerobic digestion. 2001.

12. **Toomas Tiivel**. The role of the mitochondrial outer membrane in *in vivo* regulation of respiration in normal heart and skeletal muscle cell. 2002.

13. **Olle Hints**. Ordovician scolecodonts of Estonia and neighbouring areas: taxonomy, distribution, palaeoecology, and application. 2002.

14. **Jaak Nõlvak**. Chitinozoan biostratigrapy in the Ordovician of Baltoscandia. 2002.

15. **Liivi Kluge**. On algebraic structure of pre-operad. 2002.

16. **Jaanus Lass**. Biosignal interpretation: Study of cardiac arrhytmias and electromagnetic field effects on human nervous system. 2002.

17. **Janek Peterson**. Synthesis, structural characterization and modification of PAMAM dendrimers. 2002.

18. **Merike Vaher**. Room temperature ionic liquids as background electrolyte additives in capillary electrophoresis. 2002.

19. **Valdek Mikli**. Electron microscopy and image analysis study of powdered hardmetal materials and optoelectronic thin films. 2003.

20. **Mart Viljus**. The microstructure and properties of fine-grained cermets. 2003.

21. **Signe Kask**. Identification and characterization of dairy-related *Lactobacillus*. 2003.

22. **Tiiu-Mai Laht**. Influence of microstructure of the curd on enzymatic and microbiological processes in Swiss-type cheese. 2003.

23. **Anne Kuusksalu**. 2–5A synthetase in the marine sponge *Geodia cydonium*. 2003.

24. **Sergei Bereznev**. Solar cells based on polycristalline copper-indium chalcogenides and conductive polymers. 2003.

25. **Kadri Kriis**. Asymmetric synthesis of C_2-symmetric bimorpholines and their application as chiral ligands in the transfer hydrogenation of aromatic ketones. 2004.

26. **Jekaterina Reut**. Polypyrrole coatings on conducting and insulating substracts. 2004.

27. **Sven Nõmm**. Realization and identification of discrete-time nonlinear systems. 2004.

28. **Olga Kijatkina**. Deposition of copper indium disulphide films by chemical spray pyrolysis. 2004.

29. **Gert Tamberg**. On sampling operators defined by Rogosinski, Hann and Blackman windows. 2004.

30. **Monika Übner**. Interaction of humic substances with metal cations. 2004.

31. **Kaarel Adamberg**. Growth characteristics of non-starter lactic acid bacteria from cheese. 2004.

32. **Imre Vallikivi**. Lipase-catalysed reactions of prostaglandins. 2004.

33. **Merike Peld**. Substituted apatites as sorbents for heavy metals. 2005.

34. **Vitali Syritski**. Study of synthesis and redox switching of polypyrrole and poly(3,4-ethylenedioxythiophene) by using *in-situ* techniques. 2004.

35. **Lee Põllumaa**. Evaluation of ecotoxicological effects related to oil shale industry. 2004.

36. **Riina Aav**. Synthesis of 9,11-secosterols intermediates. 2005.

37. **Andres Braunbrück**. Wave interaction in weakly inhomogeneous materials. 2005.

38. **Robert Kitt**. Generalised scale-invariance in financial time series. 2005.

39. **Juss Pavelson**. Mesoscale physical processes and the related impact on the summer nutrient fields and phytoplankton blooms in the western Gulf of Finland. 2005.

40. **Olari Ilison**. Solitons and solitary waves in media with higher order dispersive and nonlinear effects. 2005.

41. **Maksim Säkki**. Intermittency and long-range structurization of heart rate. 2005.

42. **Enli Kiipli**. Modelling seawater chemistry of the East Baltic Basin in the late Ordovician–Early Silurian. 2005.

43. **Igor Golovtsov**. Modification of conductive properties and processability of polyparaphenylene, polypyrrole and polyaniline. 2005.

44. **Katrin Laos**. Interaction between furcellaran and the globular proteins (bovine serum albumin β-lactoglobulin). 2005.

45. **Arvo Mere**. Structural and electrical properties of spray deposited copper indium disulphide films for solar cells. 2006.

46. **Sille Ehala**. Development and application of various on- and off-line analytical methods for the analysis of bioactive compounds. 2006.

47. **Maria Kulp**. Capillary electrophoretic monitoring of biochemical reaction kinetics. 2006.

48. **Anu Aaspõllu.** Proteinases from *Vipera lebetina* snake venom affecting hemostasis. 2006.

49. **Lyudmila Chekulayeva**. Photosensitized inactivation of tumor cells by porphyrins and chlorins. 2006.

50. **Merle Uudsemaa**. Quantum-chemical modeling of solvated first row transition metal ions. 2006.

51. **Tagli Pitsi**. Nutrition situation of pre-school children in Estonia from 1995 to 2004. 2006.

52. **Angela Ivask**. Luminescent recombinant sensor bacteria for the analysis of bioavailable heavy metals. 2006.

53. **Tiina Lõugas**. Study on physico-chemical properties and some bioactive compounds of sea buckthorn (*Hippophae rhamnoides* L.). 2006.

54. **Kaja Kasemets**. Effect of changing environmental conditions on the fermentative growth of Saccharomyces cerevisae S288C: auxo-accelerostat study. 2006.

55. **Ildar Nisamedtinov**. Application of ^{13}C and fluorescence labeling in metabolic studies of Saccharomyces spp. 2006.

56. **Alar Leibak**. On additive generalisation of Voronoï's theory of perfect forms over algebraic number fields. 2006.

57. **Andri Jagomägi**. Photoluminescence of chalcopyrite tellurides. 2006.

58. **Tõnu Martma**. Application of carbon isotopes to the study of the Ordovician and Silurian of the Baltic. 2006.

59. **Marit Kauk**. Chemical composition of $CuInSe_2$ monograin powders for solar cell application. 2006.

60. **Julia Kois**. Electrochemical deposition of $CuInSe_2$ thin films for photovoltaic applications. 2006.

61. **Ilona Oja Açik**. Sol-gel deposition of titanium dioxide films. 2007.

62. **Tiia Anmann**. Integrated and organized cellular bioenergetic systems in heart and brain. 2007.

63. **Katrin Trummal**. Purification, characterization and specificity studies of metalloproteinases from *Vipera lebetina* snake venom. 2007.

64. **Gennadi Lessin**. Biochemical definition of coastal zone using numerical modeling and measurement data. 2007.

65. **Enno Pais**. Inverse problems to determine non-homogeneous degenerate memory kernels in heat flow. 2007.

66. **Maria Borissova**. Capillary electrophoresis on alkylimidazolium salts. 2007.

67. **Karin Valmsen**. Prostaglandin synthesis in the coral *Plexaura homomalla*: control of prostaglandin stereochemistry at carbon 15 by cyclooxygenases. 2007.

68. **Kristjan Piirimäe**. Long-term changes of nutrient fluxes in the drainage basin of the gulf of Finland – application of the PolFlow model. 2007.

69. **Tatjana Dedova**. Chemical spray pyrolysis deposition of zinc sulfide thin films and zinc oxide nanostructured layers. 2007.

70. **Katrin Tomson**. Production of labelled recombinant proteins in fed-batch systems in *Escherichia coli*. 2007.

71. **Cecilia Sarmiento**. Suppressors of RNA silencing in plants. 2008.

72. **Vilja Mardla**. Inhibition of platelet aggregation with combination of antiplatelet agents. 2008.

73. **Maie Bachmann**. Effect of Modulated microwave radiation on human resting electroencephalographic signal. 2008.

74. **Dan Hüvonen**. Terahertz spectroscopy of low-dimensional spin systems. 2008.

75. **Ly Villo**. Stereoselective chemoenzymatic synthesis of deoxy sugar esters involving *Candida antarctica* lipase B. 2008.

76. **Johan Anton**. Technology of integrated photoelasticity for residual stress measurement in glass articles of axisymmetric shape. 2008.

77. **Olga Volobujeva**. SEM study of selenization of different thin metallic films. 2008.

78. **Artur Jõgi**. Synthesis of 4'-substituted 2,3'-dideoxynucleoside analogues. 2008.

79. **Mario Kadastik**. Doubly charged Higgs boson decays and implications on neutrino physics. 2008.

80. **Fernando Pérez-Caballero**. Carbon aerogels from 5-methylresorcinol-formaldehyde gels. 2008.

81. **Sirje Vaask**. The comparability, reproducibility and validity of Estonian food consumption surveys. 2008.

82. **Anna Menaker**. Electrosynthesized conducting polymers, polypyrrole and poly(3,4-ethylenedioxythiophene), for molecular imprinting. 2009.

83. **Lauri Ilison**. Solitons and solitary waves in hierarchical Korteweg-de Vries type systems. 2009.

84. **Kaia Ernits**. Study of In_2S_3 and ZnS thin films deposited by ultrasonic spray pyrolysis and chemical deposition. 2009.

85. **Veljo Sinivee**. Portable spectrometer for ionizing radiation "Gammamapper". 2009.

86. **Jüri Virkepu**. On Lagrange formalism for Lie theory and operadic harmonic oscillator in low dimensions. 2009.

87. **Marko Piirsoo**. Deciphering molecular basis of Schwann cell development. 2009.

88. **Kati Helmja**. Determination of phenolic compounds and their antioxidative capability in plant extracts. 2010.

89. **Merike Sõmera**. Sobemoviruses: genomic organization, potential for recombination and necessity of P1 in systemic infection. 2010.

90. **Kristjan Laes**. Preparation and impedance spectroscopy of hybrid structures based on $CuIn_3Se_5$ photoabsorber. 2010.

91. **Kristin Lippur**. Asymmetric synthesis of 2,2'-bimorpholine and its 5,5'-substituted derivatives. 2010.

92. **Merike Luman**. Dialysis dose and nutrition assessment by an optical method. 2010.

93. **Mihhail Berezovski**. Numerical simulation of wave propagation in heterogeneous and microstructured materials. 2010.

94. **Tamara Aid-Pavlidis**. Structure and regulation of BDNF gene. 2010.

95. **Olga Bragina**. The role of Sonic Hedgehog pathway in neuro- and tumorigenesis. 2010.

96. **Merle Randrüüt**. Wave propagation in microstructured solids: solitary and periodic waves. 2010.